

The HUNGARIAN JOURNAL OF INDUSTRY AND CHEMISTRY (HJIC)

formerly (until 2012) the Hungarian Journal of Industrial Chemistry

The HJIC is an international periodical that focuses on results of fundamental and applied research in the field of

- Biotechnology
- Chemical Engineering Science
- Chemical Processes
- Energetics
- Environmental Chemistry
- Environmental Engineering & Technology
- Industrial Management
- Material Science
- Mechanical Engineering
- Mechatronics
- Process & System Engineering
- Recycling

in the form of original papers, technical reports, reviews, communications, and conference proceedings written in English. HJIC is abstracted by Chemical Abstracts, indexed by Hungarian Scientific Bibliographic Database (MTMT), and archived by REAL-J Repository of the Hungarian Academy of Sciences.

EDITORIAL BOARD

Editor-in-chief: RÓBERT K. SZILÁGYI

Department of Chemistry and Biochemistry, Montana State University, Bozeman, MT, U.S.A.

MTA-ELTE "Lendület" Chemical Structure/Function Laboratory, Budapest, Hungary

Associate Editors:

JÁNOS ABONYI

Department of Process Engineering,
University of Pannonia, Veszprém, Hungary

DEZSŐ BODA

Department of Physical Chemistry,
University of Pannonia, Veszprém, Hungary

NORBERT MISKOLCZI

MOL Department of Hydrocarbon and Coal Processing,
University of Pannonia, Veszprém, Hungary

DÓRA RIPPEL PETHŐ

Department of Chemical Engineering Science,
University of Pannonia, Veszprém, Hungary

Editors:

KATALIN BÉLAFI-BAKÓ

Research Institute of Bioengineering,
Membrane Technology and Energetics,
University of Pannonia, Veszprém, Hungary

PETER CZERMAK

Institute of Bioprocess Engineering and
Pharmaceutical Technology, Mittelhessen University of
Applied Sciences, Giessen, Germany

DÉNES FODOR

Institute of Mechanical Engineering,
University of Pannonia, Veszprém, Hungary

MARIA GAVRILESCU

Department of Environmental Engineering
and Management,
Gheorghe Asachi Technical University of Iasi, Romania

DIRK GILLESPIE

Department of Molecular Biophysics and Physiology,
Rush University Medical Center, Chicago, U.S.A

LÁSZLÓ GUBICZA

Research Institute of Bioengineering, Membrane
Technology and Energetics,
University of Pannonia, Veszprém, Hungary

JENŐ HANCSÓK

MOL Department of Hydrocarbon and Coal Processing,
University of Pannonia, Veszprém, Hungary

JIŘÍ KLEMEŠ

Centre for Process Integration and Intensification,
University of Pannonia, Veszprém, Hungary

ZOLTÁN KOVÁCS

Department of Management,
University of Pannonia, Veszprém, Hungary

JÁNOS KRISTÓF

Department of Analytical Chemistry,
University of Pannonia, Veszprém, Hungary

ISTVÁN SZALAI

Institute of Physics and Mechatronics,
University of Pannonia, Veszprém, Hungary

JÁNOS SZÉPVÖLGYI

Research Centre for Natural Sciences,
University of Pannonia, Veszprém, Hungary

GYULA VATAI

Department of Food Engineering,
Corvinus University of Budapest, Hungary

GÁBOR VERESS

Federation of Technical and Scientific Societies –
MTESZ Budapest, Hungary

IBOLYA ZSOLDOS

Department of Material Science and Technology,
Széchenyi István University, Győr, Hungary

EDITORIAL OFFICE: UNIVERSITY OF PANNONIA, P.O. BOX 158, VESZPRÉM, 8201 (HUNGARY)

Tel.: +36 (88) 624-746, e-mail: hjic@almos.uni-pannon.hu; web: hjic.mk.uni-pannon.hu

Felelős szerkesztő: Szilágyi Róbert Károly

Nyelvi lektor: Matthew Chen

Kiadja: Pannon Egyetem, 8200 Veszprém, Egyetem u. 10.

Elektronikus terjesztés: De Gruyter Open (formerly Versita), Warsaw, Poland

Levél cím: H-8201 Veszprém, Postafiók 158, Tel.: (88) 624-000

Felelős kiadó: a Pannon Egyetem, Mérnöki Kar dékánja (Prof. Dr. Szalai István, Ph.D.)

TABLE OF CONTENTS

REVIEW

Some Analytic Expressions for the Capacitance and Profiles of the Electrical Double Layer Formed by Ions near an Electrode

DOUGLAS HENDERSON 55–66
DOI: 10.1515/hjic-2015-0010

ARTICLES

Comparison of Two Variable Interpolation Methods for Predicting the Vapour Pressure of Aqueous Glycerol Solutions

ISTVÁN SZALKAI, ATTILA SEBESTYÉN, B. DELLA-VECCHIA, TAMÁS KRISTÓF, LÁSZLÓ KÓTAI,
FERENC BÓDI 67-71
DOI: 10.1515/HJIC-2015-0011

Comparison of Decontamination Standards

LE CONG HAO, MAI DIHN THUY, DO TRUNG HIEU, ZOLTÁN SAS 73–78
DOI: 10.1515/hjic-2015-0012

A Study of the Adsorption Characteristics of Cobalt and Caesium from a Solution by using Vietnamese Bentonite

LE PHUOC CUONG, PHAM HOANG GIANG, BUI DANG HANH, GERGŐ BÁTOR 79–83
DOI: 10.1515/hjic-2015-0013

Application of Ionic Liquids in the Utilization of the Agricultural Wastes: Towards the One-Step Pre-treatment and Cellulose Hydrolysis

GÁBOR MEGYERI, NÁNDOR NEMESTÓTHY, MILAN POLAKOVIC, KATALIN BÉLAFI-BAKÓ,
LÁSZLÓ GUBICZA 85–89
DOI: 10.1515/hjic-2015-0014

Mineral Matter in Nigerian Coals and Tar Sand and Their Implications in Binary Blend Formulation/Co-Carbonisation

SOLOMON A. RYEMSHAK, ALIYU JAURO, ISTIFANUS Y. CHINDO, ENO O. EKANEM 91–95
DOI: 10.1515/hjic-2015-0015

Comparative Study of Advanced Oxidation Processes to Treat Petroleum Wastewater

DHEEAA AL DEEN ATALLAH ALJUBOURYA, PUGANESHWARY PALANIANDY,
HAMIDI BIN ABDUL AZIZ, SHAIK FEROZ 97–101
DOI: 10.1515/hjic-2015-0016

SOME ANALYTIC EXPRESSIONS FOR THE CAPACITANCE AND PROFILES OF THE ELECTRIC DOUBLE LAYER FORMED BY IONS NEAR AN ELECTRODE

DOUGLAS HENDERSON *

Department of Chemistry and Biochemistry, Brigham Young University, Provo, Utah 84602, USA

The electric double layer, which is of practical importance, is described. Two theories that yield analytic results, the venerable Poisson-Boltzmann or Gouy-Chapman-Stern theory and the more recent mean spherical approximation, are discussed. The Gouy-Chapman-Stern theory fails to account for the size of the ions nor for correlations among the ions. The mean spherical approximation overcomes, to some extent, these deficiencies but is applicable only for small electrode charge. A hybrid description that overcomes some of these problems is presented. While not perfect, it gives results for the differential capacitance that are typical of those of an ionic liquid. In particular, the differential capacitance can pass from having a double hump at low concentrations to a single hump at high concentrations.

Keywords: Electric double layer, capacitance, Gouy-Chapman-Stern theory, mean spherical approximation, density functional theory, computer simulation

1. Introduction

A double layer (DL) or an electric double layer (EDL) is formed when charged particles are attracted to a charged surface. The most obvious case is an electrolyte near a charged electrode (as in a battery). However, DNA can play a role that is analogous to the electrode. Ions can be attracted to membranes. A membrane can be thought of as a pseudo electrode. Ions are absorbed (often selectively) into physiological channels in membranes. Such channels permit the transport of nutrients into the cell and the removal of waste from the cell and are essential to the functioning of cells and life. The reader's attention is drawn to some recent reviews of EDLs [1–3].

It is the case of an electrolyte near a charged flat surface that is considered here. This is the simplest case; it is an interesting and important application of statistical mechanical theory. The theory of the DL is important to our understanding of batteries. It can be used in the analysis of experimental electrochemical data and in analytical chemistry.

In the model DL that is presented here, the electrode is approximated as a smooth flat charged surface located at $x = 0$. This surface is impenetrable and the ions are confined to the region $x > 0$. The charge of the electrode is located on the surface. There is no charge inside the electrode ($x < 0$). The electric field does not penetrate the surface. The electrode is a classical metal. Obviously, this is an approximation but there has been very

little work that takes into account the electronic structure of the electrode. The electrode charge is presumed to be uniform; the charge density of the electrode is σ and has the units of C/m^2 . Ions in the electrolyte near an electrode that have a charge opposite to that of the electrode are attracted to the electrode and form a layer whose net charge is equal in magnitude, but opposite in electric sign, to the charge of the electrode. The electrode and the attracted charge are together called an EDL. The charge in the EDL of the electrolyte can be spread over an extended region, usually called the diffuse layer, and need not consist solely of counterions whose charge is opposite to the electrode charge. The counterions can bring some coions with them. There may be regions of alternating charge where the coions predominate. However, the net charge of the attracted charged region in the electrolyte is equal in magnitude but opposite in sign to that of the electrode. Otherwise, the electric field would not vanish far from the electrode.

For simplicity, the model electrolyte that is employed here is a fluid of charged hard spheres of diameter d . In this study, the electrolyte is assumed to be binary. For additional simplicity, the ions are assumed in this article to be symmetric both in the magnitude of their charge and diameter. The value of the charge of an ion of species i is $z_i e$, where z_i is the ion valence and has the sign of the ion charge. The magnitude of the elementary charge is e . Because the ions are symmetric, $|z_i| = z$. In the bulk, the density of the ions of species i is $\rho_i = N_i/v$, where N_i is the number of ions of species i in the bulk

*Author for correspondence: doug@chem.byu.edu

and v is the volume of the system. Electrical neutrality requires that $N_1 = N_2$ or $\rho_1 = \rho_2$ or $\sum z_i \rho_i = 0$. The solvent (usually water) of the electrolyte is characterized by a dielectric constant, ϵ . Any change of the dielectric constant with a change of ion concentration is ignored. This model electrolyte is appropriately called the primitive model (PM). In the particular case considered here, where the ions all have the same diameter, this model is called the restricted primitive model (RPM).

In this model, the interaction between a pair of ions, whose centers are separated by the distance r , is given by

$$u_{ij}(r) = \begin{cases} \infty & \text{for } r < d \\ \frac{z_i z_j e^2}{4\pi\epsilon_0\epsilon r} & \text{for } r \geq d \end{cases}, \quad (1)$$

where ϵ_0 is the permittivity of free space, and the interaction of an ion with the surface is given by

$$u_{wi}(x) = \begin{cases} \infty & \text{for } x < d/2 \\ -\frac{\sigma z_i e x}{\epsilon_0 \epsilon} & \text{for } x \geq d/2 \end{cases}, \quad (2)$$

where x is the distance between the center of the ion and the surface.

Our task is to determine the density profile, $\rho_i(x)$, of the ions, or equivalently, $g_i(x) = \rho_i(x)/\rho_i$. Note that $\rho_i(\infty) = \rho_i$, so that $g_i(\infty) = 1$. Once, the $g_i(x)$ are known, the charge profile (C/m²), for $x > d/2$, is given by

$$q(x) = e \sum_i z_i \rho_i h_i(x), \quad (3)$$

where $h_i(x) = g_i(x) - 1$. In writing Eq. 3, the global charge neutrality condition $\sum z_i \rho_i = 0$ has been invoked. The charge density on the electrode is given by

$$\sigma = -e \sum_i z_i \rho_i \int_{d/2}^{\infty} h_i(t) dt. \quad (4)$$

There is no point including the region $0 < t < d/2$ in the integral since $\sum h_i(t) = 0$ in this region. The potential profile (in Volts) is given by

$$\phi(x) = -\frac{e}{\epsilon_0 \epsilon} \sum_i z_i \rho_i \int_x^{\infty} (t-x) h_i(t) dt. \quad (5)$$

In particular, the potential (Volts) of the electrode is given by

$$V = \phi(0) = -\frac{e}{\epsilon_0 \epsilon} \sum_i z_i \rho_i \int_0^{\infty} t h_i(t) dt. \quad (6)$$

Note that these equations satisfy Poisson's equation

$$\frac{d^2 \phi(x)}{dx^2} = -\frac{q(x)}{\epsilon_0 \epsilon}. \quad (7)$$

Indeed, Eqs. 3 and 5 are obtained by integrating Poisson's equation. An alternative procedure for computing the potential profile has been proposed by Boda and Gillespie [4] for simulation purposes.

It is often convenient to use dimensionless, or reduced, values that are denoted by an asterisk. For a system whose temperature (K) is T , the reduced temperature is $T^* = 4\pi\epsilon_0 d k T / z^2 e^2$. The reduced density is $\rho_i^* = \rho_i d^3$, the reduced electrode charge density is $\sigma^* = \sigma d^2 / e$, and the reduced potential is $\phi^* = \beta e \phi$, where $\beta = 1/kT$, with k being the Boltzmann constant (the gas constant per particle).

2. Poisson–Boltzmann or Gouy–Chapman–Stern theory: comparison with simulations

The classic theory of the EDL was developed by Gouy [5], Chapman [6], and Stern [7] (GCS) a century ago. The theory is based on Poisson's equation together with the Boltzmann formula,

$$g_i(x) = \begin{cases} 0 & x < d/2 \\ \exp[-\beta z_i e \phi(x)] & x \geq d/2 \end{cases}. \quad (8)$$

In electrostatics, Poisson's equation is exact and is equivalent to one of Maxwell's equations. The Boltzmann formula is approximate and neglects ion size and correlations between the ions. Eq. 8 states that $g_i(x)$ for the cations is the reciprocal of $g_i(x)$ for the counterions. This is not true, in general [8].

Equation 8, when inserted into Poisson's equation, yields what may be called the Poisson-Boltzmann (PB) or GCS approximation. This approximation is also employed in the Debye-Hückel (DH) theory for bulk electrolytes that was developed some years later. However, because of the three dimensional geometry of the DH theory, the nonlinear PB equation cannot be solved analytically and the PB equations in the DH theory are usually linearized. In the GCS theory, the resultant PB equation is a nonlinear second order differential equation. As has been pointed out, such equations generally do not yield analytic solutions. However, for the one dimensional geometry of the planar DL that is considered here, an analytic solution is possible in the case of the GCS theory.

The resulting PB/GCS potential is

$$\frac{\beta z e \phi(x)}{2} = \ln \left\{ 1 + \frac{b/2}{1 + \sqrt{1 + b^2/4}} \exp[-\kappa y] \right\} - \ln \left\{ 1 - \frac{b/2}{1 + \sqrt{1 + b^2/4}} \exp[-\kappa y] \right\}, \quad (9)$$

where $y = x - d/2 > 0$ and

$$b = \frac{\beta z e \sigma}{\epsilon_0 \epsilon \kappa}, \quad (10)$$

where κ is the Debye screening parameter that is given by

$$\kappa = \sqrt{\frac{\beta z^2 e^2 \rho}{\epsilon_0 \epsilon}} \quad (11)$$

with $\rho = \sum \rho_i$. The parameter b is another dimensionless measure of the electrode charge density. However, it is not as fundamental a quantity as σ^* since it arises from a theory. The parameter κ is a screening parameter; it is an inverse measure of the distance over which the profiles reach their asymptotic values within the GCS and DH theories.

In the GCS theory the relationship between the potential difference and electrode charge density is given by

$$\sinh \left[\frac{\beta z e \phi_{d/2}}{2} \right] = \frac{b}{2}, \quad (12)$$

where $\phi_{d/2} = \phi(d/2)$ is often called the diffuse layer potential. Some relations that are equivalent to Eq. 12 are

$$\cosh \left[\frac{\beta z e \phi_{d/2}}{2} \right] = \sqrt{1 + b^2/4}, \quad (13)$$

$$\tanh \left[\frac{\beta z e \phi_{d/2}}{2} \right] = \frac{b/2}{\sqrt{1 + b^2/4}}, \quad (14)$$

and

$$\tanh \left[\frac{\beta z e \phi_{d/2}}{4} \right] = \frac{b/2}{1 + \sqrt{1 + b^2/4}}. \quad (15)$$

The equivalence of Eqs. 12–15 is a result of identities among the hyperbolic functions.

Thus, Eq. 9 can be written as

$$\frac{\beta z e \phi(x)}{2} = \ln \left\{ 1 + \tanh \left[\frac{\beta z e \phi_{d/2}}{4} \right] \exp(-\kappa y) \right\} - \ln \left\{ 1 - \tanh \left[\frac{\beta z e \phi_{d/2}}{4} \right] \exp(-\kappa y) \right\}. \quad (16)$$

Alternative forms of Eqs. 9 and 16 are

$$\tanh \left[\frac{\beta z e \phi(x)}{4} \right] = \tanh \left[\frac{\beta z e \phi_{d/2}}{4} \right] \exp(-\kappa y) \quad (17)$$

or

$$\tanh \left[\frac{\beta z e \phi(x)}{4} \right] = \frac{b/2}{1 + \sqrt{1 + b^2/4}} \exp(-\kappa y). \quad (18)$$

In the GCS theory, the potential difference across the EDL is

$$V = -\frac{ze}{\epsilon\epsilon_0} \sum_i \rho_i \int_0^\infty th_i(t) dt = \frac{\sigma d}{2\epsilon\epsilon_0} + \phi_{d/2}, \quad (19)$$

where $\phi_{d/2}$ is given by Eq. 12. Thus, the capacitance, $C = \sigma/V$, of the EDL is

$$\frac{1}{C} = \frac{d}{2\epsilon\epsilon_0} + \frac{2 \sinh^{-1}(b/2)}{\epsilon\epsilon_0 \kappa b} \quad (20)$$

and the differential capacitance, $C_d = \partial\sigma/\partial V$, of the EDL is given by

$$\frac{1}{C_d} = \frac{d}{2\epsilon\epsilon_0} + \frac{1}{\epsilon\epsilon_0 \kappa \sqrt{1 + b^2/4}}. \quad (21)$$

Equations 20 and 21 are formally identical to a diffuse layer capacitor with capacitance,

$$C^{dl} = \epsilon\epsilon_0 \kappa \frac{b/2}{\sinh^{-1}(b/2)}, \quad (22)$$

or differential capacitance

$$C_d^{dl} = \epsilon\epsilon_0 \kappa \sqrt{1 + b^2/4} \quad (23)$$

in series with an inner-layer parallel plate capacitor with capacitance (or differential capacitance),

$$C^{il} = C_d^{il} = \frac{2\epsilon\epsilon_0}{d}. \quad (24)$$

At contact,

$$g_i(d/2) = \exp[\beta z_i e \phi_{d/2}] = 1 + \frac{b^2}{2} - \frac{z_i}{z} b \sqrt{1 + \frac{b^2}{4}}, \quad (25)$$

so that $g_{\text{sum}}(d/2) = \frac{1}{2}[g_1(d/2) + g_2(d/2)]$ is, in the GCS theory, given by

$$g_{\text{sum}}(d/2) = 1 + \frac{b^2}{2}. \quad (26)$$

This is to be compared with the exact result (for the restricted PM) due to Henderson and Blum [9] and Henderson, Blum, and Lebowitz [10],

$$g_{\text{sum}}(d/2) = \frac{p}{\rho kT} + \frac{b^2}{2}, \quad (27)$$

where p is the osmotic pressure of the electrolyte. The second term in the above equation is just the Maxwell electrostatic stress. Thus, Eq. 27 is just a force balance condition where the momentum transfer to the electrode is equal to the sum of the osmotic term and the Maxwell stress. The GCS theory deals with the electrostatic term correctly but replaces the osmotic pressure with the ideal gas result $p = \rho kT$ because of the neglect of the ion diameters.

For comparison with the mean spherical approximation (MSA), which is a linear response theory that will be considered in the next section, it is worthwhile to give the linearized GCS theory results, obtained for the case of small electrode charge. In this case,

$$g_i(x) = \begin{cases} 0 & \text{for } x < d/2 \\ 1 - \beta z_i e \phi(x) & \text{for } x \geq d/2 \end{cases}, \quad (28)$$

or

$$g_i(x) = \begin{cases} 0 & \text{for } x < d/2 \\ 1 + \frac{\beta z_i e \sigma}{\epsilon\epsilon_0 \kappa} \exp(-\kappa y) & \text{for } x \geq d/2 \end{cases}. \quad (29)$$

The potential profile in the diffuse layer is given by

$$\phi(x) = \phi_{d/2} \exp(-\kappa y) \quad (30)$$

with $\phi_{d/2}$ given by

$$\phi_{d/2} = \frac{\sigma}{\epsilon\epsilon_0 \kappa}. \quad (31)$$

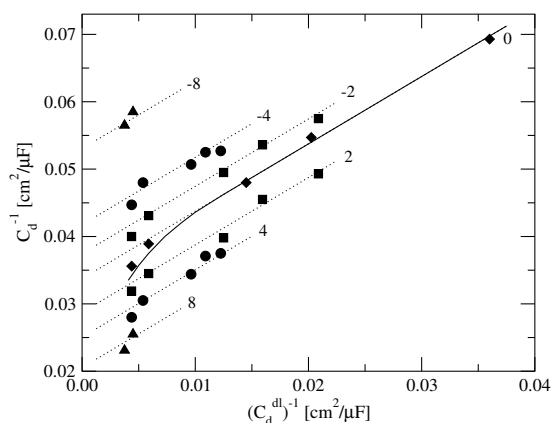


Figure 1: Experimental values of the inverse differential capacitance, C_d , of an aqueous solution of NaH_2PO_4 at 25°C near a hanging drop mercury electrode as a function of the inverse diffuse layer capacitance, C_d^{dl} , obtained from Eq. 23. The points are the experimental results of Parsons and Zobel. The light straight lines of unit slope give the results of the GCS theory but with the experimental inner layer capacitance obtained empirically. The numbers at the low concentration end of the lines give the electrode charges in units of μCcm^{-2} . The heavy solid curve gives the results of the MSA using a dipolar hard sphere model for the solvent together with an estimate of the contribution of the electronic structure of the electrode and is intended only as an aid to the eye. This figure has been reproduced, with permission, from Ref. [1].

The potential difference across the EDL is

$$V = \frac{\sigma d}{2\epsilon\epsilon_0} + \frac{\sigma}{\epsilon\epsilon_0\kappa} \quad (32)$$

and the capacitance (and differential capacitance) of the EDL is given by

$$\frac{1}{C} = \frac{d}{2\epsilon\epsilon_0} + \frac{1}{\epsilon\epsilon_0\kappa}. \quad (33)$$

In the GCS theory, in the limit of large κ (high concentration) or large b (high electrode charge), the diffuse layer capacitance is large and, as a result, the inner layer capacitance dominates, due to the reciprocal or series additivity of Eqs. 20 and 21. Hence, in the GCS theory, $C = 2\epsilon\epsilon_0/d$ is the limiting (maximum) value of C or C_d at large concentrations or large electrode charges. Further, the differential capacitance at low concentrations looks something like a parabola but flattens out at large σ . At high concentrations, the differential capacitance is constant. Any additional shape in the experimental differential capacitance is added by an empirical fit of the inner layer capacitance to the experimental results. However, the diffuse layer capacitance is presumed to be given adequately by the GCS theory.

Parsons and Zobel (PZ) [11] have plotted their experimental results for the *inverse* of the differential capacitance as a function of the *inverse* of the diffuse layer dif-

ferential capacitance, given by Eq. 23. Such a plot is often called a Parsons-Zobel plot. If the GCS theory were correct, this should result in a straight line. The extrapolation of the straight line to $1/C_d^{dl} = 0$ (high concentration and/or high electrode charge density) should, if the GCS theory were correct, yield the reciprocal of the inner layer capacitance. As is seen in Fig. 1, at first sight the experimental results of PZ (the points) do seem to follow a straight line and, conventionally, are presumed to provide an experimental verification of the GCS theory. In Fig. 1, the light straight lines are the GCS results. The solid curve is the result of the MSA that has not yet been discussed. For the moment the solid line can be considered to be an aid to the eye in following the trend of the experimental results. In the conventional GCS picture, the inner layer capacitance might not be given by Eq. 24 but might differ because of the presumed effect of the presence and nature of the solvent molecules and the electronic structure of the electrode that are beyond the GCS theory. Possible solvent effects might be a lower dielectric constant due to the alignment of the solvent molecules because of the strength of the electrode charge. The important point is that, in the GCS theory, such solvent effects are presumed to be confined only to the inner layer. The GCS theory is conventionally considered to provide an adequate description of the diffuse layer where the ions are present. Also, it is thought to provide a description of the EDL when combined with some treatment of the solvent molecules in the inner layer, or even an empirical fit. Indeed, the extrapolation of the straight lines to $1/C_d^{dl} = 0$ is one method of obtaining presumed “experimental” values of C_d^{il} .

However, a careful examination of the PZ experimental results in Fig. 1 indicates that the experimental differential capacitance does not follow Eq. 21 at high concentrations (the left side of the figure) but rises above the extrapolated intercept, possibly without limit. Until recently, most experimentalists have ignored this point and did not concern themselves with this issue because ions are not soluble in water when their concentration is large and it is difficult to obtain results with other solvents. Additionally, experimental results are difficult to obtain at high electrode charges for conventional electrolytes. However, as we shall see, DLs in ionic liquids can be formed at high concentrations and the deficiencies of the GCS theory become quite apparent.

Given that experiments on aqueous systems are difficult in regimes where problems with the GCS theory become apparent, it is useful to consider computer simulations. One simulation technique is the Monte Carlo (MC) method. Until recently, it has been the most common simulation tool in DL studies. In MC simulations the ions undergo a random walk and the profiles and other properties of interest are obtained by averages over this random walk. A simple random walk would take forever before useful results could be obtained. However, meaningful results can be obtained by means of a biased random walk that confines the ions to regions in which they

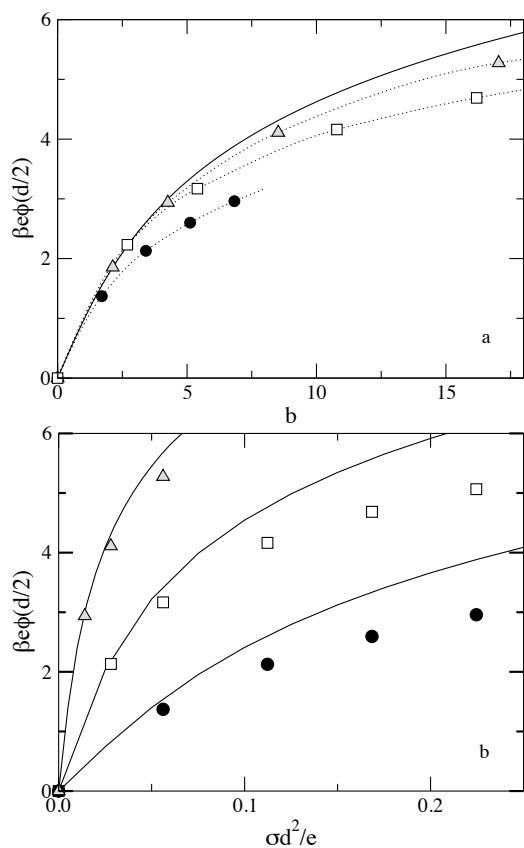


Figure 2: Diffuse layer potential of a 1:1 electrolyte ($d = 3 \text{ \AA}$) at room temperature as a function of b (part a) and σ (part b). The curves are, from top to bottom, for 0.01, 0.1, and 1 M solutions. The symbols give the simulation results. The solid curve in part a gives the GCS results. The dotted lines connect the MC results for easier visualization. The lines in part b give the GCS results. Part a is reproduced, with permission, from Ref. [1].

have a high probability of residing. The simulation cell consists of a parallelepiped with a charged wall (the electrode) at $x = 0$ and another wall (charged or uncharged) at $x = L$, where L is so large that the two walls do not interfere. Periodic boundary conditions are used in the other two directions. The size of the cell is chosen to be large enough that electrostatic screening eliminates the effects of the periodic image cells. The number of ions of each species is chosen so that the system is electroneutral. The first use of MC simulations for the study of the EDL was that of Torrie and Valleau [12, 13]. After their seminal studies, there was a hiatus in simulation studies of the EDL. However in recent years, there has been a renewed interest in simulations of the EDL that includes the work of Bhuiyan *et al.* [8], Boda *et al.* [14, 15], and Lamperski *et al.* [16, 17].

Another simulation technique is the molecular dynamics (MD) method in which the equations of motion are solved and the properties of the system of interest are obtained by averaging over the positions and velocities of the ions. A simulation cell that is similar to that used

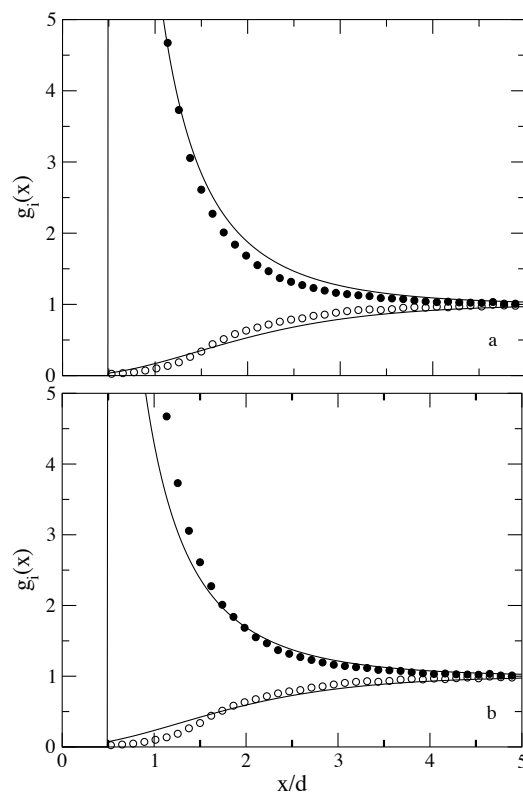


Figure 3: Normalized density profiles, $g_i(x)$, of a 1:1 electrolyte ($d = 3 \text{ \AA}$) at 1 M and room temperature for the state for which the MC values are $\sigma d^2/e = 0.1685$ and $\beta e \phi(d/2) = 2.6$. The points give the simulation results and the curves give the GCS results. The comparison is made at the same charge density (part a) and the same diffuse layer potential (part b).

in MC simulations is employed. In recent years, there has been an interest in MD simulations of the EDL, especially for ionic liquids. Some representative studies are those of Vatamanu *et al.* [18, 19], Hu *et al.* [20], and Feng [21] *et al.*.

A comparison with simulation gives an unambiguous test of the GCS theory since uncertainties resulting from empirical fits of the diffuse layer capacitance cannot arise. The GCS theory and simulations both use the same model and interaction parameters that are defined in Eqs. 1 and 2. Additionally, simulations and theory give results for the density profiles, $g_i(x)$, that cannot be obtained by present experimental methods. The simulations plotted in Figs. 2–5 are those of Boda *et al.* [22]. In Fig. 2a, the electrostatic potential $\beta e \phi(d/2)$ for a 1:1 electrolyte is plotted as a function of b for three concentrations (0.01M, 0.1M, and 1M). If the GCS theory were correct, these curves would be identical and independent of concentration. Hence, there can be only one GCS curve in Fig. 2a. As is seen, $\phi(d/2)$ as a function of b actually decreases with increasing concentration. In Fig. 2b, $\phi(d/2)$ is plotted as a function of $\sigma d^2/e$. The CGS curves are greater than the simulation results, espe-

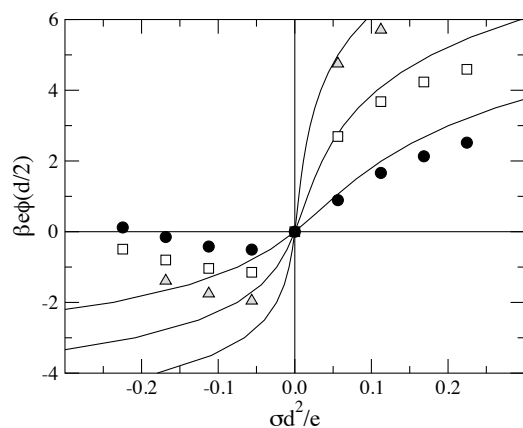


Figure 4: Diffuse layer potential of a 2:1 electrolyte ($d = 3 \text{ \AA}$) at room temperature as a function of σ . The curves are, from top to bottom, for 0.01, 0.1, and 1 M for positive σ and the reverse for negative σ . The symbols give the simulation results. The curves give the GCS results.

cially as the concentration increases. The density profiles for a 1:1 electrolyte are plotted in Fig. 3. The comparison is made at the same value of σ in part a and the same value of $\phi(d/2)$ in part b. In principle, there is no reason to choose whether the comparison should be made at the same σ , the same $\phi(d/2)$, or the same $\phi(0)$. It was natural for Torrie and Valleau to make their comparisons at the same σ because σ is the input variable in their method. However, ϕ is the natural variable in the GCS theory. In any case, the GCS theory looks best when σ is used as the input variable. Torrie and Valleau overstated things when they said that the GCS theory was reasonable for a 1:1 electrolyte. Their statement is most applicable if the comparison is made at the same value of σ . The value of the counterion profile would be in poor agreement at $x = d/2$ if $\phi(d/2)$ or $\phi(0)$ were used as the input variable. A similar comparison is made for a 2:1 electrolyte in Figs. 4 and 5. The agreement of the GCS theory with simulations is much poorer. The electrostatic interactions are stronger because of the presence of the divalent ions. When the divalent ions are the counterions, the potential, $\phi(d/2)$ has a maximum and then decreases with increasing electrode charge. This is not seen in the GCS results which are monotonic. Further, the simulation profiles are not monotonic whereas the GCS results are monotonic. The simulation profiles have oscillations. The EDL can consist of regions where counterions or coions predominate. When the coions predominate, this phenomenon is known as charge inversion. Of course, the net charge in the diffuse layer is still equal in magnitude, but opposite in sign, to that of the electrode charge. This is required to screen the electrode charge and potential far from the electrode.

Generally, experimentalists have been content to ignore the discrepancies in the results of the GCS theory and state that these differences are unimportant since they occur at high electrode charges or high concentrations

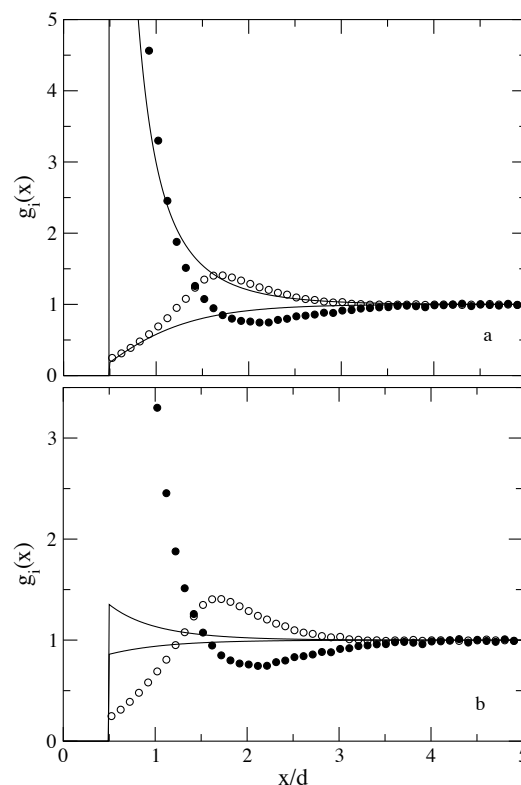


Figure 5: Normalized density profiles, $g_i(x)$ of a 2:1 electrolyte ($d = 3 \text{ \AA}$) at 1 M and room temperature for the state for which the MC values are $\sigma d^2/e = -0.1685$ and $\beta e \phi(d/2) = -0.15$. The points give the simulation results and curves give the GCS results. The comparison is made at the same charge density (part a) and the same diffuse layer potential (part b).

or for high valence electrolytes or nonaqueous systems, where experimental results are difficult to obtain. However, this is short-sighted. As scientists, one of our goals is to understand what is happening. This cannot be done with an inaccurate theory even with curve fitting. In the remainder of this article, attention is directed to more accurate, but still analytic, theories.

3. Mean spherical approximation

The mean spherical approximation (MSA) is a natural extension of the linearized GCS theory in which the size of the ions is taken into account. It was first applied to the EDL by Blum [23]. The GCS is usually obtained by means of the solution of a differential equation whereas the MSA is obtained from the solution of an integral equation. At first sight, the connection between the GCS and MSA theories is unclear. However, Henderson and Blum [24] demonstrated that the GCS theory could also be obtained from an integral equation. In fact, the linearized GCS integral equation is just the MSA integral equation with the effect of ion size ignored. Actually, Henderson and Blum proved a more general result. They showed that the GCS theory followed from the

hypernetted-chain approximation (HNCA) when ion size was neglected. The MSA can be regarded as a linearized version of the HNCA and, because of this, the stated relation of the linearized GCS theory to the MSA follows. In this article, the HNCA is not considered because it does not yield analytic results and has severe problems when σ is large [25]. Also, the emphasis in this article is upon analytic, or at least explicit, results that can be valuable in practical calculations.

The MSA result that is analogous to Eq. 29 is

$$g_i(x) = \begin{cases} 0 & \text{for } x < d/2 \\ g_0(x) - \frac{\beta z_i e \sigma}{\epsilon \epsilon_0 \kappa} f(y) & \text{for } x \geq d/2 \end{cases}, \quad (34)$$

where $g_0(x)$ is the Percus-Yevick (PY) profile for hard spheres near a hard surface. Earlier, Henderson, Abraham, and Barker (HAB) [26] obtained an integral equation for $g_0(x)$. The second term gives the electrostatic part of the profile for charged hard spheres near a charged hard surface. Blum [23] did not obtain a result for $f(y)$ but he did obtain an analytic result for the Laplace transform of $f(y)$,

$$\int_0^\infty \exp(-sy) f(y) dy = \frac{s}{s^2 + 2(\Gamma\sigma)s + 2(\Gamma\sigma)^2(1 - \exp[-s])}, \quad (35)$$

where 2Γ is a renormalized screening parameter that is related to κ by $\kappa = 2\Gamma(1 + \Gamma\sigma)$ or $2\Gamma\sigma = \sqrt{1 + 2\kappa\sigma} - 1$. Note that for small κ (small concentrations), $2\Gamma\sigma = \kappa\sigma - (\kappa\sigma)^2/2 + \dots$. Thus, the MSA screening parameter is smaller than the GCS screening parameter. This suggests that the MSA EDL is wider than that of the GCS theory. This agrees with the simulation results. The notation of Blum has been followed. However, it might have been preferable if he had incorporated the factor of 2 into the definition of Γ so that Γ became κ at low concentrations.

Note that at low concentrations, the Laplace transform of $f(y)$ becomes $1/s(1 + \kappa s)$. This means that

$$f(y) = \exp(-\kappa y), \quad (36)$$

in the limit of low concentrations. Also, $g_0(x) = 1$ in this limit. Thus, at low concentrations, the MSA becomes the GCS theory. Blum did not invert the Laplace transform of $f(y)$. However, he did obtain the contact value of $f(y)$ by examining the Laplace transform of $f(y)$ at large s . He showed that $f(0) = 1$. Using the earlier result of HAB for $g_0(d/2)$, the contact value of $g_i(x)$ is

$$g_i(d/2) = \frac{1 + 2\eta}{(1 - \eta)^2} - \frac{\beta z_i e \sigma}{\epsilon \epsilon_0}, \quad (37)$$

where $\eta = \pi\rho d^3/6$. The MSA contact value is an improvement over the GCS result that contains only the ideal gas term. However, the osmotic pressure should have both a hard sphere term and an electrostatic term. Additionally, the hard sphere term is accurate only for low values of ρ .

Equation 37 does not contain the quadratic term b^2 of Eq. 27. This is because the MSA is a linearized theory. A better expression for the osmotic term is

$$\frac{p}{\rho kT} = \frac{1 + \eta + \eta^2 - \eta^3}{(1 - \eta)^3} - \frac{\Gamma^3}{3\pi\rho}, \quad (38)$$

where Γ is the renormalized screening parameter that has been defined above. This result is obtained from the application of the MSA to bulk electrolytes. The MSA, as is the case for most theories, is not fully self-consistent. Henderson *et al.* [27] have compared this expression with their simulations (see their Fig. 1) and found it to be very accurate. Despite these problems, the MSA contact value given in Eq. 37 does represent an advance.

By expansion of the Laplace transform of $f(y)$, it is easy to show that the MSA EDL satisfies electroneutrality. That is, the charge in the EDL is equal in magnitude, but opposite in sign, to the electrode charge. Again, by expanding the Laplace transform, the MSA expressions for the total and diffuse layer potentials of the EDL are found to be

$$V = \frac{\sigma}{\epsilon \epsilon_0 (2\Gamma)} \quad (39)$$

and

$$\phi_{d/2} = \frac{\sigma}{\epsilon \epsilon_0 \kappa} [1 - (\Gamma d)^2]. \quad (40)$$

Thus, in the MSA, the capacitance (and differential capacitance) of the EDL is

$$\frac{1}{C} = \frac{1}{\epsilon \epsilon_0 (2\Gamma)}. \quad (41)$$

Expanding the expression that defines Γ ,

$$2\Gamma = \kappa - \kappa^2 d/2 + \kappa^3 d^2/2 + \dots \quad (42)$$

Therefore,

$$\frac{1}{C} = \frac{1}{\epsilon \epsilon_0 \kappa} + \frac{d}{2\epsilon \epsilon_0} - \frac{\kappa d^2}{4\epsilon \epsilon_0} + \dots \quad (43)$$

The MSA capacitance does not reach a maximum at $2\epsilon\epsilon_0/d$ but continues to increase, as is indicated in Fig. 1. The MSA (solid) curve in Fig. 1 was not calculated from Eq. 41 but from a more sophisticated version of the MSA, that is not discussed in detail here, which includes the contribution resulting from explicit solvent molecules and the electronic structure of the metal [28–30]. However, the results of Eq. 41 are qualitatively similar to the more sophisticated results. In this paper, the solid curve serves to guide the eye. The inner layer capacitance continues to be $2\epsilon\epsilon_0/d$ but it is simply the electrode charge divided by potential difference across the inner layer and not a ‘catch all’ for the deficiencies of the GCS theory. The diffuse capacitance is the electrode charge divided by the potential difference from the distance of closest approach to the bulk electrolyte and contains correction terms to the GCS theory. This is the reverse of the usual interpretation of the GCS theory where the GCS expressions are assumed to be accurate for the diffuse layer

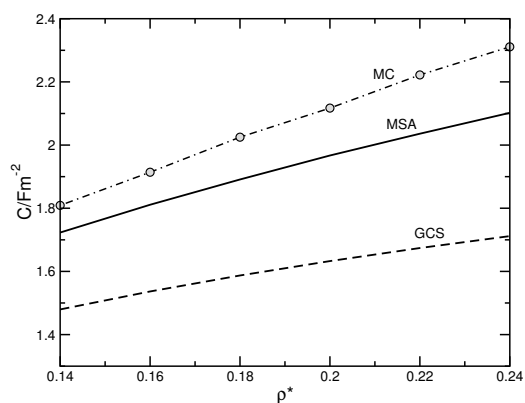


Figure 6: Double layer capacitance, C , as a function of the reduced density, $\rho^* = \rho d^3$, at the reduced temperature $T^* = 0.08$. The circles are the MC data of Henderson *et al.* [27] and the lines are the MSA and GCS results. The line through the circles is given as a guide to the eye. Because the MSA is a linearized theory, the MC, MSA, and GCS capacitances are for $\sigma = 0$.

capacitance and everything else is ‘lumped’ into the inner layer capacitance. In the more sophisticated version MSA, the contributions due to the solvent molecules appear in both the diffuse and inner layer potentials. The solvent molecule profile is as diffuse as that of the ions. The effect of the molecular nature of the solvent is not confined to the inner layer.

The initial slope of the $\phi(d/2)$ vs. σ curves in Figs. 2 and 4 is just the inverse of the diffuse portion of the capacitance. It is seen that the initial slope of the MC curves is well described by the GCS theory at low concentrations but increasingly falls below the GCS initial slope (the inverse of the differential capacitance) with increasing concentration as was seen in the experimental results in Fig. 1. Henderson *et al.* [27] compared the GCS and MSA differential capacitances with their simulation results for a broad range of densities and at a temperature that was meant to be qualitatively representative of an ionic liquid. As is seen in Figs. 6 and 7, the MSA results are considerably improved over the GCS results. The comparison with the MC results is made for a small value of σ because the MSA is a linearized theory that is applicable only for small σ .

Although an analytic expression for $f(y)$ is not available, Henderson and Smith [31] were able to obtain a zonal expansion for $f(y)$. They showed that

$$f(x) = \sum_{n=1}^{\infty} f_n(z)u(z), \quad (44)$$

where $z = t - n + 1$, $t = x/d$, $u(z)$ is the Heaviside step function that is zero for $z < 0$ and one for $z \geq 0$ and

$$f_n(z) = \exp(-\mu) \frac{\mu^n}{(n-1)!} [j_{n-2}(\mu) - j_{n-1}(\mu)] \quad (45)$$

with $\mu = (\Gamma d)z$. The function $j_m(\mu)$ is the spherical

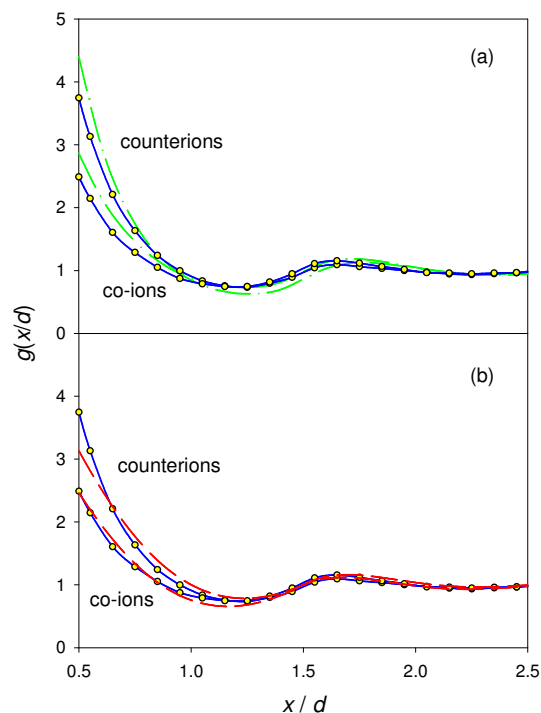


Figure 7: The electrode-ion normalized density profiles, $g_i(x/d)$, at the reduced density $\rho^* = \rho d^3 = 0.5$ for the reduced temperature $T^* = 0.8$ and surface charge density, $\sigma = 0.05 \text{ C/m}^2$, is small enough that the MSA is applicable. The circles are the MC results of Henderson *et al.* [26] and the dashed line gives the MSA result. The line through the circles is given as a guide to the eye. This figure is reproduced, with permission, from Ref. [26].

Bessel function that is easily calculated using the recurrence formula for this function. Hundreds of $j_m(\mu)$ can be calculated without difficulty, even with a laptop computer.

Henderson and Smith [31] also obtained a zonal expansion for $g_0(x)$. Their result is

$$g_0(x) = \sum_{n=1}^{\infty} g_0^n(z)u(z), \quad (46)$$

where z is again given by $z = t - n + 1$ with $t = x/d$. The expressions for the $g_0^n(x)$ are rather complex. However, Henderson and Smith gave results for $n \leq 5$. The formulae for $g_0(x)$ and $f(x)$ are not quite analytic since they involve infinite series. However, these results are explicit and easily used. Fortran programs to obtain $g_0(x)$ and $f(x)$ are given in Supplementary Material. Note that the program for $g_0(x)$ consists of two parts. One part calculates those parameters that depend only on the state of the electrolyte and the other subroutine in each code calculates profiles for a given x . The user should resist the temptation to combine the two parts into one. McQuarrie [32] did this in an appendix to his excellent book and produced an inefficient, and probably incorrect, code that he referred to as ‘Henderson’s code’. Fortunately, his code

is illegible in the later printing of his book. If the reader does combine the codes, the reader is on his/her own and should not refer to the combined, or otherwise modified, code as ‘Henderson’s code’.

The functions $g_0(x)$ and $f(x)$ are oscillatory, in accord with the simulations. They are improvements, qualitative and quantitative, to the monotonic functions of the GCS theory.

4. A useful hybrid description

As has been mentioned, the deficiencies of the GCS theory could, until recently, be dismissed as appearing mainly under conditions that are of limited experimental interest. However, there has been considerable recent interest in EDLs formed by ionic liquids. Ionic liquids can be thought of as room-temperature molten salts. Because there is no solvent, the ions do not become insoluble in some solvent and experimental results can be obtained at high concentrations. The fact that they exist at room temperature is a great experimental convenience. Kornyshev [33] has drawn attention to these electrochemical systems and aptly suggested that they provide a paradigm change in electrochemistry. He modestly ends the title of his important paper with a question mark. An exclamation mark might have been more appropriate. As well as exposing the deficiencies of the GCS theory, EDLs in ionic liquids are important in green technologies, the design of novel energy storage devices, such as high-tech batteries and super-capacitors [34]. Ionic liquid DLs have attracted recent experimental [35, 36] and theoretical interest [18–21, 37–39]. The differential capacitance, as determined by MC simulations, of a simple model [38] of an ionic salt in which $T^* = 0.8$ and $d = 8 \text{ \AA}$ is given in Fig. 8 for $\rho^* = 0.04, 0.14$ and 0.24 . At low concentrations, the differential capacitance is parabolic-like, as the GCS theory suggests. However, C_d does not become flat at large electrode charges. At higher concentrations, C_d at small electrode charges continues to increase with increasing concentration. This has been seen in Fig. 6. At high electrode charges, the capacitance decreases. The nature of this decrease seems to be independent of the concentration. This is similar to the GCS theory except that the capacitance is not flat at high electrode charges but decreases. The decrease is due to the fact that the ions are not point charges but occupy space and cannot sit on top of each other. The diffuse layer must become thicker and the capacitance decreases as the electrode charge increases. This is not because the distance of closest approach of the ions increases. Strong secondary peaks in the counterion profile appear [37]. The beginnings of this trend were first observed by Torrie and Valleau [12] and seem to be quite universal.

The GCS theory satisfies Eq. 27 at high electrode charges but fails at low electrode charges whereas the MSA gives reasonable results at small electrode charges. This implies that a repair of the GCS so that it gives the MSA results in the regime of the low electrode charges

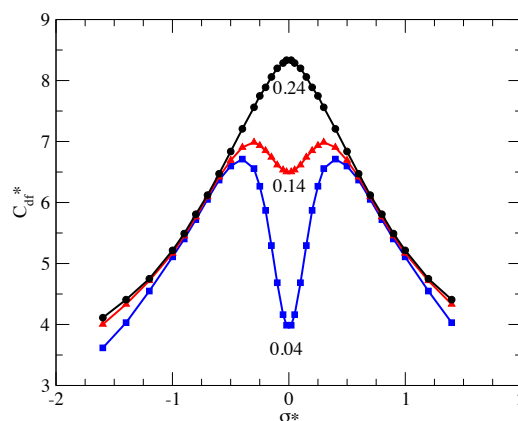


Figure 8: Differential capacitance, $C_{df}^* = C_d d / 4\pi\epsilon_0$, obtained from MC simulation for the EDL of a model ionic liquid with $d = 4 \text{ \AA}$ and $T^* = 0.8$. The curves are, from bottom to top, for $\rho^* = 0.04, 0.14$, and 0.24 . This figure has been reproduced, with permission, from Ref. [40].

but leaves the high electrode charge part unchanged might be useful. Likely, there is no way to accomplish this in a fundamental way. Additionally, there are probably several semi-empirical ways in which this could be done. Henderson and Lamperski [40] have presented one procedure. Because it is not based on any fundamental ideas, it is not a theory. It would be more appropriate to refer to their procedure as a description. They proposed that the differential capacitance for a symmetric salt could usefully be written as

$$\frac{1}{C_d} = \frac{d'}{2\epsilon\epsilon_0} + \frac{d'}{2\epsilon\epsilon_0\sqrt{1+b^2/4}} \left(\frac{1}{\Gamma d'} - 1 \right). \quad (47)$$

The parameter d' is an adjustable parameter and represents the effective thickness of the diffuse layer. At small b (small electrode charge), Eq. 47 yields

$$\frac{1}{C_d} = \frac{1}{2\Gamma\epsilon\epsilon_0}, \quad (48)$$

which is the MSA result. At large b (large electrode charge), Eq. 47 yields

$$\frac{1}{C_d} = \frac{d'}{2\epsilon\epsilon_0}. \quad (49)$$

The results of Eq. 47, using $d' = 2d$ for the system that Lamperski *et al.* simulated, were given by Henderson and Lamperski. Qualitatively, the results are very similar to the simulation results shown in Fig. 8. Better agreement could be obtained by making d' increase with electrode charge. Figure 2 of Henderson and Lamperski suggests that C_d is proportional to $1/\sigma^*$ at large σ^* (electrode charge) with the proportionality constant being independent of concentration. This behavior was first predicted by Kornyshev [33] on the basis of a lattice theory and seems to be universal. As well as the simulations of Henderson and Lamperski, it has been seen experimentally

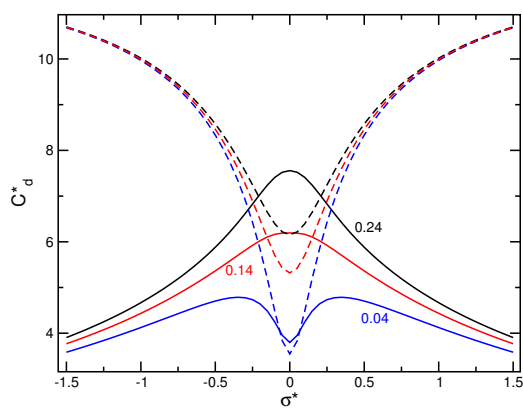


Figure 9: Differential capacitance, $C_d^* = C_d d / 4\pi\epsilon_0$, obtained from the hybrid description of the EDL of a model ionic liquid with $d = 4 \text{ \AA}$ and $T^* = 0.8$. The curves are, from bottom to top, for $\rho^* = 0.04, 0.14$, and 0.24 . The solid and broken curves give the results of the hybrid approach and GCS theory, respectively.

by Islam *et al.* [35]. Something of the nature of

$$d' = d_1 + d_2|\sigma^*| \quad (50)$$

would give the desired decrease of C_d at large σ^* . Equation 50 is sensible because it is consistent with the diffuse layer becoming thicker as the electrode charge increases. The results of this ansatz with $d_1 = 2d$ and $d_2 = d$ are given in Fig. 9. The results are similar to the simulation results in Fig. 8. This hybrid approach is capable of yielding a capacitance with a double hump at low concentrations and a single hump at high concentrations. This behavior is predicted by simulations and all the good theories of the DL of ionic liquids.

A hybrid treatment of the profiles, $g_i(x)$, is possible. One could start with the MSA expression for $g_i(x)$ and add to this $g_i^{\text{GCS}}(x; b) - g_i^{\text{GCS}}(x; b = 0)$. However, it must be realized that the MSA expressions for the profiles are less accurate than the MSA expressions for the potential and capacitance. The potential and capacitance are integrals and tend to average out any inaccuracies in the profiles.

5. Conclusion

The study of the electric DL is an important application of statistical mechanics that is of experimental and applied interest. The GCS theory is popular with experimentalists because it is intuitively simple and easy to use in the routine analysis of experiments. However, the GCS theory has deficiencies. Its use leads to the idea that any problems with the GCS theory can be ‘swept under the carpet’ by placing all of these problems into an empirical treatment of the inner layer. In reality, the deficiencies of the GCS theory lie with the GCS treatment of the diffuse layer. Admittedly, it is difficult to observe this in aqueous systems. However, it is not impossible.

The departure from linearity in the Parsons-Zobel plot (Fig. 1) is real and should not be ignored. The important field of ionic liquid electrochemistry requires something more adequate than the GCS theory. The best theories of the EDL are the modified Poisson-Boltzmann theory [41] and the density functional theory [42]. However, both theories are numerical and require an iterative numerical solution of a fairly large set of equations and may not be appealing in an experimental analysis. A hybrid description, such as that explored here, preserves the advantage of an analytic treatment of the capacitance and is no more cumbersome than the GCS theory.

Supplementary Information

Fortran programs to calculate $g_0(x)$ and $f(x-d/2)$ using MSA. The codes can be downloaded free of charge from <http://tinyurl.com/hjic-2015-0010-suppl>.

Acknowledgement

Professor Dezső Boda assisted with the preparation of this paper. Professor Lutful Bari Bhuiyan read the manuscript prior to submission and suggested several important modifications. The author is grateful to both colleagues for their continuing wise advice.

REFERENCES

- [1] Henderson, D., Boda, D.: Insights from theory and simulation on the electrical double layer, *Phys. Chem. Chem. Phys.*, 2009 **11**(20), 3822–3830 10.1039/b815946g
- [2] Cherstvy, A.G.: Electrostatic interactions in biological DNA-related systems, *Phys. Chem. Chem. Phys.*, 2011 **13**, 9942–9968 10.1039/C0CP02796K
- [3] Merlet, C., Rotenberg, B., Madden, P.A., Salanne, M.: Computer simulations of ionic liquids at electrochemical interfaces, *Phys. Chem. Chem. Phys.*, 2013 **15**, 15781–15792 10.1039/c3cp52088a
- [4] Boda, D., Gillespie, D.: Calculating the electrostatic potential profiles of double layers from simulation ion density profiles, *Hung. J. Ind. Chem.*, 2013 **41**(2), 125–132 ISSN: 0133-0276
- [5] Gouy, G.: Sur la constitution de la charge électrique à la surface d’un électrolyte, *J. de Phys.*, 1910 **9**(1), 457–468 10.1051/jphys:019100090045700
- [6] Chapman, D.L.: A contribution to the theory of electrocapillarity, *Phil. Mag. Ser. 6*, 1913 **25**(148), 475–481 10.1080/14786440408634187
- [7] Stern, O.: Zur Theorie der elektrolytischen Doppelschicht, *Zeit. Elektrochem.*, 1924 **30**(21–22), 508–516
- [8] Bhuiyan, L.B., Outhwaite, C.W., Henderson, D.: Some simulation and modified Poisson-Boltzmann theory results for the contact values of an electrolyte near a charged electrode, *J. Electroanal. Chem.*, 2007 **607**(1–2), 54–60 10.1016/j.jelechem.2006.10.010

- [9] Henderson, D., Blum, L.: Some exact results and the application of the mean spherical approximation to charged hard spheres near a charged hard wall, *J. Chem. Phys.*, 1978 **69**(12), 5441–5449 10.1063/1.436535
- [10] Henderson, D., Blum, L., Lebowitz, J.L.: Exact formula for the contact value of the density profile of a system of charged hard-spheres near a charged wall, *J. Electroanal. Chem.*, 1979 **102**(3), 315–319 10.1016/S0022-0728(79)80459-3
- [11] Parsons, R., Zobel, F.: The interphase between mercury and aqueous sodium dihydrogen phosphate, *J. Electroanal. Chem.*, 1965 **9**(5–6), 333–348 10.1016/0022-0728(65)85029-X
- [12] Torrie, G.M., Valleau, J.P.: Electrical double-layers 1. Monte Carlo study of a uniformly charged surface, *J. Chem. Phys.*, 1980 **73**(11), 5807–5816 10.1063/1.440065
- [13] Torrie, G.M., Valleau, J.P.: Electrical double-layers 4. Limitations of the Gouy-Chapman theory, *J. Phys. Chem.*, 1982 **86**(16), 3251–3257 10.1021/j100213a035
- [14] Boda, D., Henderson, D., Chan, K.Y.: Monte Carlo study of the capacitance of the double layer in a model molten salt, *J. Chem. Phys.*, 1999 **110**(11), 5346–5350 10.1063/1.478429
- [15] Boda, D., Henderson, D., Chan, K.Y., Wasan, D.T.: Low temperature anomalies in the properties of the electrochemical interface, *Chem. Phys. Lett.*, 1999 **308**(5–6), 473–478 10.1016/S0009-2614(99)00643-0
- [16] Lamperski, S., Outhwaite, C.W.: Exclusion volume term in the inhomogeneous Poisson–Boltzmann theory for high surface charge, *Langmuir*, 2002 **18**(9), 3423–3424 10.1021/la011852v
- [17] Lamperski, S., Bhuiyan, L.B.: Counterion layering at high surface charge in an electric double layer. Effect of local concentration approximation, *J. Electroanal. Chem.*, 2003 **540**, 79–87 10.1016/S0022-0728(02)01278-0
- [18] Vatamanu, J., Borodin, O., Smith, G.D.: Molecular insights into the potential and temperature dependences of the differential capacitance of a room-temperature ionic liquid at graphite electrodes, *J. Am. Chem. Soc.*, 2010 **132**(42), 14825–14833 10.1021/ja104273r
- [19] Vatamanu, J., Borodin, O., Bedrov, D., Smith, G.D.: Molecular dynamics simulation study of the interfacial structure and differential capacitance of Alkylimidazolium Bis(trifluoromethanesulfonyl)imide [Cnmim][TFSI] ionic liquids at graphite electrodes, *J. Phys. Chem. C*, 2012 **116**(14), 7940–7951 10.1021/jp301399b
- [20] Hu, Z., Vatamanu, J., Borodin, O., Bedrov, D.: A molecular dynamics simulation study of the electric double layer and capacitance of [BMIM][PF₆] and [BMIM][BF₄] room temperature ionic liquids near charged surfaces, *Phys. Chem. Chem. Phys.*, 2013 **15**(34), 14234–14247 10.1039/c3cp51218e
- [21] Feng, G., Jiang, D., Cummings, P.T.: Curvature effect on the capacitance of electric double layers at ionic liquid/anion-like carbon interfaces, *J. Chem. Theor. Comp.*, 2012 **8**(3), 1058–1063 10.1021/ct200914j
- [22] Boda, D., Fawcett, W.R., Henderson, D., Sokołowski, S.: Monte Carlo, density functional theory, and Poisson-Boltzmann theory study of the structure of an electrolyte near an electrode, *J. Chem. Phys.*, 2002 **116**(16), 7170–7176 10.1063/1.1464826
- [23] Blum, L.: Theory of electrified interfaces, *J. Phys. Chem.*, 1977 **81**(2), 136–147 10.1021/j100517a009
- [24] Henderson, D., Blum, L.: The Gouy-Chapman theory as a special case of the hypernetted chain approximation, *J. Electroanal. Chem.*, 1978 **93**(2), 151–154 10.1016/S0022-0728(78)80228-9
- [25] Woelki, S., Henderson, D.: Application of the SRISM approach to the study of the capacitance of the double layer of a high density primitive model electrolyte, *Cond. Matt. Phys.*, 2011 **14**(4), 43801 10.5488/CMP.14.43801
- [26] Henderson, D., Abraham, F.F., Barker, J.A.: The Ornstein-Zernike equation for a fluid in contact with a surface, *Mol. Phys.*, 1976 **31**(4), 1291–1295 10.1080/00268977600101021
- [27] Henderson, D., Lamperski, S., Outhwaite, C.W., Bhuiyan, L.B.: A mean spherical approximation study of the capacitance of an electric double layer formed by a high density electrolyte, *Coll. Czechoslovak Chem. Comm.*, 2010 **75**(3), 303–312 10.1135/cccc2009094
- [28] Carnie, S.L., Chan, D.Y.C.: The structure of electrolytes at charged surfaces: Ion–dipole mixtures, *J. Chem. Phys.*, 1980 **73**(6), 2949–2957 10.1063/1.440468
- [29] Blum, L., Henderson, D.: Mixtures of hard ions and dipoles against a charged wall - the Ornstein-Zernike equation, some exact results, and the mean spherical approximation, *J. Chem. Phys.*, 1981 **74**(3), 1902–1910 10.1063/1.441282
- [30] Schmickler, W., Henderson, D.: The interphase between jellium and a hard sphere electrolyte. A model for the electric double layer, *J. Chem. Phys.*, 1984 **80**(7), 3381–3386 10.1063/1.447092
- [31] Henderson, D., Smith, W.R.: Exact analytical formulas for the distribution functions of charged hard spheres in the mean spherical approximation, *J. Stat. Phys.*, 1978 **19**(2), 191–200 10.1007/BF01012511
- [32] McQuarrie, D.A.: Statistical mechanics (University Science Books, Mill Valley), 2000 ISBN-13: 978-1891389153
- [33] Kornyshev, A.A.: Double-Layer in Ionic Liquids: Paradigm Change?, *J. Phys. Chem. B*, 2007 **111**(20), 5545–5557 10.1021/jp067857o
- [34] Winter, M., Brodd, R.J.: What Are Batteries, Fuel Cells, and Supercapacitors?, *Chem. Rev.*, 2004 **104**(10), 4245–4270 10.1021/cr020730k

- [35] Islam, M.M., Alam, M.T., Ohsaka, T.: Electrical double-layer structure in ionic liquids: A corroboration of the theoretical model by experimental results, *J. Phys. Chem. C*, 2008 **112**(42), 16568–16574 10.1021/jp8058849
- [36] Lockett, V., Horne, M., Sedev, R., Rodopoulos, T., Ralston, J.: Differential capacitance of the double layer at the electrode/ionic liquids interface, *Phys. Chem. Chem. Phys.*, 2010 **12**(39), 12499–12512 10.1039/C0CP00170H
- [37] Wu, J., Jiang, T., Jiang, D., Jin, Z., Henderson, D.: A classical density functional theory for interfacial layering of ionic liquids, *Soft Matter*, 2011 **7**(23), 11222–11231 10.1039/c1sm06089a
- [38] Lamperski, S., Henderson, D.: Simulation study of capacitance of the electrical double layer of an electrolyte near a highly charged electrode, *Mol. Sim.*, 2011 **37**(4), 264–268 10.1080/08927022.2010.501973
- [39] Lamperski, S., Sosnowska, J., Bhuiyan, L.B., Henderson, D.: Size asymmetric hard spheres as a convenient model for the capacitance of the electrical double layer of an ionic liquid, *J. Chem. Phys.*, 2014 **140**(1), 014704 10.1063/1.4851456
- [40] Henderson, D., Lamperski, S.: Simple Description of the Capacitance of the Double Layer of a High Concentration Electrolyte, *J. Chem. Eng. Data*, 2011 **56**(4), 1204–1208 10.1021/je101106z
- [41] Outhwaite, C.W., Bhuiyan, L.B.: An improved modified Poisson-Boltzmann equation in electric-double-layer theory, *J. Chem. Soc. Faraday. Trans. II.*, 1983 **79**, 707–718 10.1039/F29837900707
- [42] Jiang, J., Cao, D., Henderson, D., Wu, J.: A contact-corrected density functional theory for electrolytes at an interface, *Phys. Chem. Chem. Phys.*, 2014 **16**(9), 3934–3938 10.1039/C3CP55130J

COMPARISON OF TWO VARIABLE INTERPOLATION METHODS FOR PREDICTING THE VAPOUR PRESSURE OF AQUEOUS GLYCEROL SOLUTIONS

ISTVÁN SZALKAI,^{1*} ATTILA SEBESTYÉN,^{2,†} BIANCAMARIA DELLA-VECCHIA,³ TAMÁS KRISTÓF,⁴ LÁSZLÓ KÓTAI,⁵ AND FERENC BÓDI⁶

¹ Department of Mathematics, University of Pannonia, Veszprém, 8201, HUNGARY

² Department of Inorganic Chemistry, University of Pannonia, Veszprém, 8201, HUNGARY

³ Dipartimento di Matematica, Istituto G. Castelnuovo, Università degli Studi di Roma 'La Sapienza', Rome, 00185, ITALY

⁴ Department of Physical Chemistry, University of Pannonia, Veszprém, 8201, HUNGARY

⁵ Institute of Materials and Environmental Chemistry, Research Centre for Natural Sciences, Hungarian Academy of Sciences, PO Box 17, Budapest, 1525, HUNGARY

⁶ Faculty of Engineering, University of Pannonia, Veszprém, 8201, HUNGARY

Several general mathematical methods for approximating two variable functions are applied for the study of the relationships between the temperature, concentration, and vapour pressure of aqueous glycerol solutions. The general properties of each of the applied methods are discussed in respect of possible alternative applications.

Keywords: vapour-pressure approximation, splines, glycerol, aqueous solutions, multi-dimensional interpolation

1. Introduction

Recently, the evaporation of aqueous solutions with low glycerol concentrations from the combined processes of ion-exchange and chemisorption of diluted solutions is preferred instead of the expensive purification of concentrated glycerol solutions. These processes are important in the cosmetic industry [1–3]. During the atmospheric evaporation of highly concentrated glycerol solutions, glycerol molecules condense by losing water and convert into acrolein or polyglycerols. Thus, the control of the appropriate temperature and pressure limits is of great importance in industrial processes.

In the present work, mathematical relationships with regard to concentration, vapour pressure, boiling point, and temperature data are studied for aqueous glycerol solutions. The possibilities for data interpolation using several two variable spline-interpolation methods are investigated with the aim of calculating low pressure evaporation conditions and upper temperature limits for aqueous glycerol solutions with given concentrations as a continuation of our previous work [4, 5].

2. Data and Methods

We use the data shown in *Table 1* that were taken from Ref. [6]. The dataset is graphically presented in *Fig. 1*. Approximating a two valued function means that we are given the measured values $z_{i,j} \in \mathbb{R}$ at the measured points $P_{i,j} = (x_i, y_j)$ for $1 < i < M$, $1 < j < N$ and we want to construct a smooth function $S: \mathbb{R}^2 \rightarrow \mathbb{R}$ such that $S(x_i, y_j) = z_{i,j}$ for $1 < i < M$, $1 < j < N$. In the present paper we considered the following general approximation methods:

- iterated one-dimensional (1D) cubic splines [8],
- Hermite type, two-dimensional (2D) interpolation, improved by Lénárd in three versions [10–12], and
- Shepard's generalised method for a scattered dataset with certain parameters in two versions [15, 17].

These methods are general approximation methods that are applicable not only to the present problem. When discussing the errors in computer outputs, we differentiate between general mathematical and chemical (material) specific reasons.

In order to test the practical applicability of these methods we used every second column of the original dataset (*Table 1*, pressures of 5.3, 20.2, ..., 101.3 kPa) as inputs, then we computed the approximations for the omitted columns, and finally we compared the computed values to the measured data from *Table 1* in the omitted columns (13.3, 26.6, ..., 93.3). These

*Correspondence: szalkai@almos.uni-pannon.hu

†Deceased in 2001.

Table 1. The measured boiling points (in °C) of aqueous glycerol solutions as a function of pressure (kPa) and concentration (mass percent, g g⁻¹) as in Table 44 of Ref. [6].

conc.	pressure														
	5.3	13.3	20.2	26.6	33.3	39.9	46.6	53.3	59.9	66.6	73.3	79.9	86.6	93.3	101.3
0%	34.0	51.6	60.1	66.4	71.6	75.9	79.6	82.9	85.9	88.7	91.2	93.5	95.7	97.7	100.0
10%	34.4	52.1	60.7	67.0	72.3	76.6	80.3	83.7	86.7	89.5	92.0	94.3	96.6	98.6	100.9
20%	34.9	52.7	61.3	67.7	73.0	77.3	81.1	84.4	87.5	90.3	92.9	95.2	97.4	99.5	101.8
30%	35.5	53.4	62.1	68.6	73.8	78.2	82.0	85.3	88.4	91.3	93.8	96.2	98.4	100.4	102.8
40%	36.5	54.4	63.1	69.5	74.9	79.3	83.1	86.4	89.5	92.4	95.0	97.3	99.6	101.7	104.0
50%	37.5	55.7	64.5	71.1	76.4	80.9	84.8	88.2	91.3	94.2	96.8	99.2	101.5	103.6	106.0
60%	39.5	58.0	66.9	73.5	79.0	83.5	87.4	90.9	94.1	97.0	99.7	102.1	104.4	106.0	109.0
70%	43.0	61.7	70.8	77.6	83.1	87.7	91.7	95.2	98.4	101.4	104.1	106.6	109.0	111.1	113.6
80%	49.1	68.2	77.4	84.3	90.0	94.6	98.7	102.3	105.6	108.7	111.4	113.9	116.3	118.5	121.0
90%	59.5	80.2	90.3	97.7	103.9	109.1	113.5	117.4	121.0	124.4	127.4	130.2	132.8	135.2	138.0

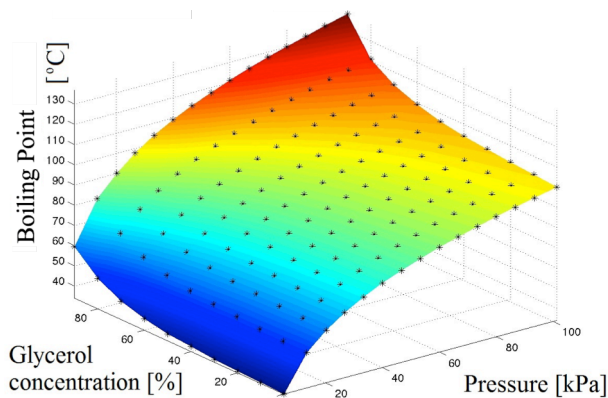


Figure 1. The original dataset from Table 1.

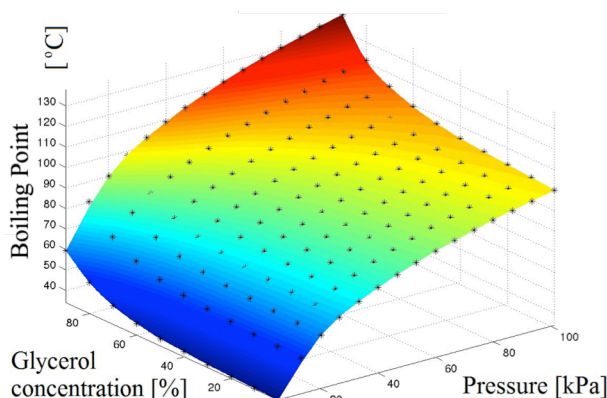


Figure 2. Estimated boiling points from iterated 1D splines.

approximations and comparisons are shown in Table S1 (not included in the paper due to its size) and are graphically summarised in Figs.2–6.

We did not consider specific semi-empirical relationships such as those in Ref. [7]:

$$\ln(p) = A(c) \cdot t^{a(c)},$$

where p , c , and t stand for pressure (MPa), concentration (%), and temperature (°C), respectively.

2.1. Iterated One-Dimensional Interpolations

In Refs. [8] and [9], one finds the well-known method of two variable spline interpolations, which repeatedly uses 1D spline interpolations. The details can be found in Ref. [2] as well. This method requires that the domain of the function we are approximating is rectangular $[a, b] \times [c, d]$. Furthermore, the measured points $P_{i,j}$ lie on lines ℓ_j parallel to the ordinate axis for $1 < j < N$. For calculating $S(x, y)$ at each inner point $(x, y) \in [a, b] \times [c, d]$ we follow a two-step calculation. First, we use 1D splines s_j in each horizontal line ℓ_j to compute the values $\ell_j(x, y_j) = s_j(x)$ for $1 < j < N$. Next, we use another 1D spline along the vertical line crossing the point (x, y) . Then, we calculate the value $S(x, y)$ using the numbers $\ell_j(x, y_j)$ for $1 < j < N$ and a 1D spline on them. In practice we can compute all the formulae of the splines s_j in advance, so later the values of $s_j(x)$ can be obtained by an easy substitution. In our computations, we used cubic splines as described in

Refs. [2], [8] and [9]. The approximating function $S(x, y)$ for our glycerol data is plotted in Fig.2, detailed numeric values can be found in Table S1. The similarity between Figs.1 and 2 shows the small error of iterated 1D spline interpolation, while magnification can reveal some differences.

The advantages of this method include that the 1D approximation is widely known, no equidistance tabulated (measured) points y_j or x_i are needed, and only the parallel lines ℓ_j are assumed. The method also gives an approximation at the margins of the closed rectangle $[a, b] \times [c, d]$ and it can be easily generalised for higher dimensions.

A disadvantage of this method is the repeated use of the final spline approximation (“vertical step”) for getting $S(x, y)$ at each point (x, y) , which makes the computation slightly slower. We repeatedly have to build up and solve a tridiagonal $N \times N$ size system of linear equations.

2.2. Direct Two-Dimensional Interpolations

In Ref. [10], one can find simple, but general direct 2D methods for constructing directly a 2D spline interpolation of minimal degree of Hermite type, invented by Lénárd. She investigated 2D and higher dimensional methods as discussed also in Refs. [2], [11], and [12]. This method requires that the dataset (measured data points) form a rectangular grid, i.e. each quadruple of

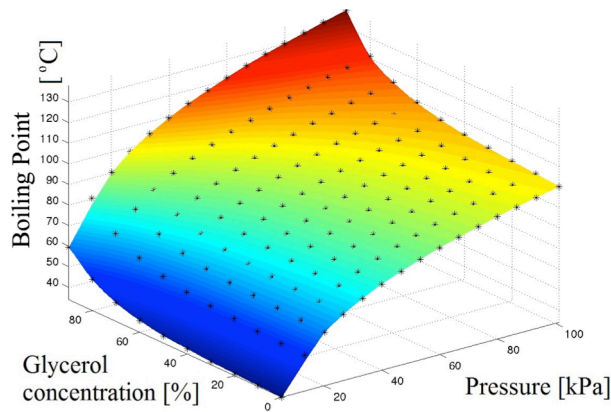


Figure 3. Estimated boiling points from Lénárd’s Hermite-type interpolation.

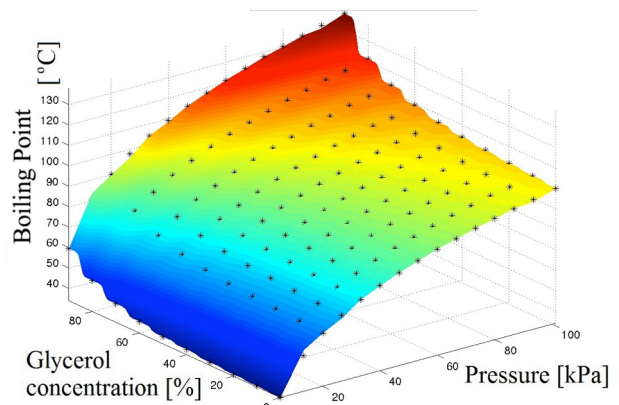


Figure 4. Estimated boiling points from Shepard’s method.

$$\{ (x_i, y_j), (x_{i+1}, y_j), (x_i, y_{j+1}), (x_{i+1}, y_{j+1}) \} \quad (1)$$

forms a rectangle, but not necessarily of the same size. Ref. [11] requires equidistant grids. The problem associated with this is discussed in Ref. [2]. The method we currently use is from Ref. [10] that gives us separate formulae for each rectangle in Eq.(1) as

$$S(x, y) = S_{i,j}(x, y) \text{ if } (x, y) \in [x_i, x_{i+1}] \times [y_j, y_{j+1}] \quad (2)$$

such that finally

- a) S is twice continuously partially differentiable in both variables on its whole domain $[a, b] \times [c, d]$,
- b) $S_{i,j}$ values are polynomials in both variables of minimal degree and their degrees, as two variable polynomials, are minimal, too.

Moreover, Lénárd provided three different formulae for points a) and b) with the details described in Eqs.(1,3), (2,3), and (3,3) of Ref. [10]. The implementation of each of these three methods with numeric values can be found in Table S1. The differences among the approximated results using these methods are not so significant, so we present here the plot only for the results of the first method in Fig.3. The similarity between Figs.1 and 3 shows the small error of Lénárd’s Hermite-type interpolation.

An advantage of this method is that although the precomputation of the higher dimensional arrays takes some time, $S(x, y)$ can then be computed as a polynomial at any point (x, y) , making the computation fast. Furthermore, the method can be easily generalised for higher dimensions as described in Ref. [12].

One disadvantage of this method is that we ultimately need rectangular tabulated, measured data points, $P_{i,j} = (x_i, y_j)$. If required, the data points can be transformed to form an equidistant grid, i.e. the rectangles in Eq.(1) would become congruent as in Ref.[2], for example. Furthermore, the method gives no approximation at certain margins of the rectangle $[a, b] \times [c, d]$, since we cannot compute the finite partial differences of higher order at the margins.

2.3. Shepard’s Method

In Ref.[13], Shepard presented a more general method for continuous approximation in any dimension as was also discussed in Refs. [14–17]. This method does not require any special assumption on the positions of the data points $P_{i,j} \in \mathbb{R}^n$ as it works for arbitrary distribution as well. This method can be introduced as follows:

Let the arbitrary measured data points

$$P_1, P_2, \dots, P_M \in \mathbb{R}^n$$

and the corresponding values

$$F_1, F_2, \dots, F_M \in \mathbb{R}$$

be given. Then the formula for each $P \in \mathbb{R}^n$

$$U(P) = \frac{\sum_{i=1}^M F_i \cdot \sigma(d(P, P_i))}{\sum_{i=1}^M \sigma(d(P, P_i))} \quad (3)$$

gives a continuous and exact approximation:

$$U(P_i) = F_i \text{ for any } i \leq M \quad (4)$$

where $d(P, P_i)$ is the Euclidean distance of the points P and P_i and the positive “weight function” $\sigma: \mathbb{R} \rightarrow \mathbb{R}^+$ satisfies

$$\lim_{d \rightarrow 0^+} \sigma(d) = +\infty \text{ and } \lim_{d \rightarrow +\infty} \sigma(d) = 0^+ \quad (5)$$

In other words, $U(P)$ is a weighted arithmetic mean of the measured values F_i with weights, which are “inverses” of the distances of points P_i from point P . The closer P_i is to P , the greater weight F has in Eq.(3).

Theoretical and practical considerations in Refs. [15] and [17] suggest σ to be chosen as

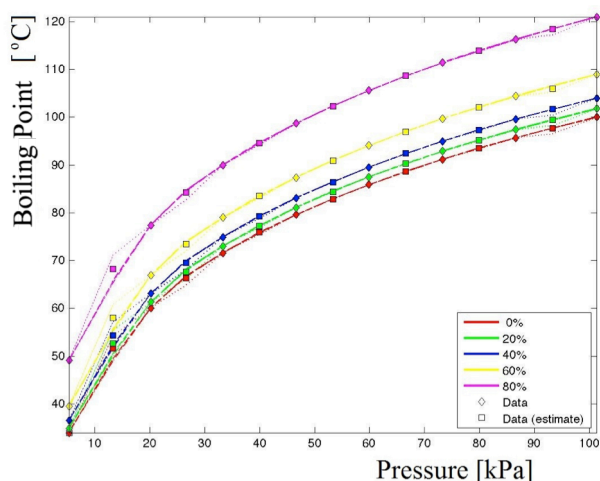


Figure 5. Boiling point dependence on glycerol concentration as a function of vapour pressure.

$$\sigma(d) = d^{-\alpha} \cdot e^{-\lambda d} \quad (6)$$

for some "appropriate" α , $\lambda \geq 1$, usually $1 \leq \alpha$, $\lambda \leq 2$ are satisfactory in practice. This problem is discussed in detail in Refs. [14–17]. In our present calculations, we used the values $\alpha = \lambda = 1$. The approximating function $U(P)$ of Shepard's method is shown in Fig.4, detailed numeric values can be found in Table S1. It is worth noting that the wave-like patterns on the surface in Fig.4 show the unique property of Shepard's interpolation (see References [15] and [17] for details).

The main advantage of Shepard's method is the simplicity of Eq.(3), which makes both theoretical investigations and practical computations easy. Furthermore, the measured points $P_1, P_2, \dots, P_M \in \mathbb{R}^n$ can be chosen totally arbitrarily, which may be of great assistance during measurements.

However, an important disadvantage of this method is that σ and thus U are sensitive to the measurement units, MPa or kPa in our case. Though U is always continuous and Eq.(4) is valid for any σ , which satisfies Eq.(5), the "shape" of U is the best when the distribution of the data points P_i is "nearly" uniform in a region of \mathbb{R}^n (see Ref. [17]). To improve our approximation we used data expressed in kPa in Table 1.

Moreover, larger data sets slow down the processing of Eq.(3) greatly, even when $M \approx 150$ the computational time can be several minutes. A workaround for managing this problem is to deal only with the data points P_i closest to P . In our example with aqueous glycerol solutions, we used 4×4 matrices of data points againsts pressure and concentration, respectively, surrounding the requested approximated point. This approximation greatly speeded up the execution times. The continuity property of U in this variant is discussed in Refs. [15] and [16].

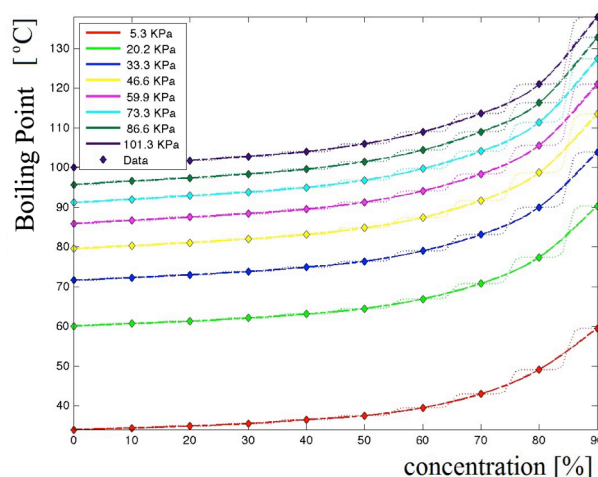


Figure 6. Boiling point dependence on glycerol vapour pressure as a function of concentration.

3. Discussion

For an alternative comparison of the methods considered in this paper, we present Figs.5 and 6. In Fig.5, we displayed the boiling points for different fixed concentrations. In Fig.6, the pressure is examined. Iterated 1D splines are the dashed-dotted lines, Lénárd's Hermite-type 2D spline is the dashed line, and Shepard's method is shown in dotted lines. As can be seen, Lénárd's and iterated splines are practically undistinguishable. It seems that Shepard's method works less well than the other two methods. We can see this from the 3D plot (Fig.4) with the effect of the flattening being evident. Also it is evident from the 2D plot (Fig.6) with constant concentration, where estimation in the middle (supposed missing) points is poor (plotted as squares). The flattening effect is again evident from the 2D plot (Fig.5) with constant pressure.

4. Conclusion

We conclude that although Shepard's method represented by Eqs.(3) and (4) is an easy approximating method for the measured data, it is extremely sensitive for the large and small distances among the data points. For data sets situated in a rectangular grid (as in Table 1), spline methods are more accurate.

SYMBOLS

$\tilde{z}_{i,j}$	measured values in 2D
F_i	measured values in 'n'-dimension
$P_{i,j}$	measured points in 2D
P_i	measured points in 'n'-dimension
S	approximating function in 2D
U	approximating function in 'n'-dimension
σ	weight function in Shepard's method

Acknowledgement

The research is supported by the European Union and co-funded by the European Social Fund, "Telemedicine-focused research activities in the field of Mathematics, Informatics and Medical Sciences", project number: TÁMOP-4.2.2.A-11/1/KONV-2012-0073.

Supporting Information

Table S1 can be downloaded free of charge from math.uni-pannon.hu/~szalkai/HJIC-16-Table2-150110.xls.

REFERENCES

- [1] Isahak, W.N.R.W.; Ramli, Z.A.C.; Ismail, M.; Jahim, J.M.; Yarmo, M.A.: Recovery and purification of crude glycerol from vegetable oil trans-esterification, *Sep. Purif. Rev.*, 2015, **44**(3), 250–267 DOI:10.1080/15422119.2013.851696
- [2] Ardi, M.S.; Aroua, M.K.; Hashim, N.A.: Progress, prospect and challenges in glycerol purification process: A review, *Renewable Sustainable Ene. Rev.*, 2015, **42**, 1164–1173 DOI: 10.1016/j.rser.2014.10.091
- [3] Hunsom, M.; Autthanit, C.: Adsorptive purification of crude glycerol by sewage sludge-derived activated carbon prepared by chemical activation with H_3PO_4 , K_2CO_3 and KOH, *Chem. Eng. J.*, 2013, **229**, 334–343 DOI: 10.1016/j.cej.2013.05.120
- [4] Szalkai, I.; Sebestyén, A.; Kótai, L.; Bódi, F.: Comparison of interpolation methods for predicting the vapour pressure of aqueous glycerol solutions, *Proc. 42nd Annual Conf. Canadian Soc. Chem. Engng.*, Toronto, Canada, 1992, pp. 279–280 math.uni-pannon.hu/~szalkai/Szalkai-1992c-konfTor.pdf
- [5] Szalkai, I.; Sebestyén, A.; Kótai, L.; Bódi, F.: Comparison of interpolation methods for predicting the vapour pressure of aqueous glycerol solutions, Preprint No. 036 (University of Veszprém, Veszprém, Hungary) 1995 math.uni-pannon.hu/~szalkai/Szalkai-1995Preprint-Glic.pdf
- [6] Kiss B.: Plants oil industry and household tables (Mezőgazdasági Kiadó, Budapest, Hungary) 1988 (in Hungarian)
- [7] Saburov, A.G.; Vasiliene, I.M.; Postolov, J.M.; Klibov, N.P.: Numerical formulae for thermodynamic properties of aqueous glycerol solutions, *Mashlo-Khim. Promisl.*, 1987, 21–22 (in Russian)
- [8] Djuric, M.; Ranogajec, J.; Marinkov-Neducin, R.: Predicting of floor tiles behaviour by using two-dimensional spline interpolation, *Hung. J. Ind. Chem.*, 1992, **20**(1), 39–44
- [9] Press, W.H.; Flannery, B.P.; Teukolsky, B.P.; Vetterling, W.T.: Numerical recipes - The art of scientific computing (Cambridge Univ. Press, Cambridge, UK) 1985
- [10] Lénárd M.: On the two-dimensional spline interpolation of Hermite-type, *Colloquia Math. Soc. J. Bolyai*, 1985, **49**, 531–541
- [11] Lénárd M.: Spline interpolation in two variables, *Studia Sci. Math. Hung.*, 1985, **20**, 145–154
- [12] Lénárd M.: On an N-dimensional quadratic spline approximation, *J. Approx. Theory*, 1992, **68**(2), 113–135 DOI: 10.1016/0021-9045(92)90088-6
- [13] Shepard D.: A two dimensional interpolation function for irregularly spaced data, *Proc. 23rd ACM Nat. Conf.*, New York, NY, USA, 1968, pp. 517–524 DOI: 10.1145/800186.810616
- [14] Gordon, W.J.; Wixon J.A.: Shepard's method of "Metric Interpolation" to bivariate and multivariate interpolation, *Math. Comp.*, 1978, **32**(141), 253–264 DOI: 10.1090/S0025-5718-1978-0458027-6
- [15] Szalkai I.: Scattered data interpolation via improved Shepard's method, Preprint No. 76. (University of Veszprém, Veszprém, Hungary) 1999 math.uni-pannon.hu/~szalkai/Szalkai-1999Preprint-Shepard.pdf
- [16] Allasia G.: A class of interpolating positive linear operators: theoretical and computational aspects, in *Approximation Theory, Wavelets and Approximation*, (Ed.: Singh S.P., Kluwer Publ., Dordrecht, The Netherlands) 1995, pp. 1–36 DOI: 10.1007/978-94-015-8577-4
- [17] Della-Vecchia, B.; Szalkai I.: Finding better weight functions for generalised Shepard's operator on infinite intervals, *Int. J. Comp. Math.*, 2011, **88**(13), 2838–2851 DOI: 10.1080/00207160.2011.559542



Degree programmes in English at the Faculty of Engineering

Graduate Programmes

MSc in Environmental Engineering

Duration: 4 semesters

Number of credits: 120

Tuition fee: 4500 USD/semester

Head of the programme: Dr Endre Domokos, Institute of Environmental Engineering

Contact: domokose@uni-pannon.hu

MSc in Environmental Sciences

Duration: 4 semesters

Number of credits: 120

Tuition fee: 4500 USD/semester

Head of the programme: Prof. Judit Padisak, Institute of Environmental Sciences

Contact: padisak@almos.uni-pannon.hu

BSc and MSc in Chemical Engineering

Duration: BSc 7 semesters, MSc 4 semesters

Number of credits: BSc: 210 credits MSc: 120 credit

Tuition fee: 4500 USD/semester

Head of the programme: Dr Sandor Nemeth, Institute of Chemical and Process Engineering

Contact: nemeth@fmt.uni-pannon.hu

Postgraduate Programmes

Hydrocarbon Technology Development Engineer

Duration: 2 semesters

Number of credits: 60

Tuition fee: 2000 USD/semester

Head of the programme: Dr Zoltan Varga, Institute of Chemical and Process Engineering

Contact: vargaz@almos.uni-pannon.hu

Water and Wastewater Treatment System Operation

Duration: 2 semesters

Number of credits: 60

Tuition fee: 2000 USD/semester

Head of the programme: Dr Rita Szakacsne-Foldes, Institute of Environmental Sciences

Contact: foldenyi@almos.uni-pannon.hu



COMPARISON OF DECONTAMINATION STANDARDS

LE CONG HAO,¹ MAI DINH THUY,² DO TRUNG HIEU,³ AND ZOLTÁN SAS^{4*}

¹ Nuclear Techniques Laboratory, University of Science, VNU-HCMC, Ho Chi Minh City, VIETNAM

² School of Nuclear Engineering and Environmental Physics, Hanoi University of Science and Technology, Ho Chi Minh City, VIETNAM

³ Faculty of Chemistry, University of Science, VNU, Ho Chi Minh City, VIETNAM

⁴ Institute of Radiochemistry and Radioecology, University of Pannonia, Veszprém, H-8201, HUNGARY

The quality of materials used in nuclear-related facilities is critical, especially the ease of decontamination of different paints and coatings. Standards describe different testing methods for classification. Nevertheless, compliance with these standards cannot be carried out negligibly from a safety point of view. In this study, a withdrawn Hungarian (MSZ-05 22.7662-83), an international ISO (ISO 8690:1988), and Russian (GOST 25146-82) decontamination standard were compared. Four different paints were tested as part of this survey. The ease of decontamination varied mainly from poor to fair levels in the case of the Hungarian standard, while the ISO standard exhibited very good level. In the case of the Russian standard, only a theoretical comparison was carried out. Based on the results, it was found that a special epoxy-based coating can be recommended for isotope laboratories due to being the best material from an ease of decontamination point of view. From comparison of the standards considered here, it was found that the application of ISO standard is significantly faster and simpler than the withdrawn Hungarian standard. However, in the case of the Hungarian standard the data described the ease of decontamination in more details. The use of water or some other cleaning agents can be effective to remove ¹³⁷Cs and ⁶⁰Co contamination right after early identification. Isotope ¹³⁷Cs and ⁶⁰Co contamination of a surface can be cleaned quickly and effectively using distilled water for the ¹³⁷Cs isotope removal from the surfaces being several times easier than that of ⁶⁰Co.

Keywords: surface contamination, decontamination value, ISO standard 8690:1988, Hungarian standard MSZ-05 22.7662-83, Russian standard GOST 25146-82, ⁶⁰Co isotope, ¹³⁷Cs isotope

1. Introduction

Contamination of surfaces with radionuclides can lead to human exposure depending on the type, extent of contamination, and activity of the contaminating isotope. In order to reduce the risk, quick and effective decontamination of the involved area is required. The contamination of different surfaces are common in workplaces that deal with radionuclides e.g. isotope laboratories, nuclear industry related activities, etc.[1,2]. Contamination can occur in various ways, but chemical and physical adsorption processes are the most important ones. In the case of chemical adsorption, ions exit from the hydration shell and bind directly to the surface, while in the case of physical adsorption the ions binds to the surface together with the hydration shell. Furthermore, the contaminating isotopes can infiltrate into the pores of the surface material *via* diffusion. To avoid the internal contamination of porous materials special paints and coatings should be applied which inhibits the diffusion of contaminating isotopes into

pores [3]. The decontamination capacity of surfaces greatly depends on the form of contamination media and the chemical and physical parameters of surfaces. The main influencing parameters that can affect the ease of decontamination are i) surface porosity, ii) surface roughness, iii) surface wettability, iv) chemical reactions between the radionuclide and the surface, and v) adsorption processes on the outer part of the electric double layer of the solid/liquid interface.

The efficiency of decontamination expressed by the decontamination factor (*DF*) [3] can be calculated according to the following equation:

$$DF = \frac{\text{Activity of surface after contamination}}{\text{Activity of surface after decontamination}} \quad (1)$$

However, the decontamination efficiency is greatly parameter dependent as mentioned above. Standardised protocols are necessary to classify certain paints and coatings from a decontamination point of view, which is informative about their utilisation in isotope laboratories and other relevant workplaces as well.

In this study, the comparison of different decontamination standards is presented that includes a Hungarian (withdrawn in 2003) standard MSZ-05 22.7662-83 “*Testing of painted coatings in laboratory.*

*Correspondence: ilozas@almos.uni-pannon.hu

Table 1. Properties of the coatings investigated.

ID	coating type	paint	colour	roughness
DC	base-modified silicone resin	spray	grey (Fig.1A)	slight
CV	alkyd resin	spray painted	dark grey (Fig.1B)	great
KM	enamel paint	brush painted	brown (Fig.1C)	glossy
NR	epoxy resin	brush painted	beige (Fig.1D)	semi-glossy

Determination for ease of decontamination”[3], an international ISO 8690:1988 standard “Decontamination of radioactively contaminated surfaces – Method for testing and assessing the ease of decontamination” [4], and a Russian interstate standard GOST 25146-82 “Radiochemical production and atomic power plant materials. Method for determination of decontamination ratio” [5].

2. Experimental

2.1. Sample Preparation

In order to compare the three selected standards, four different types of coatings were used for providing various conditions during the survey. The relevant properties of the applied coatings are shown in Table 1.

The selected coatings were painted on 4×4 cm aluminium test disks (Fig.1) and stored for 24 hours to dry completely. The selected standards require 5 parallel measurements for each type of coating.

2.2. Comparison of Contamination Processes

In the case of the Russian GOST 25146–82 standard, the investigated surfaces are contaminated by natural or artificial β -radiating nuclides. The activity of the samples was distributed on the surface to avoid self-absorption. The GOST standard describes in great detail the measurement conditions and apparatus, which should be enforced to ensure reliable results. The same standard allows for using any types of contamination solution, which provides numerous ways for measuring the ease of decontamination under a wide variety of conditions, while in the case of the ISO and MSZ standards specific conditions have to be maintained. In the case of the withdrawn Hungarian MSZ-05 22.7662-83 and ISO 8690:1988 standards the recommended contaminating isotopes are ^{137}Cs and ^{60}Co (carrier concentration $10^{-5} \text{ mol dm}^{-3}$ and pH value of 4) which were prepared in a laboratory before testing.

To determine the count rate of the contaminating isotopes a γ -spectrometer was used with a high purity germanium (HPGe) semiconductor detector ORTEC GMX40-76, with 40% efficiency. To obtain counts from ^{137}Cs , the 661.6 keV γ -line was measured, while in the case of ^{60}Co , the 1173.4 and 1332.5 keV lines were

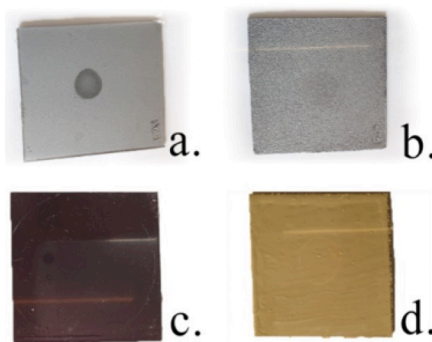


Figure 1. Applied coatings on test disks.

measured. The spectra were recorded by an ORTEC DSPEC LF 8196 MCA instrument. Before contamination the background spectra were recorded, which were extracted from all contaminated and decontaminated spectra.

2.3. Hungarian Standard MSZ-05 22.7662-83

For the Hungarian standard, the decontamination was investigated in two differentiated ways to obtain relevant information related to physical and chemical links adsorption separately. To investigate the physical adsorption, 0.1 cm^3 of contamination solution was dropped onto test samples and dried under an infrared lamp at 40°C . After drying, the count rates were measured using a HPGe detector for 1000 s to obtain the specific count rate of the contamination solution. To investigate chemical origin contamination, a special socketed cylinder-shaped contamination block (Fig.2) was used with 0.565 cm^3 of the contamination solution, which provides a 10 cm^2 contact surface between the solution and test specimens. The contamination block was put onto coated test specimens and filled with the contamination solution for 2 hours. After that period, the contamination solution was removed from the contamination block and the test specimens were gently flushed using ultrapure water.

2.4. ISO Standard 8690:1988

For the ISO standard, only chemical adsorption was investigated. The specific count rate of the contamination solution was determined before contamination of the test specimens. A micropipette was used to put 0.1 cm^3 of contamination solution onto glass sheets. The test specimens were inserted between the upper and lower parts of the contamination block for contamination, which was prepared according to the ISO standard (Fig.3).

Before filling the upper part with 1 cm^3 of contamination solution both parts were fastened together tightly to avoid leakage. After filling the holder, disks were covered to avoid evaporation of the contamination solution for 2 hours. After this contamination process, the contamination solution was pumped out of the holder, and the test specimens inserted into the decontamination unit.

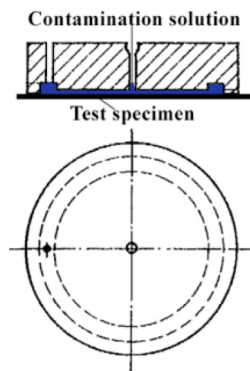


Figure 2. Scheme of the contamination block according to the withdrawn Hungarian MSZ-05 22.7662-8 standard.

2.5. Decontamination Process

In the case of the Hungarian standard, an immersion-based decontamination method was used over three steps. Firstly, upon the completion of count rate measurements, the contaminated surfaces were immersed in ultrapure water for 10 s then pulled out and tilted to allow the residual fluid to trickle down before finally being immersed again in the decontamination solution. The immersion was repeated 15 times (total immersion time: 150 s). Thereafter, the test specimens were dried under an infrared lamp and the count rate originating from the residual contaminating isotopes recorded using a γ -ray spectrometer.

In the second step, a special decontamination solution was prepared according to the method described as a standard in order to get information about the decontamination efficiency of detergents. The decontamination solution was composed of polyethylene glycol nonylphenyl ether (5 g dm^{-3}), citric acid (4 g cm^{-3}), and EDTA (4 g cm^{-3}). The test specimens were added to the decontamination cocktail and decontaminated using the same immersion/pull out technique described in the first step. The count rate was measured again after drying. For the final step 1 M HCl was used to get information about more aggressive decontamination fluids, which can cause structural changes in the case of the investigated coating but can also be beneficial from a decontamination point of view to remove isotopes from pores also. The decontamination and the measurement process were repeated for each specimen after the acidic decontamination step.

In the case of the ISO standard, the test specimens were placed immediately into a special cage-stirrer apparatus (described in the standard) after the contamination process. The apparatus was equipped with a 100 rpm motor. The cage was immersed into a glass beaker filled with ultrapure water and rotated for 150 s. Thereafter, the specimens were dried and measured using γ -ray spectrometry to obtain residual count rates. The details of the MSZ-05 22.7662-83 and ISO 8690:1988 decontamination methods are summarised in Table 2.

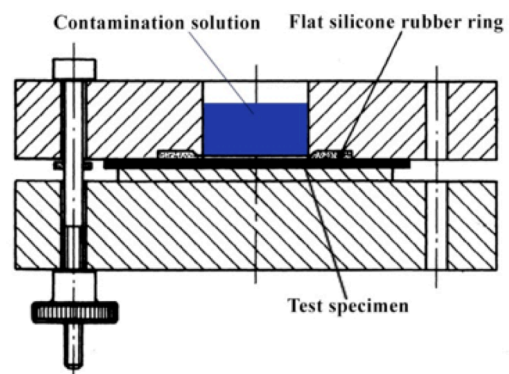


Figure 3. Scheme of the contamination block according to the ISO 8690:1988 standard.

Table 2. Results of decontamination experiments performed in this study.

standards	steps	method	agents
MSZ-05 22.7662-83	3	immersed for 150 s	ultrapure water
MSZ-05 22.7662-83		then	decontamination solution
adsorption		pulled out	1 M HCl
ISO 8690:1988	1	immersed stirring cage in ultrapure water for 150 s	

2.6. Calculation of DF Values and Classification of Specimens

The decontamination factors were calculated from recorded spectra. The peak areas corresponding to the presence of ^{137}Cs and ^{60}Co isotopes were corrected by background measurements. The specific count rates (count-per-second cm^{-3}) were calculated for all samples. The decontamination factors of each step for all samples were calculated using the Eq.(1).

3. Results and Discussion

3.1. Decontamination Factors from the Hungarian Standard MSZ-05 22.7662-83

The obtained decontamination factor of each treated surface on the basis of the Hungarian standard is shown in Fig.4, which compares the physical adsorption between the contaminating isotopes and surfaces.

The decontamination factors varied from 2.0 to 196.3 for ^{137}Cs and from 1.0 to 30.1 for ^{60}Co . The largest variation between the two isotopes was observed for the NR sample, which is an epoxy-based laboratory coating. Most of the decontaminated isotopes were removed independently from applied decontamination solutions, while the decontamination of CV-coated (strongly rough alkyd resin) samples seemed unaffected by treatment using any of the solutions. The decontamination of other surface materials was less

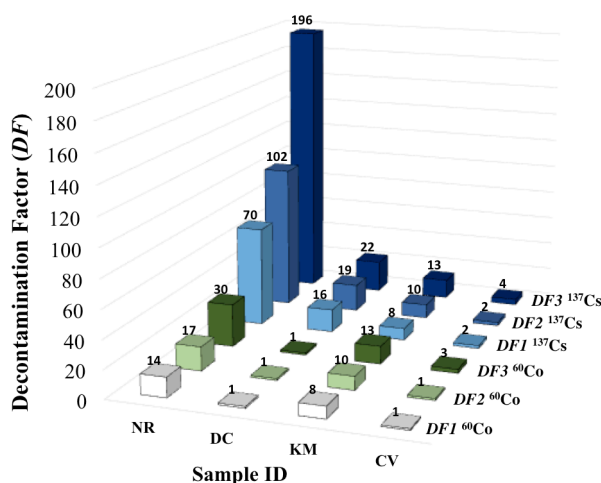


Figure 4. Decontamination factors for MSZ-05 22.7662-83 (Table 2) after drying.

effective than that of the NRs. In the case of KM (glossy enamel paint), the decontamination factor was fair for both isotopes. The results for all materials suggest that decontamination efficiency may be independent of the number of attempts, but dependent on the characteristics of the contamination and features of the surface and contaminant media. In all cases, it seemed that the HCl solution improved the efficiency of decontamination for both ¹³⁷Cs and ⁶⁰Co. Nevertheless, it is notable that distilled water is also a good nominated agent for the decontamination of less specific radioactive cleaning agents.

Table 3 presents the assessment of ease of decontamination using 0.1 cm³ of contamination solution. The ease of decontamination was found to vary from poor to fair for DC, KM and CV. An acceptable level of efficiency was found for NR.

Chemical adsorption was investigated by another decontamination experiment using 0.565 cm³ of contamination solution. Similar results (Fig.5) were observed when compared with the drying method (Fig.4). The decontamination factor using distilled water was found to be approximately the same as for the applied cocktail solution. Similar phenomena were reported by Ruhman *et al.* [1]. The reason for unacceptable efficiencies in the case of samples with CV coatings can be explained by the roughness of the surface, which allows contamination of inner pores due to diffusion, hence the surface becomes very difficult to clean. Surface degradation due to the porosity of the material or by some unknown chemical modification might be another reason. A recommended area for further study is the ease of decontamination in the light of surface changes after years of use [1].

The ease of decontamination was found to vary from poor for CV to fair for DC and KM as shown in Table 4. An acceptable efficacy was found for NR. The ease of decontamination varied from excellent for KM to good for DC and NR. A poor/bad level was found for CV.

Table 3. Assessment of ease of decontamination using 0.1 cm³ of contaminated solution.

samples	isotopes	DF	degree of ease
DC	¹³⁷ Cs	22.5	fair
	⁶⁰ Co	1.5	poor/bad
KM	¹³⁷ Cs	13.4	fair
	⁶⁰ Co	12.6	fair
CV	¹³⁷ Cs	4.0	poor/bad
	⁶⁰ Co	2.7	poor/bad
NR	¹³⁷ Cs	196.3	good
	⁶⁰ Co	30.1	fair

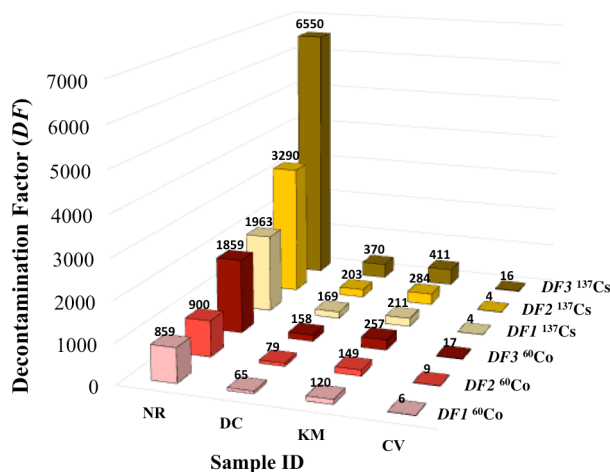


Figure 5. Decontamination factors for MSZ-05 22.7662-83 using the adsorption method (Table 2).

3.2. Decontamination Factors from the ISO Standard 8690:1988

The decontamination factors using the ISO standard method are illustrated in Fig.6. The values clearly show that in the case of epoxy-based NR resin the ease of decontamination was efficient. In the case of the KM coating, the efficiency was the highest. The worst decontamination capability was found for CV-coated samples. The results using the ISO standard clearly show that the ease of decontamination greatly depends on the types of coating. Furthermore, the ¹³⁷Cs isotope can be removed more easily than the ⁶⁰Co isotope, which can be explained by the different physical/chemical properties of investigated isotopes. The obtained decontamination factors for each isotope are summarised in Table 5.

Depending on available conditions, the task and specific conditions, the Hungarian standard method and the ISO standard will be chosen, while the Russian standard was studied only for the sake of comparison. It is important to mention that simulation exercises, for both major and minor contamination events, may be essential for coordination and execution of a response [6–12].

Table 4. Assessment of ease of decontamination in the case of the adsorption method.

samples	isotopes	DF	degree of ease
DC	^{137}Cs	370	fair
	^{60}Co	158	fair
KM	^{137}Cs	411	fair
	^{60}Co	257	fair
CV	^{137}Cs	16	poor/bad
	^{60}Co	17	poor/bad
NR	^{137}Cs	6550	excellent
	^{60}Co	1859	good

Table 5. Assessment of ease of decontamination for the ISO standard 8690:1988.

sample	isotopes	DF	degree of ease
DC	^{137}Cs	684	good
	^{60}Co	315	good
KM	^{137}Cs	4928	excellent
	^{60}Co	3444	excellent
CV	^{137}Cs	13	poor/bad
	^{60}Co	30	poor/bad
NR	^{137}Cs	934	excellent
	^{60}Co	3822	good

3.3. Comparison of DF Values from the ISO and Hungarian Standards

Although a direct comparison of the results between the Hungarian and the ISO standards has limited usefulness and relevance due to fundamental differences in the methods used, we found the same experimental phenomena in terms of ease of decontamination. As expected, similar results were observed and measured for higher decontamination factors in all cases. The most different finding, in the case of KM was that the most effective method observed was by treatment using distilled water. Most of the ^{137}Cs contamination was removed more effectively than ^{60}Co contamination for DC, KM, and NR surfaces.

In comparison with the Hungarian standard method, the ISO standard was used for testing and assessing the ease of decontamination only for chemically adsorbed contaminating isotopes. The experiment was then conducted using 20 contaminated samples of the same type, distilled water as a cleaning agent, and using different decontamination methods. The results are shown in Figs.6-7 and Table 5.

These results are in contrast to our previous observations using the Hungarian standard method and the low efficiency for CV sample. The differences can be explained by some unknown chemical bond formation between the surface of the material and the studied isotopes. This research confirms that the use of deionised water or cleaning agents described in standards may be a sufficient means of removing wet ^{137}Cs and ^{60}Co contamination when identified early.

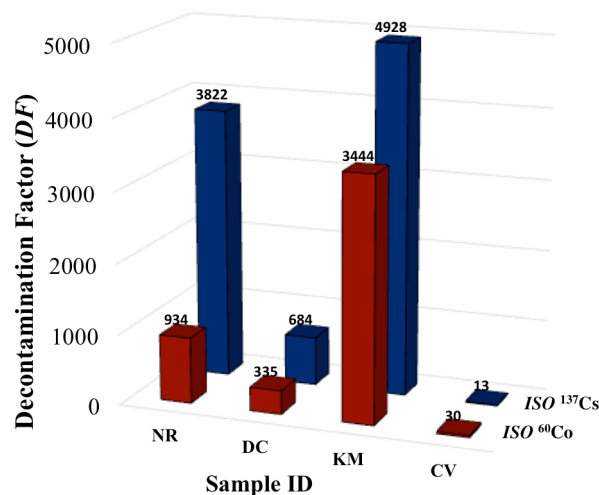


Figure 6. Decontamination factors for the ISO standard 8690:1988 (Table 2).

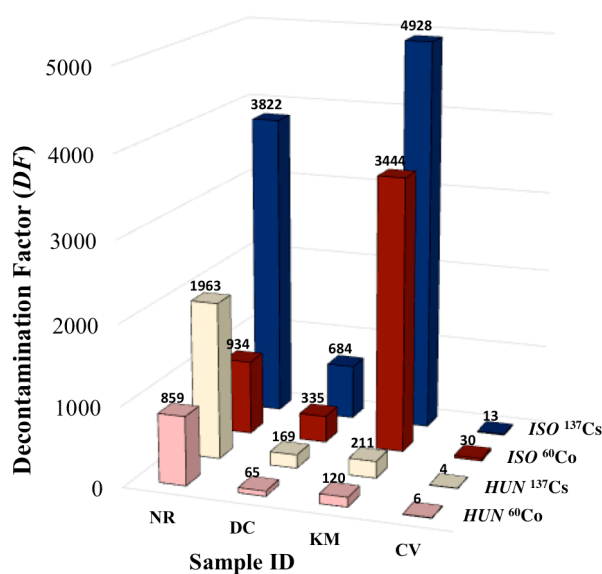


Figure 7. Decontamination factors for the ISO 8690:1988 (E) and Hungarian (adsorption-type contamination) standards.

4. Conclusion

The aim of this study was to identify some of the best surfaces, which would meet ALARA and good-manufacturing-practice requirements to set up protocols to manage contamination in laboratories. The Russian standard can provide very specific information about the ease of decontamination for a wide variety of contamination conditions. The fixed measurement parameters in the case of the ISO 8690:1988 and Hungarian MSZ-05 22.7662-83 standards provide an opportunity to compare paints and coatings and classify them. Using the Hungarian and ISO standards, the ^{137}Cs and ^{60}Co contamination on a surface can be cleaned quickly and effectively using distilled water. Based on the results obtained after the decontamination procedure for the Hungarian and ISO standards, NR can be applied to the surface, the walls of the laboratory, and where

radiation is susceptible in nuclear power plants. In the worst case scenario, when there is an accident involving radioactive contamination, the ability of cleansing the decontamination of surfaces covered by NR will be the most efficient. According to our findings, we were able to select the best materials for the floor of our laboratory.

Acknowledgement

The authors thank the Ministry of Education, Vietnam for funding this research, and the Institute of Radiochemistry and Radioecology, University of Pannonia for providing experimental conditions.

REFERENCES

- [1] Ruhman, N.; Vesper, G.; Martin C.: The effectiveness of decontamination products in the nuclear medicine department, *J. Nucl. Med. Technol.*, 2010, **38**(4), 191–194 DOI: 10.2967/jnmt.110.076919
- [2] Leonardi, N.M.; Tesán, F.C.; Zubillaga, M.B.; Salgueiro, M.J.: Radioactivity decontamination of materials commonly used as surfaces in general-purpose radioisotope laboratories, *J. Nucl. Med. Technol.*, 2014, **42**(4), 292–295 DOI: 10.2967/jnmt.114.144303
- [3] Hungarian Standard MSZ-05 22.7662-83: Testing of painted coatings in laboratory. Determination for ease of decontamination (Hungarian Patent Office, Budapest, 1983 - withdrawn in 2003)
- [4] International ISO Standard 8690:1988: Decontamination of radioactively contaminated surfaces. Method for testing and assessing the ease of decontamination (International Organization of Standardization, Switzerland, 1988) www.iso.org/iso/catalogue_detail.htm?csnumber=16094
- [5] Russian Interstate Standard GOST 25146-82: Radiochemical production and atomic power plant materials. Method for determination of decontamination ratio (Technormativ LLC, 1983 - official translation in 2015) <http://runorm.com/product/view/2/10771>
- [6] Schleipman, A.R.; Gerbaudo, V.H.; Castronovo, F.P.: Radiation disaster response: preparation and simulation experience at an academic medical center, *J. Nucl. Med. Technol.*, 2004, **32**(1), 22–27 PubMedD: 14990671; tech.snmjournals.org/content/32/1/22
- [7] Gurau, D.; Deju R.: The use of chemical gel for decontamination during decommissioning of nuclear facilities, *Rad. Phys. Chem.*, 2015, 106, 371–375 DOI: 10.1016/j.radphyschem.2014.08.022
- [8] Varga, K.; Baradlai, P.; Hirschberg, G.; Nemeth, Z.; Oravetz, D.; Schunk, J.; Tilky, P.: Corrosion behaviour of stainless steel surfaces formed upon chemical decontamination, *Electrochim. Acta*, 2001, **46**(24-25), 3783–3790 DOI: 10.1016/S0013-4686(01)00665-X
- [9] Anthofer, A.; Lippmann, W.; Hurtado, A.: Laser decontamination of epoxy painted concrete surfaces in nuclear plants, *Optics Laser Technol.*, 2014, **57**, 119–128 DOI 10.1016/j.optlastec.2013.09.034
- [10] Endo, M.; Kakizaki, T.: Washing operation of a road surface washing mechanism for decontaminating radioactive substances, *ROBOMECH J.*, 2014, **1**, 13 DOI 10.1186/s40648-014-0013-8
- [11] IAEA-TECDOC-102 2: New methods and techniques for decontamination in maintenance or decommissioning operations, Results of a coordinated research programme 1994–1998 (International Atomic Energy agency, Vienna) 1998 ISSN 1011-4289; www-pub.iaea.org/MTCD/publications/PDF/te_1022_web.pdf
- [12] IAEA-TECDOC-24 8: Decontamination of operational nuclear power plants (International Atomic Energy agency, Vienna) 1981 www-pub.iaea.org/mtcd/publications/pdf/te_248_web.pdf

A STUDY OF THE ADSORPTION CHARACTERISTICS OF COBALT AND CAESIUM FROM A SOLUTION BY USING VIETNAMESE BENTONITE

LE PHUOC CUONG,¹ PHAM HOANG GIANG,² BUI DANG HANH,³ AND GERGŐ BÁTOR^{4*}

¹ The University of Danang-University of Science and Technology, Danang, VIETNAM

² VNU University of Science, Hanoi, VIETNAM

³ Vietnam Atomic Energy Institute (VINATOM), Hanoi, VIETNAM

⁴ Institute of Radiochemistry and Radioecology, University of Pannonia, Veszprém, H-8201, HUNGARY

The radioactive waste produced from the construction of a nuclear power plant is a controversial topic. The resulting radioactive waste contains ^{60}Co and ^{137}Cs isotopes that are the most difficult to remove. Bentonite is widely used as an adsorbent for heavy metals. An important factor is the safe operation of waste management at a nuclear power plant to be built in Vietnam. Therefore, a method of degrading complexes of radionuclides and the adsorption of radionuclides onto Vietnamese Bentonite was implemented in this study. In current literature, UV radiation and heating with oxidising substances are used in general for degrading complexes of radionuclides. The experimental results for the adsorption of $\text{Co}^{(II)}$ and Cs^+ onto VNB suggest that VNB can be used in the future for large-scale liquid waste treatment due to its low cost, high efficiency, and environmentally friendliness.

Keywords: radionuclides; Vietnamese bentonite; adsorption; UV radiation; hydrogen peroxide

1. Introduction

During operation, a nuclear power plant (NPP) releases a large quantity of liquid waste containing radionuclides. The sources of liquid waste include contaminated boric acid solutions, liquid that has leaked from the primary circuit, a solution used to decontaminate the equipment of the primary circuit, and other waste sources. Radionuclides that exist in liquid waste include ^{137}Cs , ^{60}Co , ^{59}Fe , ^{51}Cr , ^{54}Mn , etc. [1–4].

In all types of nuclear reactors, the solutions that are used to decontaminate equipment containing chemicals are for example, alkalis, KMnO_4 , EDTA, etc. [4] in order to oxidise or to form complexes with radionuclides. These complexes are highly soluble in reactor solutions. Liquid waste containing radionuclides has to be stored for a certain period of time to decay. Radionuclides with short half-lives decay during this storage time. The longer-lasting radionuclides such as ^{60}Co and ^{137}Cs are still present in concentrations above the discharge limit of 1 kBq dm^{-3} . Thus, they are not allowed to be discharged into the environment even after several years of storage [5–10].

One of the most effective methods for the treatment of radioactive waste is on the basis of ion exchange and adsorption processes using inorganic ion exchangers. The desirable characteristics of high

exchange capacity and favourable selectivity for some radioisotopes made certain zeolites useful in the treatment of radioactive waste. Natural zeolites considered for radioactive waste treatment include mordenite, erionite, chabazite, clinoptilolite, and bentonite. Among these, bentonite has received much attention due to its widespread usage, large surface area, and high selectivity for some radiotoxic metals [4, 11].

Bentonite consists predominantly of the mineral montmorillonite, an aluminium hydrosilicate. Its crystal structure shows distinct layers forming a lattice (*Fig.1*). The term “bentonite” was first used by Knight in 1889 following the discovery of highly colloidal plastic clay near Fort Benton in the cretaceous bed of Wyoming. Bentonite is a naturally occurring cationic clay, which can be processed or modified to tailor its properties, so it is suitable for various applications and uses. In its pure form or with some chemical additives or modifications, bentonite can be used as a rotary mud, an anticaking agent for certain granular fertilisers, a binding agent in the agglomeration of cattle feed, in pesticides or mineral oil, for filling, oil deodorising, palletising or bleaching, and in civil construction, foundries, and the alkylation of phenols [4, 6–8].

The aim of this study was the identification of degrading and mineralising complex compounds of $\text{Co}^{(II)}$ and Cs^+ by using UV radiation and heating with oxidation substances. In addition, we also determined the adsorption efficiency of these radioactive isotopes onto VNB.

*Correspondence: kt@almos.uni-pannon.hu

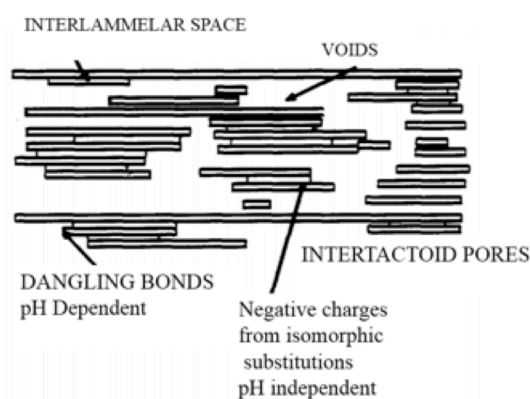


Figure 1. Structure of bentonite [6].

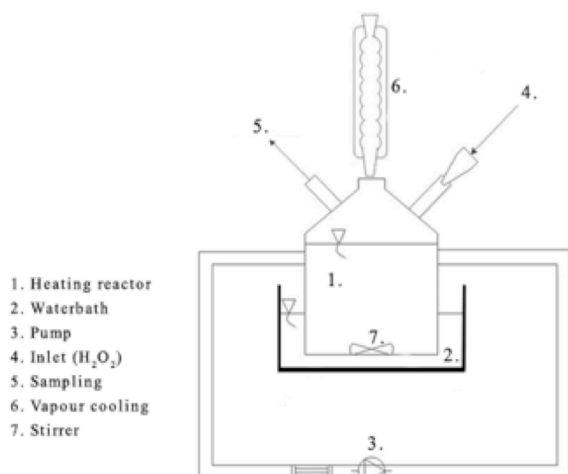


Figure 2. The experimental set-up of the heating system.

2. Experimental

2.1. Objectives

In order to extract ^{60}Co and ^{137}Cs from radioactive liquid waste, a combined treatment method was used. This method includes two stages. In the first stage, the EDTA complexed radionuclides were degraded and mineralised by UV radiation and heating with oxidising substances and then in the second stage radionuclides ions were removed by adsorption using VNB.

In order to prepare the model solutions for this study, the activity concentrations of the radioactive isotopes of ^{137}Cs and ^{60}Co in a typical liquid radioactive waste sample were determined by standard γ -spectrometry using a Gamma Múszaki Zrt scintillation (NaI) detector. Table 1 shows measurements taken from the liquid waste radioactive sample.

2.2. Research Methodology

The concentrations of radioactive elements were determined by using an iCE 3000 atomic absorption spectrometer (AAS, Thermo Scientific, USA) with an air- C_2H_2 flame at a flow rate of $0.9 \text{ dm}^3 \text{ min}^{-1}$.

The chemicals used as analytical standards were all reagent grade or better. Ethylenediaminetetraacetic

Table 1. Typical radioactive liquid waste sample (3/2/2015 measurements).

radio-nuclides	activity concentration, Bq dm^{-3}	pH	dry matter, g dm^{-3}	boric acid, g dm^{-3}	EDTA, g dm^{-3}
^{60}Co	1.23×10^4	12.5	85.23	120	4
^{137}Cs	2.51×10^5				

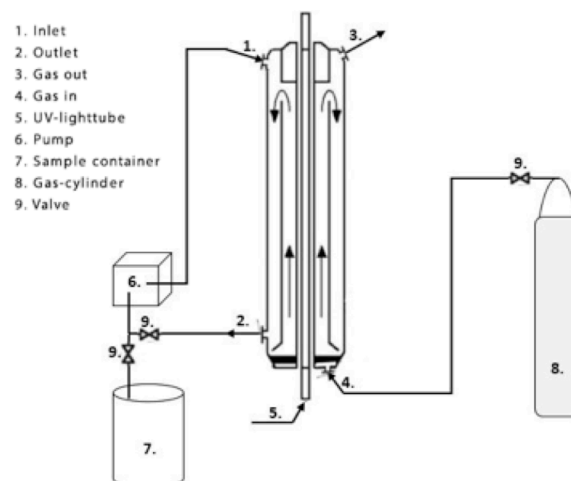


Figure 3. The experimental set-up for UV radiation system.

acid (EDTA), H_3BO_3 , NaOH , H_2O_2 , CoSO_4 , and CsCl were purchased from Merck (Germany). All glassware and polyethylene bottles were thoroughly washed and then rinsed using ultrapure water before use.

2.2.1. Degradation of Complex Compounds by Heating with an Oxidant

In the heated system (Fig.2), the degradation of complex EDTA, CoSO_4 , and H_3BO_3 was investigated under two sets of conditions at 60 and 70 °C both with and without H_2O_2 in 30 mg dm^{-3} concentration. Each experiment lasted 1 hr for three solutions with various concentrations of CoSO_4 (10, 20, and 40 mg dm^{-3}). Aliquots of samples were taken at regular intervals, such as 10, 30, and 60 min. These solutions were centrifuged and stirred with VNB for 1 hr. After that, the solution samples, with and without VNB, were analysed to determine the $\text{Co}^{(\text{II})}$ concentration.

2.2.2. Degradation of Complexes by UV Radiation and Oxidizers

Aspects of photocatalytic degradation of complexes with EDTA, CoSO_4 , and H_3BO_3 were investigated. Degradation efficiencies were studied in detail using a UV radiation system within the range of 280–315 nm and at 0.15 W m^{-2} (Fig.3) under the following conditions:

1. only with UV light;
2. UV and O_2 with flow rate of $70 \text{ dm}^3 \text{ h}^{-1}$;
3. UV, O_2 , and H_2O_2 in 3 mg dm^{-3} concentration;
4. UV, O_2 , and TiO_2 ;
5. UV, O_2 , TiO_2 and H_2O_2 .

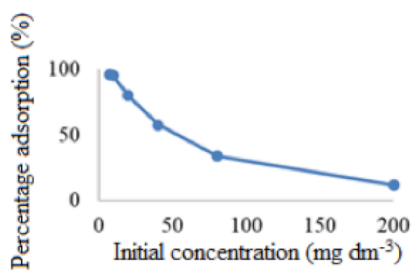


Figure 4. The effect of the initial concentration on the adsorption of Co^(II) onto VNB.

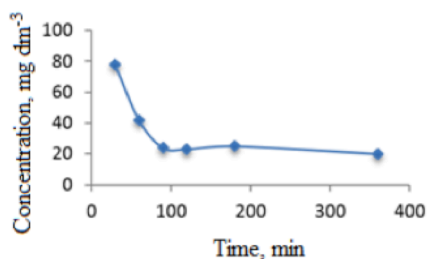


Figure 5. Cs⁺ content in the solution after different periods of time.

Each experiment lasted for 2 hr for the three solutions using various concentrations of CoSO₄ (10, 20, and 40 mg dm⁻³). Samples were taken at regular intervals of 10, 30, 60, and 120 min. The solutions were centrifuged and stirred with VNB for 1 hr. After that, the solution samples, with and without VNB, were analysed to determine the Co^(II) concentration.

2.2.3. Adsorption of Radioactive Elements onto VNB

Experiments on the adsorption of Co^(II) and Cs⁺ onto bentonite were performed in batches to determine their adsorption time and equilibrium isotherms. A volume of 30 cm³ of radioactive solution at various initial concentrations for CoSO₄ (10, 20, and 40 mg dm⁻³); and CsCl (60 and 120 mg dm⁻³) was stirred with bentonite for 1 hr within a pH range of 12 to 13, depending on the initial concentrations of EDTA and H₃BO₃ in the model solution. Samples were taken at regular intervals, centrifuged, and the concentration of Co^(II) and Cs⁺ ions were measured.

2.2.4. Adsorption Isotherms

To evaluate the adsorption ability of ions onto bentonite, the Langmuir and Freundlich isotherm models were employed. On the basis of experimental data, the typical parameters of the adsorption process were determined by using the linear regression method. The Langmuir equation is given by:

$$q_e = q_m k_a C_e / (1 + K_a C_e) \tag{1}$$

Its linear form is

$$C_e / q_e = (1/q_m) C_e + 1/(K_a q_m) \tag{2}$$

where q_e is the amount of ions adsorbed (mg g⁻¹) at equilibrium; C_e is the equilibrium concentration (mg

dm⁻³); q_m is the maximum adsorption capacity (mg g⁻¹); and K_a is the adsorption equilibrium constant. A plot of C_e/q_e against C_e expected to give a straight line with a gradient of $1/q_m$ and an intercept of $1/(K_a q_m)$. The Freundlich equation is given by:

$$q_e = K_f C_e^{1/n} \tag{3}$$

Its linear form is:

$$\ln q_e = \ln K_f + (1/n) \ln C_e \tag{4}$$

where K_f and n are constants.

3. Results and Discussion

3.1. Efficiency of the Adsorption of Radioactive Elements onto VNB

For the estimation of the adsorption ability of Co^(II) onto VNB, 0.1 g of VNB was stirred with 50 cm³ of Co^(II) solution (8–200 mg dm⁻³). After equilibrium was achieved, the residual concentration of Co^(II) was measured using an iCE 3000 AAS (atomic absorption spectrometer).

The effect of initial concentrations on the adsorption of Co^(II) by VNB can be seen in Fig.4. When the initial Co^(II) concentration was increased from 8 to 200 mg dm⁻³ the absolute amount of Co^(II) adsorbed per unit weight of VNB increased from 2.31 mg g⁻¹ (96.5%) to 6.95 mg g⁻¹ (11.8%). However, the percentage adsorption decreased with increasing initial concentration. The results showed that at higher initial concentrations, the number of available adsorption sites decreased and hence, the removal of Co^(II) ions depends upon the initial concentration.

To determine the optimal reaction time in order to achieve an equilibrium state, flasks containing a mix of solutions (CsCl, NaOH, H₃BO₃) with VNB were stirred for different periods of time (10, 30, 60, and 120 min). The concentrations of Cs⁺ ions in the solutions were measured using an atomic absorption spectrometer. The reaction time required to achieve an equilibrium state was defined between the start of stirring and when the analyte concentration remained constant. Fig.5 describes the Cs⁺ content in the solution after different periods of time. According to Fig.5, a period of 100 min can be considered optimal reaction time to achieve equilibrium. This optimal time was implemented for the experiments on the adsorption of Cs⁺ ions onto VNB.

3.2. Study of the Kinetics of the Adsorption of Radionuclides onto Bentonite

3.2.1. Adsorption Isotherms of Co^(II)

Fig.6 shows the adsorption isotherms of Co^(II) onto VNB, which can be described by the Langmuir model with a correlation coefficient (R^2) of 0.9791 and a maximum adsorption capacity of 8.15 mg g⁻¹. The equilibrium data also corresponded to the Freundlich isotherm with a correlation coefficient (R^2) of 0.9640.

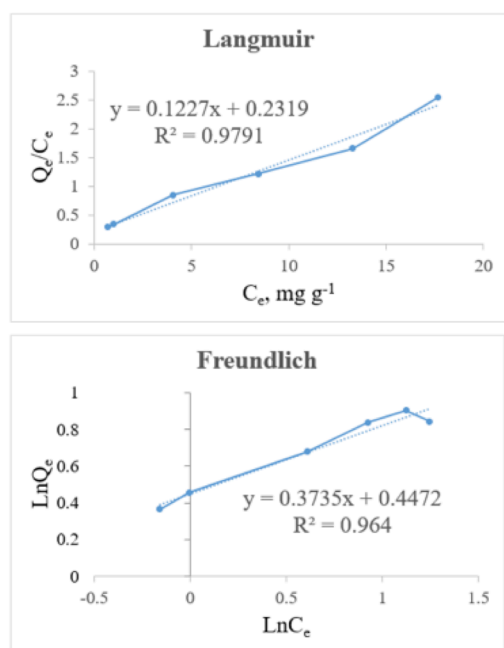


Figure 6. Adsorption Isotherms of $\text{Co}^{(II)}$ onto VNB.

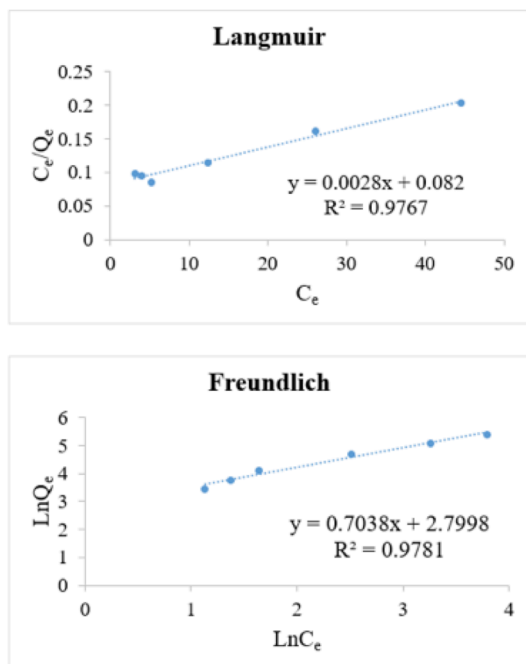


Figure 8. Adsorption Isotherms of Cs^+ onto VNB.

Regarding the four experiments with heating, only Exp. 4 with reaction at 90°C and 30 mg dm^{-3} of H_2O_2 could reduce the concentration of $\text{Co}^{(II)}$ otherwise the $\text{Co}^{(II)}$ concentration remained unchanged or showed no significant change. Fig.7 shows that the concentration of $\text{Co}^{(II)}$ decreased as time increased within 30 minutes, but after that, it practically remained constant. Moreover, initial concentrations also affected the efficiency of removing $\text{Co}^{(II)}$ with initial concentrations of 10, 20, and 40 mg dm^{-3} . The corresponding efficiency values for removing $\text{Co}^{(II)}$ were 22.2%, 31.5% and 61.7%, respectively for samples that were not stirred with VNB, and 22.7%, 43.3%, and 67.7% for samples that were stirred with VNB.

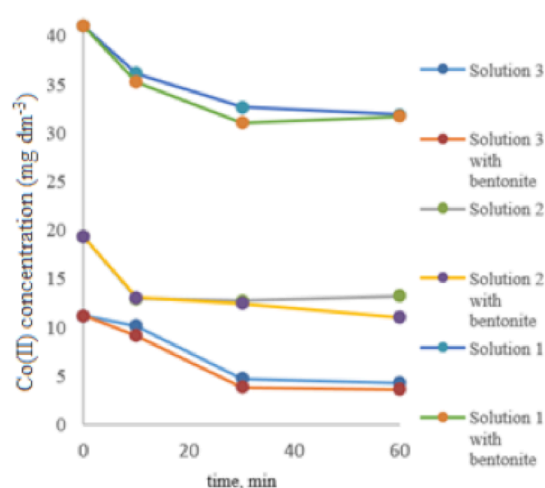


Figure 7. Degradation of $\text{Co}^{(II)}$ over different time periods (Ex. 4) using solution 1: $40\text{ mg dm}^{-3}\text{ Co}^{(II)}$; solution 2: $20\text{ mg dm}^{-3}\text{ Co}^{(II)}$; and solution 3: $10\text{ mg dm}^{-3}\text{ Co}^{(II)}$.

Thus, the experimental adsorption capacity of VNB indicate that it can adsorb $\text{Co}^{(II)}$ at the highest value of adsorption capacity of 8.15 mg g^{-1} , but in the four experiments with heating, the efficiency of removing $\text{Co}^{(II)}$ with VNB did not show significant differences without VNB. Previous research [2, 4, 6] showed that bentonite exhibits good adsorption capacities toward organic matter. However, these results showed that the adsorption ability of EDTA onto bentonite is low, and $\text{Co}^{(II)}$ still remains complexed with EDTA. It is removed only when EDTA is completely degraded.

With regard to the UV system, the results from all experiments show that the outcome of this method was not affected by decreasing $\text{Co}^{(II)}$ concentration. Rekab *et al.* showed [2] that the efficiencies of UV/ TiO_2 and UV/ H_2O_2 treatments are 67% and 42%, respectively at low pH. On the other hand, the degradation efficiency was greater under acidic pH conditions, likely due to the dissociation of H_2O_2 into HO_2^- at alkaline pH, and the photolytic generation of OH^\bullet radicals is therefore hindered. The amine functional groups in EDTA is dominantly converted to ammonia, which forms a complex compound with $\text{Co}^{(II)}$ [2].

3.3. Adsorption Isotherms of Cs

Fig.8 shows that the adsorption isotherm of Cs^+ onto VNB could be described by both the Langmuir and Freundlich models with correlation coefficients (R^2) of 0.98 for both respectively. On the basis of both of these models, the highest value of adsorption capacity was 1.15 mg g^{-1} showing that VNB can adsorb Cs.

4. Conclusion

VNB was tested as an adsorbent material for the removal of cobalt and caesium ions from sulphate and chloride waste solutions. The adsorption of $\text{Co}^{(II)}$ ions

onto VNB followed the pseudo-second order rate model. The adsorption isotherm of Co^(II) was described by the Langmuir and Freundlich models. These show that radioactive isotopes can be highly efficiently adsorbed onto VNB. The adsorption isotherm of Cs⁺ corresponded to both the Freundlich and Langmuir models with high correlation coefficients. In the presence of EDTA in radioactive waste solution, radioactive isotopes could not be adsorbed onto VNB due to forming stronger complexes with EDTA. Therefore, in this study two pre-treatment systems were implemented to remove EDTA from the liquid waste. Heating achieves an efficiency of 67% while the UV radiation did not exhibit satisfactory improvement of treatment efficiency. We are planning to scale up the UV system to include the optimisation of pH values and the effect of ammonium converted from EDTA in order to apply these findings to radioactive solution waste on a large scale.

Acknowledgement

The authors would like to thank the Ministry of Education and Training, Vietnam for funding this research, and the Institute of Radiochemistry and Radioecology at the University of Pannonia for providing the experimental conditions.

REFERENCES

- [1] Manohar, D.; Noeline, B.; Anirudhan, T.: Adsorption performance of Al-pillared bentonite clay for the removal of cobalt(II) from aqueous phase, *Applied Clay Science*, 2006, **31**(3-4), 194–206 DOI: 10.1016/j.clay.2005.08.008
- [2] Rekab, K.; Lepeytre, C.; Dunand, M.: H₂O₂ and/or photocatalysis under UV-C irradiation for the removal of EDTA, a chelating agent present in nuclear waste waters, *Appl. Cat. A: General*, 2014, **488**(11), 103–110 DOI: 10.1016/j.apcata.2014.09.036
- [3] Omar, H.; Arida, H.; Daifullah, A.: Adsorption of ⁶⁰Co radionuclides from aqueous solution by raw and modified bentonite, *Appl. Clay Sci.*, 2009, **44**(1), 21–26 DOI: 10.1016/j.clay.2008.12.013
- [4] Egamediev, S.Kh.; Nurbaeva, D.A.; Tashtemirova, N.G.: Modified bentonite as adsorbents for radionuclides: adsorption of carrier-free radiocobalt-57 on acid modified and calcined bentonite, *Proc. Int. Conf. "Nuclear Science and its Application"*, Samarkand, Uzbekistan, September 25-28, 2012, pp. 345–346 INIS: RN:44129011
- [5] IAEA: Modified Combined Methods for liquid radioactive waste treatment, Final Report (Int. Atomic Energy Agency, TECDOC-1336) 1997–2001 ISSN: 1011-4289
- [6] Dale Ortego, J.; Kowalska, M.; Cocke, D.: Interactions of montmorillonite with organic compounds - adsorptive and catalytic properties, *Chemosphere*, 1991, **22**(8), 769–798 DOI: 10.1016/0045-6535(91)90052-F
- [7] Milyuin, V.V.; Kononenko, O.A.: Sorption of caesium on finely dispersed composite ferrocyanide sorbents, *Radiochem.*, 2010, **52**(3), 281–283 DOI: 10.1134/S1066362210030100
- [8] Tofalvi, R.; Sepsey, A.; Horvath, K.; Hajos, P.: Environmental significance and identification of metal-chelate complexes using ion chromatography, *Hung. J. Ind. Chem.*, 2011, **39**(1), 95–99
- [9] Frerich, J.K., Flugge, U.: High performance catalytic tubular membrane reactors owing to forced convective flow operation, *Hung. J. Ind. Chem.*, 2005, **33**(1–2), 31–42
- [10] Varga, K.; Hirschberg, G.: Accumulation of radioactive corrosion products on steel surface of VVER-type nuclear reactors. II. ⁶⁰Co, *J. Nucl. Mater.*, 2001, **298**(3), 231–238 DOI: 10.1016/S0022-3115(01)00658-4
- [11] Kolics, A.; Varga, K.: Study of cobalt sorption on polyethylene, *J. Colloid Interface Sci.*, 1994, **168**(2), 451–457 DOI: 10.1006/jcis.1994.1441



Degree programmes in English at the Faculty of Engineering

Graduate Programmes

MSc in Environmental Engineering

Duration: 4 semesters

Number of credits: 120

Tuition fee: 4500 USD/semester

Head of the programme: Dr Endre Domokos, Institute of Environmental Engineering

Contact: domokose@uni-pannon.hu

MSc in Environmental Sciences

Duration: 4 semesters

Number of credits: 120

Tuition fee: 4500 USD/semester

Head of the programme: Prof. Judit Padisak, Institute of Environmental Sciences

Contact: padisak@almos.uni-pannon.hu

BSc and MSc in Chemical Engineering

Duration: BSc 7 semesters, MSc 4 semesters

Number of credits: BSc: 210 credits MSc: 120 credit

Tuition fee: 4500 USD/semester

Head of the programme: Dr Sandor Nemeth, Institute of Chemical and Process Engineering

Contact: nemeth@fmt.uni-pannon.hu

Postgraduate Programmes

Hydrocarbon Technology Development Engineer

Duration: 2 semesters

Number of credits: 60

Tuition fee: 2000 USD/semester

Head of the programme: Dr Zoltan Varga, Institute of Chemical and Process Engineering

Contact: vargaz@almos.uni-pannon.hu

Water and Wastewater Treatment System Operation

Duration: 2 semesters

Number of credits: 60

Tuition fee: 2000 USD/semester

Head of the programme: Dr Rita Szakacsne-Foldes, Institute of Environmental Sciences

Contact: foldenyi@almos.uni-pannon.hu



APPLICATION OF IONIC LIQUIDS IN THE UTILIZATION OF THE AGRICULTURAL WASTES: TOWARDS THE ONE-STEP PRE-TREATMENT AND CELLULOSE HYDROLYSIS

GÁBOR MEGYERI,¹ NÁNDOR NEMESTÓTHY,¹ MILAN POLAKOVIC,² KATALIN BÉLAFI-BAKÓ,¹ LÁSZLÓ GUBICZA^{1,*}

¹ Membrane Technology and Energetics, Research Institute of Bioengineering, Faculty of Engineering, University of Pannonia, Egyetem u. 10., Veszprém, 8200, HUNGARY

² Department of Chemical and Biochemical Engineering, Institute of Chemical and Environmental Engineering, Faculty of Chemical and Food Technology, Slovak University of Technology, Radlinského 9., Bratislava, 81237, SLOVAKIA

Cheap, renewable lignocellulosic materials are relevant to the future of biofuel production. Wood and agricultural wastes (e.g. straw, corn stover) provide a raw material source that cannot be used for human consumption, thus biofuels from such sources do not threaten the food supply. The aim of the work was to carry out the pre-treatment and hydrolysis of lignocellulosic material in the same ionic liquid solvent (1-n-butyl-3-methyl-imidazolium-chloride, [Bmim]Cl), using ground wheat straw and a mixture of corn (*Zea mays*) leaf and stover, as substrates. Our measurements show that it is possible to achieve an acceptable glucose content from the cellulose by applying Cellic® CTec2 and Cellic® HTec2 enzyme complexes.

Keywords: ionic liquid, enzyme, hydrolysis, glucose, agricultural waste, lignocellulose

1. Introduction

Nowadays, lignocellulosic plant biomass is considered as a renewable and cheap natural source of energy for second-generation alcohol production and a source of other platform compounds [1]. The main components of plant biomass are cellulose, hemicellulose, and lignin, which form a quite complex molecular structure [2]. Among these substances, the glucose content of cellulose is desirable, which can be obtained in an enzymatic hydrolysis process. However, it is a difficult process, since cellulose is barely soluble in water [3] and thus various pre-treatment methods are required. Physical, chemical, physico-chemical, and biological pre-treatments can be used [4], such as steam explosion [5], dilute and concentrated acids [6], etc. These techniques may liberate certain inhibitory compounds that are not desirable, because they can significantly hinder enzymatic hydrolysis. Some ionic liquids, on the other hand, are able to dissolve cellulose selectively making it accessible to the enzymes while unwanted components are not formed.

Ionic liquids are salts with low melting points [7, 8]. They are considered as green solvents [9] due to their negligible surface tension. A large number of anions and cations are available in countless variations for forming ionic liquids [10]. The asymmetric organic

cation causes the low melting point, because it reduces the lattice energy in 1-alkyl-3-methyl-imidazolium salts [11].

According to literature examples [12, 13], the ionic liquid (IL) formed from 1-butyl-3-methyl-imidazolium chloride salt ([Bmim]Cl) was used to dissolve cellulose. This is the most effective ionic liquid in cellulose pre-treatment, but some have found that it could cause the deactivation of the enzymes. Hydrolysis cellulase enzyme complexes can be used including endo-cellulases, (EC 3.2.1.4), exo-cellulases (EC 3.2.1.91) and cellobiases or β -glucosidases (EC 3.2.1.21).

The aims of this work were i) to study these two key steps (pre-treatment and enzymatic hydrolysis) using pure cellulose, ii) to decide if it is possible to carry out the two steps in the same IL solvent, and iii) to study the processes by using real agricultural waste materials.

2. Materials and Methods

The ionic liquid 1-butyl-3-methyl-imidazolium chloride ([Bmim]Cl) was provided by Io-Li-Tec (Heilbronn, Germany). The enzymes Celluclast 1.5L, Cellic HTec2, and Cellic CTec2 were supplied by Novozymes (Bagsvaerd, Denmark). A description of the enzyme (mixtures) can be found on the websites of the producers as in the case of the chemicals. Cellic CTec2 is a brown liquid with a density of 1.15 g cm⁻³ and a slightly fermented odour that contains cellulase (IUB:

*Correspondence: gubiczal@almos.uni-pannon.hu



Figure 1. Cellulose in IL before pre-treatment (scale in mm is shown below the picture).



Figure 2. Cellulose in IL after pre-treatment.

3.2.1.4) and xylanase. Cellic HTec2 is a yellow liquid with a density of 1.09 g cm^{-3} and lightly fermented odour that contains xylanase (endo-1,4 derivative, IUB: 3.2.1.8). The optimal temperature and pH for both enzymes are $45\text{--}50 \text{ }^\circ\text{C}$ and $5.0\text{--}5.5$, respectively.

The enzymatic reaction was followed by measuring either the glucose content using a GOD glucose kit (Sigma-Aldrich, Budapest, Hungary) or the reducing sugar concentration by the ortho-toluidine (Sigma-Aldrich) spectrophotometric method (Hack-Lange DR 3800 spectrophotometer). Sodium acetate buffer (pH = 5) was used in the hydrolysis experiments with a mixture of acetic acid from Scharlau (Debrecen, Hungary) and NaOH from Spektrum 3D (Debrecen, Hungary).

Purified cellulose powder (Macherey-Nagel, Düren, Germany), grounded corn leaf and stover (CLS), and wheat straw from local (Veszprém) farmers were used as substrates. The ash contents of the CLS and wheat straw were 7.7% and 7.3%, respectively, while the maximum obtained reducing sugar yield (RD_{max}) was 44.9% and 29.6% in the cases of CLS and wheat straw, respectively.

For the pre-treatment, a specified amount of lignocellulosic substance was dissolved in 0.5 g of ionic liquid in a glass reactor then mixed slowly (50 rpm) for 10 minutes in a $100 \text{ }^\circ\text{C}$ oil bath. Afterwards some buffer and 0.015 cm^3 enzyme preparation were added to the mixture. Then hydrolysis was carried out for 2 hours in a $50 \text{ }^\circ\text{C}$ water bath with vigorous mixing (650 rpm). When the hydrolysis finished, the samples were centrifuged in Eppendorf tubes. After that the reducing sugar content was measured using ortho-toluidine.

3. Results and Discussion

The first set of experiments was carried out using pure cellulose to study the effectiveness of the pre-treatment as well as enzymatic hydrolysis. Then ground corn stover and leaf, and finally wheat straw were used as substrates.

Table 1. The glucose content after 2 hr of hydrolysis of pure cellulose.

Enzyme	Glucose content (mg)
Celluclast 1.5 L	0.7
Cellic HTec2	8.4
Cellic CTec2	9.6

3.1. Pure Cellulose

For the pre-treatment, 25 mg of cellulose (5%) was added into 0.5 cm^3 of ionic liquid. Following the description of sample preparation in Ref. [14], the highly viscous mixture was incubated at $100 \text{ }^\circ\text{C}$ for 10 min, and stirred slowly. Pictures were taken under a microscope to follow changes during the pre-treatment. The pictures of the pure cellulose particles dispersed in IL before and after the 10 min pre-treatment are shown in Figs.1-2. On the basis of these photos, it seems that a 10 min pre-treatment time is enough for the cellulose to dissolve into the IL.

For the hydrolysis acetate buffer (pH = 5) and enzyme were added to the mixture. On the basis of our preliminary experiments 3.5 cm^3 of buffer and 0.015 cm^3 of Cellic CTec2 enzyme seemed to be suitable amounts for the reaction. Since the total amount of the mixture is still quite small, the glucose concentration of only the final sample was determined by using the GOD glucose kit. A reaction time of 2 hours was selected on the basis of preliminary measurements. The glucose content was measured in the reaction mixture right after the pre-treatment as well.

No glucose was found in the pre-treated mixture, but 9.6 mg of glucose was detected in the reaction mixture after the enzymatic hydrolysis, which corresponds to approximately 35% conversion. This indicates that the enzyme was able to function in IL in spite of literature data [15-17] suggesting that IL may inhibit enzymatic function. Thus, our experiment confirmed that it was possible to carry out the pre-treatment and enzymatic hydrolysis in the same IL without needing to separate IL from the reaction mixture before the degradation of cellulose.

Table 2. The amount of reducing sugar (mg) in the various samples.

Amount of buffer (cm ³)	Cellic HTec2	Cellic CTec2
1.0	7.16	9.36
3.5	33.10	64.48
7.0	32.84	76.19



Figure 3. Corn leaf and stover in IL before pre-treatment (scale in mm is shown below the picture).

As follow-up measurements, similar conditions were applied, but the other two enzymes were employed. The glucose content was determined by using the simpler ortho-toluidine reducing sugar method rather than the expensive GOD glucose kit. The results are shown in Table 1.

It can be seen from Table 1 that the Celluclast 1.5L enzyme was practically ineffective, while the performance of Cellic CTec2 was similar to the Cellic HTec2 enzyme. Hence, it was decided to use the two Cellic enzymes in our further experiments.

In the next set of measurements, a higher substrate concentration of at least 20% was applied, although, according to the literature [10], the solubility of cellulose in a similar IL is only 5%. However, in industry it is not practical to use excessively diluted cellulose solutions. Cellulose of 0.1 g was added to 0.5 cm³ of IL (20%) and the mixture was treated as described above. The higher initial substrate concentration caused difficulties in stirring the mixture. Its viscosity was extremely high and the texture was rather tacky. Elevated stirring was necessary for complete mixing.

After the pre-treatment, the mixtures were treated using buffers and enzymes for the hydrolysis. Firstly, the same conditions were applied as earlier, then the amount of buffer was varied from 1 to 7 cm³. The corresponding results are shown in Table 2.

On the basis of data in Table 2, it was concluded that 1 cm³ of buffer seems to be insufficient for the hydrolysis. A larger buffer amount, however, does not necessarily result in a higher conversion rate; rather it dilutes the samples considerably. Therefore the 3.5 cm³

Table 3. Amount of reducing sugar (mg) in the corn leaf and stover samples.

Amount of substrate (mg)	Cellic HTec2	Cellic CTec2
0.075	6.99	10.06
0.100	13.82	11.61
0.125	9.11	11.14



Figure 4. Corn leaf and stover in IL after pre-treatment (scale in mm is shown below the picture).

buffer amount was used in further experiments, which corresponds to a 1:7 ratio of IL solution to buffer. This ratio is similar to the literature data found beneficial for the hydrolysis [17].

The conversion rates of the hydrolysis seem quite high especially in the case of the Cellic CTec2 (64.5–76.2%), but these results can be attributed to the usage of pure cellulose and the higher activity enzymes developed lately.

3.2. Corn Leaf and Stover

After the successful experiments using the model substrate: pure cellulose, measurements using ground corn leaf and stover were carried out applying the conditions found suitable earlier: 0.5 cm³ IL, 100 °C, and 10 min pre-treatment time. The initial amounts of the substrate were chosen to be 0.750, 0.100, and 0.125 g corresponding to 15, 20, and 25%, respectively. The process was followed again by taking pictures under a microscope (Figs.3-4).

The higher initial substrate concentration (25%) also caused difficulties in stirring the mixture, but finally the increased stirring applied was enough to achieve complete mixing. It seems, however, that 25% of substrate poses a physical limit for the process. The pictures proved that the biomass dissolved in the IL during the pre-treatment.

Enzymatic hydrolysis was carried out in the pre-treated CLS by adding buffer (3.5 cm³) and either enzymes Cellic CTec2 or Cellic HTec2 (0.015 cm³). After the degradation (2 hours of reaction time) sufficiently high amounts of glucose were found in the

Table 4. Amount of reducing sugar (mg) in the hydrolysed wheat straw samples.

Enzyme	Amount of reducing sugar (mg)
Cellic HTec2	7.07
Cellic CTec2	8.89

mixture (Table 3), though these values are lower than the ones in the case of pure cellulose.

From the data in Table 3, it can be seen that both enzymes were able to degrade the cellulose content of the biomass, and a quite high amount of glucose was produced. It seems that the differences between the glucose concentrations obtained are not too high, which means that we are approaching the substrate saturation limit, where increased substrate content does not result in a higher amount of glucose production.

The conversion data obtained in the range of 7.2–14% indicate that the cellulose content of this biomass is rather difficult for the enzyme to access, thus the hydrolysis is less effective than in the case of pure cellulose. The hydrolytic effectiveness of the enzyme Cellic CTec2 was similar to that of Cellic HTec2.

3.3. Wheat Straw

In the final set of experiments, wheat straw was ground and processed in a similar way to other sources used as a substrate in the experiments by applying similar conditions as mentioned earlier. The initial substrate concentration was 25%, which means that 0.125 g of wheat straw was added to 0.5 cm³ of IL. The results are summarized in Table 4. It can be seen that it is possible to carry out the bioconversion processes using wheat straw as a substrate, but the conversion rate is even lower than for in the case of CLS.

4. Conclusion

It can be stated that the pre-treatment and enzymatic hydrolysis of the cellulose content of various types of plant biomass can be carried out using the same ionic liquid, 1-butyl-3-methyl-imidazolium-chloride. Our experiments have proven that acceptable conversion rates could be achieved. Thus, this technique is considered as a chemically feasible approach for the utilisation of the cellulose content of agricultural waste materials for energetic and other purposes.

Acknowledgement

This work was supported by the projects TÁMOP-4.2.2.B-15/1/KONV-2015-0004 and Slovakian-Hungarian cooperation SK-HU-2013-0008.

REFERENCES

- [1] Abels, C.; Thimm, K.; Wulforth, H.; Spiess, A.C.; Wessling, M.: Membrane-based recovery of glucose from enzymatic hydrolysis of ionic liquid pretreated cellulose, *Biores. Technol.*, 2013, **149**, 58–64 DOI: 10.1016/j.biortech.2013.09.012
- [2] Ha, S.H.; Mai, N.L.; An, G.; Koo, Y.M.: Microwave-assisted pre-treatment of cellulose in ionic liquid for accelerated enzymatic hydrolysis, *Biores. Technol.*, 2011, **102**(2), 1214–1219 DOI: 10.1016/j.biortech.2010.07.108
- [3] Iguchi, M.; Aida, T.M.; Watanabe, M.; Smith, R.L.: Dissolution and recovery of cellulose from 1-butyl-3-methylimidazolium chloride in presence of water, *Carbohydrate Polymers*, 2013, **92**(1), 651–658 DOI: 10.1016/j.carbpol.2012.09.021
- [4] Chandra, R.; Bura, R.; Mabee, W.; Berlin, A.; Pan, X.; Saddler, J.: Substrate pre-treatment: The key to effective enzymatic hydrolysis of lignocellulosic, *Adv. Biochem. Engng./Biotechnol.*, 2007, **108**, 67–93 DOI: 10.1007/10_2007_064
- [5] Van Eylen, D.; Van Dongen, F.; Kabel, M.; De Bont, J.: Corn fiber, cobs and stover: Enzyme-aided saccharification and co-fermentation after dilute acid pre-treatment, *Biores. Technol.*, 2011, **102**(10), 5995–6004 DOI: 10.1016/j.biortech.2011.02.049
- [6] Lozano, P.; Bernal, B.; Jara, A.G.; Belleville, M.-P.: Enzymatic membrane reactor for full saccharification of ionic liquid-pretreated microcrystalline cellulose, *Biores. Technol.*, 2014, **151**, 159–165 DOI: 10.1016/j.biortech.2013.10.067
- [7] Wang, Y.; Radosevich, M.; Hayes, D.; Labbé, N.: Compatible ionic liquid-cellulase system for hydrolysis of lignocellulosic biomass, *Biotechnol. Bioengng.*, 2010, **108**(10), 1042–1048 DOI: 10.1002/bit.23045
- [8] Pinkert, A.; Marsh, K.N.; Pang, S.; Strainger, M.P.: Ionic liquids and their interaction with cellulose, *Chem. Rev.*, 2009, **109**(12), 6712–6728 DOI: 10.1021/cr9001947
- [9] Zhu, S.; Wu, Y.; Chen, Q.; Yu, Z.; Wang, C.; Jin, S.: Dissolution of cellulose with ionic liquids and its application: A mini-review, *Green Chem.*, 2006, **84**(4), 325–327 DOI: 10.1039/b601395c
- [10] Fehér, E.; Major, B.; Bélafi-Bakó, K.; Gubicza, L.: On the background of enhanced stability and reusability of enzymes in ionic liquids, *Biochem. Soc. Trans.*, 2007, **35**(6), 1624–1627 DOI: 10.1042/BST0351624
- [11] Łuczak, J.; Hupka, J.; Thöming, J.; Jungnickel C.: Self-organization of imidazolium ionic liquids in aqueous solution, *Colloids Surf. A: Physicochem. Engng. Aspects*, 2008, **329**(3), 125–133 DOI: 10.1016/j.colsurfa.2008.07.012
- [12] Swatloski, R.P.; Spear, S.K.; Holbrey, J.D.; Rogers, R.D.: Dissolution of cellulose with ionic liquids, *J. Am. Chem. Soc.*, 2002, **124**(18), 4974–4975 DOI: 10.1021/ja025790m

- [13] Lozano, P.; Bernal, B.; Bernal, J.M.; Pucheault, M.; Vaultier, M.: Stabilizing immobilized cellulase by ionic liquids for saccharification of cellulose solutions in 1-butyl-3-methylimidazolium chloride, *Green Chem.*, 2011, **13**(6), 1406–1410 DOI: 10.1039/c1gc15294g
- [14] Auxenfans, T.; Buchoux, S.; Djellab, K.; Avondo, C.; Husson, E.; Sarazin, C.: Mild pre-treatment and enzymatic saccharification of cellulose with recycled ionic liquids towards one-batch process, *Carbohydrate Polymers*, 2012, **90**(2), 805–813 DOI: 10.1016/j.carbpol.2012.05.101
- [15] Turner, M.B.; Spear, S.K.; Huddleston, J.G.; Holbrey, J.D.; Rogers, R.D.: Ionic liquid salt-induced inactivation and unfolding of cellulase from *Trichoderma reesei*, *Green Chem.*, 2003, **5**(4), 443–447 DOI: 10.1039/B302570E
- [16] Salvador, Â.C.; Santos, M. Da C.; Saraiva, J.A.: Effect of the ionic liquid [bmim]Cl and high pressure on the activity of cellulase, *Green Chem.*, 2010, **12**(4), 632–635 DOI: 10.1039/b918879g
- [17] Kamiya, N.; Matsushita, Y.; Hanaki, M.; Nakashima, K.; Narita, M.; Goto, M.; Takahashi, H.: Enzymatic *in situ* saccharification of cellulose in aqueous-ionic liquid media, *Biotechnol. Lett.*, 2008, **30**(6), 1037–1040 DOI: 10.1007/s10529-008-9638-0



Degree programmes in English at the Faculty of Engineering

Graduate Programmes

MSc in Environmental Engineering

Duration: 4 semesters

Number of credits: 120

Tuition fee: 4500 USD/semester

Head of the programme: Dr Endre Domokos, Institute of Environmental Engineering

Contact: domokose@uni-pannon.hu

MSc in Environmental Sciences

Duration: 4 semesters

Number of credits: 120

Tuition fee: 4500 USD/semester

Head of the programme: Prof. Judit Padisak, Institute of Environmental Sciences

Contact: padisak@almos.uni-pannon.hu

BSc and MSc in Chemical Engineering

Duration: BSc 7 semesters, MSc 4 semesters

Number of credits: BSc: 210 credits MSc: 120 credit

Tuition fee: 4500 USD/semester

Head of the programme: Dr Sandor Nemeth, Institute of Chemical and Process Engineering

Contact: nemeth@fmt.uni-pannon.hu

Postgraduate Programmes

Hydrocarbon Technology Development Engineer

Duration: 2 semesters

Number of credits: 60

Tuition fee: 2000 USD/semester

Head of the programme: Dr Zoltan Varga, Institute of Chemical and Process Engineering

Contact: vargaz@almos.uni-pannon.hu

Water and Wastewater Treatment System Operation

Duration: 2 semesters

Number of credits: 60

Tuition fee: 2000 USD/semester

Head of the programme: Dr Rita Szakacsne-Foldes, Institute of Environmental Sciences

Contact: foldenyi@almos.uni-pannon.hu



MINERAL MATTER IN NIGERIAN COALS AND TAR SAND AND THEIR IMPLICATIONS IN BINARY BLEND FORMULATION AND CO-CARBONISATION

SOLOMON A. RYEMSHAK,^{1,2} ALIYU JAURO,^{1*} ISTIFANUS Y. CHINDO,¹ AND ENO O. EKANEM¹

1 Department of Chemistry, Abubakar Tafawa Balewa University, P.M.B. 0248, Bauchi, Bauchi State, 740003, NIGERIA

2 Fuels and Energy Division, National Metallurgical Development Centre (NMDC), P.M.B. 2116, Jos, Plateau State, 930001, NIGERIA

In blend simulation for metallurgical applications, the knowledge of the type and amount of mineral matter in coal and other additives, as well as their derivatives as a result of combustion is important in assessing the coke quality and blast furnace efficiency. X-ray diffraction (XRD) and X-ray fluorescence (XRF) techniques were used in assessing the mineral matter contents and oxides produced up on combustion of the following Nigerian coals: Afuze (AFZ), Garin-Maiganga (GMG), Lamza (LMZ), Shankodi-Jangwa (SKJ), and Chikila (CHK) in addition to a tar sand from Ondo (OTS). Coal samples from Afuze (AFZ) and Chikila (CHK) were found to contain quartz, hematite, and anhydride as the dominant minerals. The Garin-Maiganga coal sample (GMG) was found to contain quartz, magnetite, anhydride, and magnesite. Quartz and hematite were dominant in Lamza coal (LMZ), while Shankodi-Jangwa coal (SKJ) is associated with dolomite and quartz. The bitumen was found to contain quartz, kaolinite, and rutile. The XRF analysis revealed the presence of sixteen elemental oxides: the most abundant being silicon dioxide, ferric oxide, aluminium oxide, sulphur trioxide, calcium oxide, and titanium oxide. Amongst the coal samples, CHK, AFZ and GMG coals have low acidic/basic and basic/acidic ratios, which indicate that cokes originating from them may form the least slag with the best blast furnace efficiency.

Keywords: coke, mineral content, slag formation, fouling, flux, iron extraction

1. Introduction

Mineral matter and ash resulting from decomposition processes are some of the main determining factors that produce straight carbonisation and develop blend coking technology for metallurgical coke production in the iron and steel industries. The mineral matter of coal is commonly, but incorrectly termed as ash content. Coals contain mineral matter, but not ash. The latter is the solid residue, different from the mineral matter in both amount and composition that is obtained during the combustion of coal. Mineral matter has negative and positive effects on coal resource utilisation and disposal. Therefore, the characterisation of minerals in coal is essential in order to assess the beneficial and detrimental effects, which a given mineral matter may have both on the combustion process and on ultimate application. For example, even though phosphorous-bearing minerals are often minor constituents of coal, they can be transferred from coal to coke and interact with iron ore, providing difficulties in steel production [1]. Consequently, coke containing a maximum value of 0.2% phosphorus is required for iron and steel production [2].

Compositional analysis of coal and coke ash is useful in the total coal quality description. Knowledge of the ash composition is useful in predicting the slagging and fouling characteristics of combustible materials in combustion chambers, as well as the potential utilisation of ash by-products, and environmental pollution [3]. It is well known that ash deposition on heat transfer surfaces during coal combustion is a common concern for all coal-firing boilers [4].

It is difficult to quantify the mineral matter content of a coal used in high-temperature operations (combustion and coking processes), because the minerals in coal react with organic particles. On combustion, some of the original minerals decompose and the residual substance may recombine or interact with other derivatives of the coal ash. This may lead to abrasion, corrosion, and clogging as well as fouling of the catalyst and slag formation. The ash, being inevitably a heterogeneous mixture leftover after combustion, is therefore not a true measure of the nature or amount of mineral matter originally present in the sample [5].

This paper assesses the mineral matter contents of Nigerian coals and Ondo tar sand and their implications in binary-blend formulation for coke production.

*Correspondence: ajauro@atbu.edu.ng

2. Experimental

2.1. Samples and Sample Preparation

Coal samples were collected from the following coal fields: Garin-Maiganga (GMG), Chikila (CHK), Lamza (LMZ), Shankodi-Jangwa (SKJ) and Afuze (AFZ). Tar sand was obtained from Ondo (Ondo Tar Sand, OTS). The coal samples were shade dried for three days to remove the free moisture (external or primary moisture fraction). The samples were then ground, and sieved through a 250 micron (0.25 mm) mesh.

2.2. Methodologies

2.2.1. XRD Analysis

The powdered samples were placed into a sample holder and pressed with a piston. They were then loaded into the XRD spectrometer to determine the ore mineral contents of the samples. Copper K α radiation was used as the source. The spectrometer was operated at 40 kV and 30 mA using continuous scan mode from 2 to 80 degrees.

2.2.2. XRF Analysis

Coal samples were ashed at a temperature of 825 °C for 1 hour in a muffle furnace. 5.00 g of the ash was mixed with a binder (cellulose flakes) in a ratio of 5:1 g/g and pelletised at a pressure of about 15 ton inch⁻² in a pelletising machine. The prepared samples were run on an energy-dispersed X-ray fluorescence (ED-XRF) machine by appropriating programmes for various elements, and the various oxides present detected as percentages.

3. Results and Discussion

3.1. Sample Description

Previously published data show that with the exception of Shankodi-Jangwa coal that is bituminous in rank, all other samples (AFZ, LMZ, and CHK) are of subbituminous rank [6–9].

3.2. Mineral Matter

Results from the XRD analysis of the major mineral matter in the coal samples and the Ondo tar sand (OTS) are shown in *Figs. 1* and *2*. The XRD results of the coal samples and the tar sand (OTS) revealed that quartz is dominant in all the samples, with the exception of AFZ, where hematite content is slightly higher than quartz (*Fig. 1*). Apart from quartz, halite, and anhydrite were also detected in CHK (*Fig. 1*); anhydrite, magnetite and magnesite in GMG (*Fig. 1*); hematite in LMZ (*Fig. 2*); dolomite in SKJ (*Fig. 2*); kaolinite and rutile in OTS (*Fig. 2*). The observed minerals are commonly reported in coal samples worldwide [10].

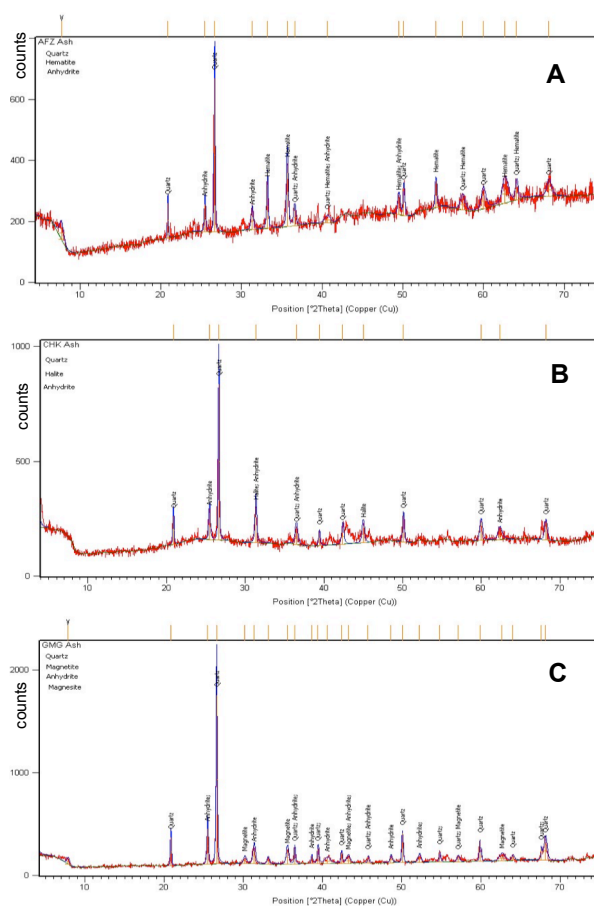


Figure 1. X-ray diffractogram of ash from A) AFZ coal (quartz 38%, hematite 41%, anhydrite 21%); B) CHK coal (quartz 63%, halite 13%, anhydrite 25%); C) GMG coal (quartz 56%, magnetite 12%, anhydrite 18%, magnesite 14%).

A mineral is an inorganic substance that affects both the processing and utilisation of an organic material. XRD analysis is a useful tool in the study of the effects of mineral matter on coal industrial applications like gasification, and liquefaction. Knowledge of the mineral matter can also be used to evaluate the behaviour of a particular coal in different utilisation processes, including to control the characteristics of fly ash, slag and other combustion by-products [11]. Coal and tar sand occur in association with mineral matters, and have different mineral compositions depending on their origins. Based on the association, there are excluded minerals (minerals that are separate from the macerals) and included minerals (minerals closely associated with the organic matter) [12]. The common major minerals identified in coals are quartz, kaolinite, illite, calcite, pyrite, plagioclase, feldspar and gypsum, and occasionally dolomite, ankerite, siderite, iron-oxyhydroxides and sulphates [10]. The amount, mode of occurrence, and composition of the mineral matter in coal are factors of great practical importance in determining its marketability and economic value.

The yield and quality of the product obtained by the use of coal also depends upon the characteristics of its mineral matter. Consequently, the quality of the coke

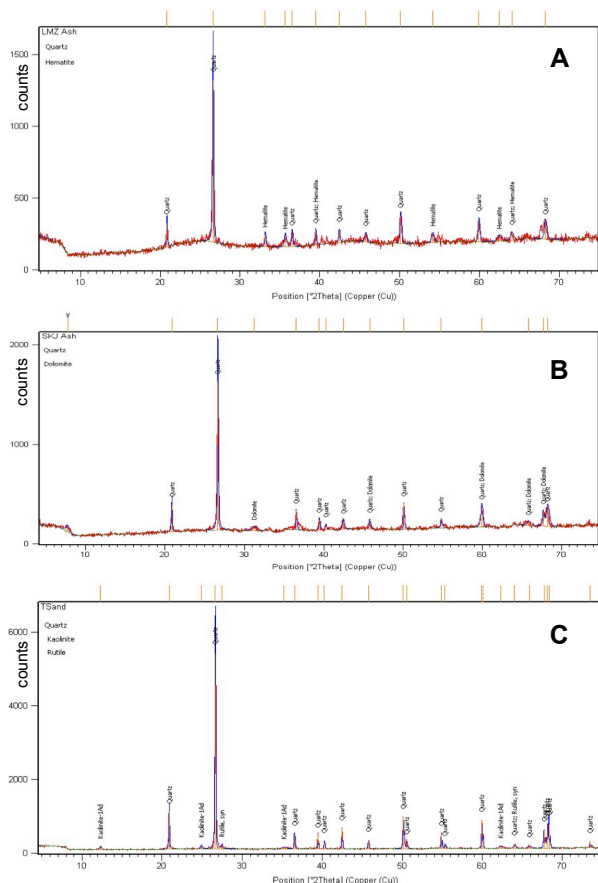


Figure 2. X-ray Diffractograms of ash from A) LMZ coal (quartz 72%, hematite 28%); B) SKJ coal (quartz 80%, dolomite 20%); C) OTS sample (quartz 86%, kaolinite 6%, and rutile 8%).

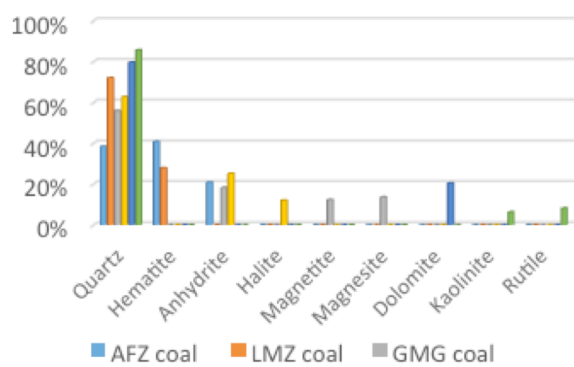


Figure 3. Mineral distribution in coal samples and the tar sand.

also depends heavily on the type and quantity of mineral matter present in the coke after carbonisation. Minerals in coals have different technological problems in metallurgy. For example, clay minerals reduce the calorific value of coal [13]. Excluded quartz and pyrite could result in the abrasion and wearing of grinding equipment [14] and pyrite could lead to slagging and fouling. However, these challenges can be mitigated by understanding coal composition, its mineralogical association and abundance.

The XRD analysis results of these samples (coals and tar sand) showed that both the coal and tar sand samples contain mineral matter impurities such as

quartz and anhydrite, commonly found associated with coal deposits (Fig.3). The minerals in these samples such as kaolinite, hematite, anhydrite, etc., are potential sources of raw materials of chemical industries. Some of the minerals in these coal samples, such as silica, dolomite (calcium magnesium carbonate) or calcium and aluminium are acidic, basic and neutral fluxes respectively, and are useful when combined with other impurities in the formation of slag in iron production [15].

3.3. Mineral Matter and Ash Content During Combustion

Some mineral matter is naturally harmful, and some can decompose to form compounds or combine with other organic components to form other derivatives during combustion. Alkali and alkali earth metals such as Li, Na, K, and Ca, Mg, respectively, at high temperatures disturb the regularity of blast furnace operation by inducing major furnace incidents like frozen hearth and burnt tuyers that cause inconsistency in iron quality. These metals also interact with other elements resulting in problems, such as clinkering, fouling, slagging and corrosion [16–17]. Alkali metals also cause lines of fracture by insertion in the carbon mass of the coke. Generally, alkaline elements were found to have a serious impact on coke production by causing decreased burden permeability and low yields [18]. The alkaline vapour sometimes acts as a glue in binding impacting ash particles together and enhancing fouling at high temperatures [19].

Ash is the inorganic residue that remains after ignition of the combustible substance, and a reduction in ash content improves the coking quality. The ash in coke is of great significance in metallurgy. According to Tivo *et al.* original coal ash contains various kinds of minerals, coexisting as crystal and non-crystal minerals at different temperatures [20]. Coke ash affects the operation of blast furnaces and cupolas due to both its amount and chemical composition. Industrial experience indicates that a weight percent increase of ash in the coke reduces metal production by 2 or 3 weight percent [21]. The disposal of ash is also a big problem that increases operational costs and poses some environmental challenges [22]. Ash content of less than 10% is recommended for a good coking coal [23].

3.4. Slag Formation and Blast Furnace Efficiency

Coal particles can behave differently particularly in terms of carbon conversion, mineral transformation, char fragmentation, and ash formation depending on the association of the organic (maceral) and inorganic (mineral) matter when fed into a gasifier or boiler [12]. This behaviour, which affects the efficiency of the boiler, can be predicted using the data from the XRF analysis of the samples. Table 1 shows the XRF analysis results of ash from the coals and tar samples.

Table 1. Chemical composition (% oxide content) of the coals and tar sand ashes from XRF measurements.

Oxide	AFZ	CHK	GMG	LMZ	SKJ	OTS
SiO ₂	24.61	29.41	38.60	46.40	57.36	70.39
TiO ₂	1.87	1.90	2.40	4.46	2.32	1.62
Al ₂ O ₃	7.31	8.93	7.19	15.81	16.20	14.33
Fe ₂ O ₃	23.97	18.28	16.26	22.53	19.30	5.31
SO ₃	13.70	14.70	11.00	6.20	1.10	0.09
CaO	11.20	25.00	21.10	1.64	1.36	1.26
MgO	0.35	0.31	1.96	0.11	0.20	0.49
Na ₂ O	0.07	0.15	0.10	0.05	0.33	0.30
K ₂ O	0.04	0.87	0.07	0.30	1.46	0.96
MnO	0.40	0.04	0.41	-	0.04	0.06
V ₂ O ₅	0.07	0.10	0.08	0.23	0.14	0.07
Cr ₂ O ₃	0.03	0.03	0.02	0.04	0.04	0.03
CuO	0.08	0.07	0.03	0.20	0.08	0.03
BaO	0.30	0.17	0.77	-	-	0.13
ZnO	-	-	-	-	0.04	0.07
NiO	-	0.04	0.02	0.04	0.03	0.02

A total of 16 elemental oxides were detected in the ashes resulting from combustion, but the most prominent ones are SiO₂, Fe₂O₃, Al₂O₃, and CaO. Even though the results of the oxides (ash composition) fall within the acceptable limit for iron production with the exception of silicon dioxide in OTS, which is above the maximum limit of 64% [2].

The ratio of acidic-to-basic (A/B) oxides (Al₂O₃+SiO₂ versus Fe₂O₃+CaO+MgO) characterises the ash with respect to refractoriness. The A/B ratio indicates the ash fusion temperature and blast furnace efficiency, a high ratio leads to a high fusion temperature resulting in a high slag volume and low blast furnace efficiency [24]. The basic constituents are iron, alkali earth metals (Ca, Mg) and the alkali metals (Na, K). The acidic constituents are Si, Al, and Ti. For instance, the coke from SKJ coal (Fig.4), which has the highest A/B ratio is expected to exhibit the highest fusion temperature and the lowest efficiency during blast furnace operation, while the one from CHK coal would guarantee the highest efficiency of the furnace. Considering the high A/B ratio value of 12 for the OTS sample (Fig.4), a small quantity of its bitumen may be good for blend formulation with the coal samples.

The ratio of basic-to-acidic oxides (B'/A') calculated from Fe₂O₃+CaO+MgO+K₂O+Na₂O content versus SiO₂+Al₂O₃+TiO₂ content [25]), corresponds to the slagging tendency of the coal; the higher the ratio the lower the slag formation [25]. Ash with a high B'/A' ratio, generally exhibits high ash fusion and melting temperatures. However, ash with a medium B'/A' ratio, tends to exhibit low fusion and melting temperatures, hence high slag volume. Ash with a low fusion temperature can cause problems during combustion.

The melting and viscosity behaviour has been described as a function of the composition of the coal ash in terms of acids and bases. Therefore it is expected that CHK and AFZ coals with high B'/A' ratios (Fig.5), would generate coke that may exhibit the least slag formation, closely followed by GMG coal. The highest slag volume is expected in OTS and SKJ coal.

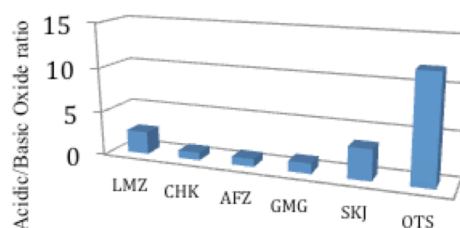


Figure 4. Blast furnace efficiencies of the coal samples.

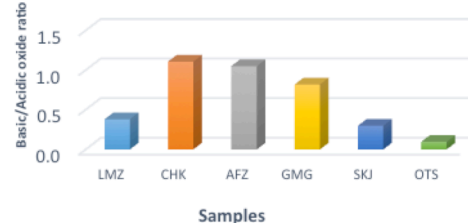


Figure 5. Slag formation tendencies of the coal and tar sand samples.

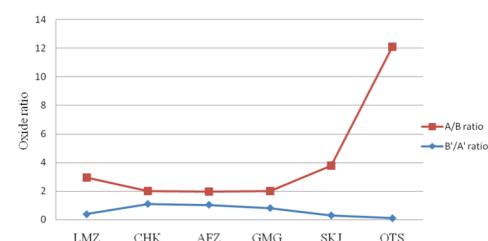


Figure 6. Slag formation tendencies and blast furnace efficiencies.

Overall, the parallel values of A/B and B'/A' ratios for CHK, AFZ, and GMG coals in Fig.6 indicate that cokes produced from them may form the least slag and therefore the best blast furnace efficiency. Excessive ash in metallurgical coke gives rise to high slag volume and low blast furnace efficiency.

4. Conclusion

The relatively low ash contents of these coal samples suggest that they can safely form part of blend formulation for the production of both domestic and industrial cokes without any or significant adverse effects on fouling and slagging, and minimal corrosion and clogging tendencies. The high A/B and low B'/A' ratios of the tar sand (OTS), suggest that a small amount of bitumen may be beneficial for binary blend formulation with the coals, for coke production. Based on the oxide ratios, CHK, AFZ and GMG coals may produce cokes by coking technology that may create the least slag with the best blast furnace efficiency.

Acknowledgement

We acknowledge the Department of Chemistry ATBU in Bauchi and the National Metallurgical Research and Development Centre in Jos for the use of their laboratories. The publication of this article was

supported by Professor János Szépvölgyi (Hungarian Academy of Science, Research Centre for Natural Sciences), Professor Jude Onwudili (University of Leeds) and Dr. Biswajit Ruj (CSIR-Central Mechanical Engineering Research Institute).

REFERENCES

- [1] Ward, C.R.; Corcoran, J.F.; Saxby, J.D.; Read, H.W.: Occurrence of phosphorous mineral in Australian coal seams, *Int. J. Coal Geol.*, 1996, **30**(3), 185–210 DOI: 10.1016/0166-5162(95)00055-0
- [2] ASTM: Petroleum Products, Lubricants and Fossil Fuels (Annual book of ASTM standard, Easton, MD, U.S.A.) 1992
- [3] Shimogori, M.; Ooyatsu, N.; Takarayama, N.; Mine, T.: Ash deposition characteristics determined in pilot plant tests burning bituminous and sub-bituminous coals, *Proc. Int. Conf. Coal Sci. & Tech. (ICCS&T), Oviedo, Spain*, 2011
- [4] Basu, A.: Coal classification and analysis: coal rank, classification by heat value, *Coal Industry News*, 2010 <http://www.coalgeology.com/coal-classification-and-analysis-coal-rank-classification-by-heat-value/8603/>
- [5] Ryemshak, S.A.; Jauro, A.: Proximate analysis, rheological properties and technological applications of some Nigerian coals, *Int. J. Ind. Chem.*, 2013, **4**(1), 1–7 DOI: 10.1186/2228-5547-4-7
- [6] Jauro, A.: Organic geochemistry of Benue Trough coals; Biomarkers, hydrocarbon generation and coking potentials (LAP Lambert Academic Publishing, Saarbrücken, Germany) 2011
- [7] Jauro, A.; Agho, M.O.; Abayeh, O.J.; Obaje, N.G.; Abubakar, M.B.: Petrographic studies and coking properties of Lamza, Chikila and Lafia-Obi Coals of Benue Trough, *J. Mining & Geol.*, 2008, **44**(1), 37–43 DOI: 10.4314/jmg.v44i1.18882
- [8] Ohimain, E.I.: Can Nigeria generate 30% of her electricity from coal?, *Int. J. Energy Power Engr.*, 2014, **3**(1), 28–37 DOI: 10.11648/j.ijep.20140301.15
- [9] Stanislav, V.V.; Vassileva, C.G.: Occurrence, abundance and origin of minerals in coals and coal ashes, *J. Fuel Processing Techn.*, 1996, **48**(2), 85–106 DOI: 10.1016/S0378-3820(96)01021-1
- [10] Ward, C.R.: Analysis and significance of mineral matter in coal seams, *Int. J. Coal Geol.*, 2002, **50**(1), 135–168 DOI: 10.1016/S0166-5162(02)00117-9
- [11] Leonard, D.C.; Bonte, L.; Dufour, A.; Ferstl, A.; Raipala, K.; Scmole, P.; Schoone, P.; Verduras, J. L.; Willmers, R.R.: Coke quality requirements of European blast furnace engineers, *Proc. 3rd European Coke Making Cong., CRM-VDEh, Gent, Belgium*, 1996, pp. 1–10
- [12] Soundarraja, N.; Krishnamurthy, N.; Gibson, L.M.; Shadle, L.J.; Pisupati, S.V.: A study of the transformation of mineral matter in bituminous coal fractions during gasification in a drop-tube reactor, *Proc. 2013 ICCS&T, EMS Energy Institute, State College, USA*, 2013, pp. 356–359
- [13] Shirazi, A.R.; Bortin, O.; Eklund, L.; Lindqvist, O.: The impact of mineral matter in coal on its combustion and a new approach to the determination of the calorific value of coal, *J. Fuel*, 1995, **74**(2), 247–251 DOI: 10.1016/0016-2361(95)92661-0
- [14] Spears, D.A.: Role of clay minerals in United Kingdom coal combustion, *J. Appl. Clay Sci.*, 2000, **16**(1-2), 87–95 DOI: 10.1016/S0169-1317(99)00048-4
- [15] Dippenaar, R.: Industrial uses of slag – the use and re-use of iron and steel-making slags, *Proc. 7th Int. Conf. Molten Slags Fluxes and Salts* (Symposium Series S36, South African Institute of Mining & Metallurgy), 2004, pp. 57–70
- [16] Poos, A.: Future requirements for blast furnace coke making, *Proc. 2nd Int. Coke Making Congress, London*, 1992, **4**, 29–30
- [17] James, G.S.: The chemistry and technology of coal (CRC, Boca Raton, USA) 2013
- [18] Eble C.; Weisenfluh J.: Metallurgical coal resources in Eastern Kentucky. Final – PON2 127 11000027681 (Kentucky Energy and Environment Department), 2012. energy.ky.gov/fossil/Documents/Met%20Coal%20Resources%in%20Kentucky.pdf
- [19] Palanisamy, D.N.; Balakrishnan S.; Nagarajan A.: Coal desulphurisation and additive techniques to combat downstream corrosion and fouling effects: an experiment and theoretical study, *Proc. Int. Conf. Coal Sci.&Tech. (ICCS&T), Oviedo, Spain*, 2011
- [20] Tivo, B.H.; Ratale, H.M.; Zhongsheng, L.; Colin, R.W.: Mineralogical characterisation of Sasol feed coals and corresponding gasification ash constituents, *Energy & Fuels*, 2009, **23**(6), 2867–2873 DOI: 10.1021/ef8010806
- [21] Diez, M.A.; Alvarez, R.; Barriocanal, C.: Coal for metallurgical coke production: prediction of coke quality and future requirement for coke making, *Int. J. Coal Geol.*, 2002, **50**, 289–412 DOI: 10.1016/S0166-5162(02)00123-4
- [22] Jauro, A.; Chigozie, A.A.; Nasirudeen, M.B.: Determination of selected metals in coal samples from Lafia-Obi and Chikila, *Sci. World J.*, 2008, **3**(2), 79–81 www.scienceworldjournal.org/article/view/10785
- [23] Akpabio, I.O.; Chagga, M.M.; Jauro, A.: Assessment of some Nigerian coals for metallurgical application, *J. Minerals Mat. Charact. Engng.*, 2008, **7**(1), 301–306 www.scirp.org/journal/PaperDownload.aspx?paperID=20564
- [24] Bo, L.; Qihui, H.; Zihao, J.; Renfu, X.; Baixing, H.: Relationship between coal ash composition and ash fusion temperatures, *Fuel*, 2013, **105**, 293–300 DOI: 10.1016/j.fuel.2012.06.046
- [25] Rod, H.: Correlating the slagging of a utility boiler with coal characteristics, (in Applications of Advanced Technology to Ash-Related Problems in Boilers, Eds.: L. Baxter; R. DeSollar.: Springer, New York, USA), 1996, pp. 237–244 DOI: 10.1007/978-1-4757-9223-2



Degree programmes in English at the Faculty of Engineering

Graduate Programmes

MSc in Environmental Engineering

Duration: 4 semesters

Number of credits: 120

Tuition fee: 4500 USD/semester

Head of the programme: Dr Endre Domokos, Institute of Environmental Engineering

Contact: domokose@uni-pannon.hu

MSc in Environmental Sciences

Duration: 4 semesters

Number of credits: 120

Tuition fee: 4500 USD/semester

Head of the programme: Prof. Judit Padisak, Institute of Environmental Sciences

Contact: padisak@almos.uni-pannon.hu

BSc and MSc in Chemical Engineering

Duration: BSc 7 semesters, MSc 4 semesters

Number of credits: BSc: 210 credits MSc: 120 credit

Tuition fee: 4500 USD/semester

Head of the programme: Dr Sandor Nemeth, Institute of Chemical and Process Engineering

Contact: nemeth@fmt.uni-pannon.hu

Postgraduate Programmes

Hydrocarbon Technology Development Engineer

Duration: 2 semesters

Number of credits: 60

Tuition fee: 2000 USD/semester

Head of the programme: Dr Zoltan Varga, Institute of Chemical and Process Engineering

Contact: vargaz@almos.uni-pannon.hu

Water and Wastewater Treatment System Operation

Duration: 2 semesters

Number of credits: 60

Tuition fee: 2000 USD/semester

Head of the programme: Dr Rita Szakacsne-Foldes, Institute of Environmental Sciences

Contact: foldenyi@almos.uni-pannon.hu



COMPARATIVE STUDY OF ADVANCED OXIDATION PROCESSES TO TREAT PETROLEUM WASTEWATER

DHEEAA AL DEEN ATALLAH ALJUBOURYA,^{1*} PUGANESHWARY PALANIANDY,¹ HAMIDI BIN ABDUL AZIZ,¹ AND SHAIK FEROZ²

¹ School of Civil Engineering, Universiti Sains Malaysia, Nibong Tebal, Seberang Perai Selatan, Pulau Pinang, 14300, MALAYSIA

² Caledonian Center for Creativity & Innovation (CCCI), Caledonian College of Engineering, P.O.Box 2322, CPO Seeb 111, Muscat, OMAN

This study was carried out to compare the performance of different oxidation processes, such as solar photo-Fenton reaction, solar photocatalysis by TiO₂, and the combination of the two for the treatment of petroleum wastewater from Sohar Oil Refinery by a central composite design with response surface methodology. The degradation efficiency was evaluated in terms of chemical oxygen demand (COD) and total organic carbon (TOC) reductions. Solar photocatalysis by the TiO₂/Fenton method improved the performance of the photocatalyst at neutral pH for petroleum wastewater without the need to adjust the pH during this treatment. Under acidic conditions, the solar photo-Fenton process is more efficient than solar TiO₂ photocatalysis while it is less efficient under alkaline conditions. The TiO₂ dosage and pH are the two main factors that improved the TOC and COD reductions in the solar photocatalysis using combined TiO₂/Fenton and the solar TiO₂ photocatalysis processes while the pH and H₂O₂ concentration are the two key factors that affect the solar photo-Fenton process.

Keywords: solar photo-Fenton process, solar photocatalysis by TiO₂, petroleum wastewater, chemical oxygen demand, total organic carbon

1. Introduction

A major problem facing industrialised nations is contamination of the environment by hazardous chemicals. A wide range of pollutants have been detected in petroleum wastewater at Sohar Oil Refinery (SOR). Therefore, the elimination of these chemicals from petroleum wastewater is presently one of the most important aspects of pollution control in Oman.

Advanced oxidation processes (AOPs) have the capability of rapid degradation of recalcitrant pollutants in aquatic environments. Remediation of hazardous substances is linked to the hydroxyl radical since it has the potential to degrade organic pollutants [1]. The advantages of AOPs are that these processes can occur at very low concentrations and do not form environmentally hazardous byproducts [2]. During the solar photocatalysis by TiO₂, upon exposure to sunlight an electron hole is created in the valence band of TiO₂ and concomitantly an electron is injected into the conduction band in response to light absorption. This electron hole causes the oxidation of hydroxyl anions and produces the hydroxyl radicals at the TiO₂ surface. During the photo-Fenton process the hydroxyl radicals are formed from the reaction of Fe²⁺ with H₂O₂ under

sunlight irradiation. In the treatment of non-biodegradable and toxic compounds, the photocatalytic processes have shown promising results [3].

Previous studies have reported the enhanced oxidation of contaminants by TiO₂ photocatalysis in the presence of Fenton reactivity. Kim *et al.* [4] reported that the combination of TiO₂ photocatalysis and the Fenton-like reaction synergistically increased the degradation of organic compounds at around neutral pH (6.5–7.5) by the increased production of reactive oxidants and their improved reactivity. However, it has not been clearly addressed whether the integration of the UV/TiO₂ and Fe²⁺/H₂O₂ systems exhibits synergistic results with respect to the degradation of contaminants. Little data are available on the role of Fe²⁺ ions in the UV/Fe²⁺/TiO₂ system at neutral pH, where the Fe²⁺/H₂O₂ or UV/Fe²⁺/H₂O₂ system alone is not effective for oxidant production and pollutant oxidation due to the low aqueous iron solubility and H₂O₂ decomposition via a non-radical mechanism without hydroxyl radical generation [1,4,5]. Zarei *et al.* [6] showed that the removal efficiency of phenol was 69% after 150 min using photoelectro-Fenton (PEF)/Mn²⁺/TiO₂ nanoparticles for the removal of phenol from aqueous solutions. Nogueira [7] showed that the role of Fe²⁺ ions and H₂O₂ are much more important than that of TiO₂ in the photodegradation of both 4-chloro-phenol (4CP) and dichloro-acetic acid (DCA) under solar irradiation [7].

*Correspondence: msc.dheea@yahoo.com

Table 1. Overview of research done in the area of Fenton/TiO₂ processes in recent years.

No.	Wastewater	method	material removed	Ref.
1	aqueous imidacloprid	photocatalysis by TiO ₂ photo-Fenton	imidacloprid	[1]
2	Milli-Q water	TiO ₂ /Fenton-like/solar	2,4-dinitrophenyl hydrazine (DNPH)	[4]
3	aqueous solutions	TiO ₂ /photoelectro-Fenton/Mn ²⁺ /UV	phenol	[6]
4	aqueous media	TiO ₂ /Fenton-like/solar	4-chloro-phenol (4CP) and dichloro-acetic acid (DCA)	[7]
5	oil-water emulsions	TiO ₂ /H ₂ O ₂ /Fe ²⁺ /UV TiO ₂ /H ₂ O ₂ /Fe ²⁺ /UV/air ZnO/H ₂ O ₂ /Fe ²⁺ /UV	organics measured by reduction in COD value	[9]
6	dye polluted water	TiO ₂ /H ₂ O ₂ /Fe ²⁺ /UV TiO ₂ /H ₂ O ₂ /Fe ²⁺ /solar	azo dye basic blue 4	[11]
7	petroleum wastewater	TiO ₂ /H ₂ O ₂ /Fe ²⁺ /solar solar photocatalysis by TiO ₂ solar photo-Fenton	organics measured by reduction in COD and TOC values	This study

Table 2. Characteristics of petroleum wastewater from Sohar Oil Refinery (SOR).

parameters	units	ranges of concentration in petroleum wastewater	average concentration	standard discharge limit
pH	-	6–8	7	6–9
Conductivity	μS cm ⁻¹	2600–3950	3275	2000–2700
TDS	ppm(mg dm ⁻³)	1200–1500	1350	1500–2000
TOC	ppm (mg dm ⁻³)	220–265	243	50–75
COD	ppm(mg dm ⁻³)	550–1600	1075	150–200

The aims of the given study are as follows: (i) comparison of the homogenous (solar photo-Fenton) and heterogeneous photocatalytic systems (solar photocatalysis by TiO₂ and solar photocatalysis using combined TiO₂/Fenton processes) by central composite design (CCD) with response surface methodology (RSM) on the basis of their performances with regard to the chemical oxygen demand (COD) and total organic carbon (TOC) in petroleum wastewater and (ii) assessment of treatment efficiencies and the main factors with regard to these methods by CCD and RSM.

To our knowledge there are no reports in the literature of a similar comparison by a central composite design (CCD) with response surface methodology (RSM) applied to the homogeneous and heterogeneous photocatalytic systems for treatment of petroleum wastewater as shown in Table 1.

2. Materials and Methods

2.1. Wastewater Characterisation

The physicochemical characteristics of the petroleum wastewater from SOR are summarised in Table 2. Samples of the petroleum wastewater were collected on different days. Samples were transferred to the laboratory and stored in a refrigerator at 4 °C until use. Samples were characterised before the analysis for their chemical and physical properties. The petroleum wastewater was characterised by the quantification of pH and chemical oxygen demand (COD) according to the Standard Methods for the Examination of Wastewater methodology [12].

2.2. Materials

The catalyst used was TiO₂ Aeroxide P-25 manufactured by Evonik Industries Co., Germany. Hydrogen peroxide (H₂O₂) (35% dm³ dm⁻³) and iron sulphate hydrate (FeSO₄·xH₂O) were supplied by EMPROVE Exp. (USA). Sulphuric acid and sodium hydroxide were used to set the desired pH values.

2.3. Analytical Procedures

A Shimadzu TOC analyser (LCSH/CSN) was used to measure the total organic content (TOC). Chemical oxygen demand (COD) was measured by a COD photometer (manufactured by CHEMetrics). The pH levels were monitored by using a digital pH meter. TOC and COD were determined before and after treatment. Before each analysis, samples were filtered by using a 0.22 μm Millipore Durapore membrane (40 ashless, diameter 150 mm) filter paper.

2.4. Experimental Procedure

The solar photocatalytic equipment used is shown schematically in Fig.1 consisting of a stirred glass recirculation tank (1.5 dm³). The tubular solar reactor contained four tubes 50 cm in length × 2 cm in inner diameter × 0.1 cm in thickness. The solution was recirculated through the reactor at a flow rate of 1.5 dm³ min⁻¹ using a peristaltic pump. Natural sunlight was used as a light source. The added materials and their concentrations such as TiO₂, H₂O₂, and Fe²⁺ were varied according to a central composite design (CCD) with response surface methodology (RSM) to determine the COD and TOC removal efficiencies under the optimum operational conditions.

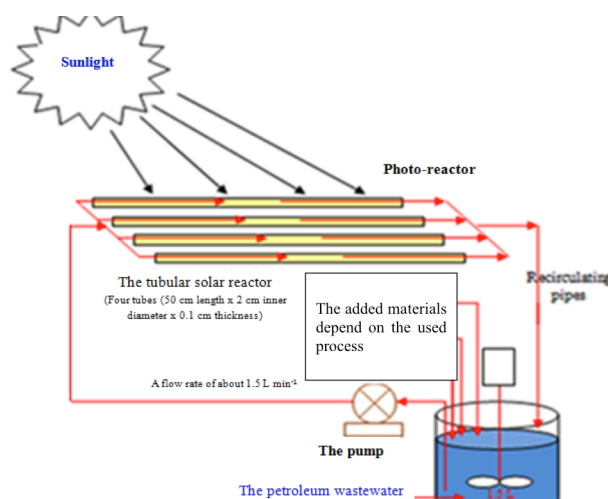


Figure 1. Schematic view of the experimental setup for solar photo-Fenton, solar TiO₂ photocatalysis and solar photocatalysis using combined TiO₂/Fenton processes.

3. Results and Analysis

3.1. Effect of pH

There are two types of Advanced Oxidation Processes (AOPs) depending on the reaction medium: a homogeneous process such as the solar photo-Fenton process, a heterogeneous process such as solar TiO₂ photocatalysis, and their combined processes. According to previous results [13], the solar photo-Fenton process is more efficient for petroleum wastewater treatment than solar TiO₂ photocatalysis under acidic conditions.

By comparing solar photocatalysis using combined TiO₂/Fenton processes with the solar photo-Fenton process under the same pH values, the TOC and COD removal efficiencies improved from 16% to 23% and from 27% to 38%, respectively at pH 7 as shown in Table 3. This enhancement is attributed to increased hydroxyl radical ($\bullet\text{OH}$) production by the presence of TiO₂. As shown in Fig. 2, solar photocatalysis using combined TiO₂/Fenton processes improves performance at neutral pH for petroleum wastewater. Therefore, there is no need to adjust the pH during this treatment.

By comparing these results with previous studies, the results of this work are in agreement with some studies. Ardhendu *et al.* [2] reported that the greatest TOC reduction took place under photo-Fenton process (PFP). It was found to be more efficient than UV/TiO₂ photocatalysis (UVPC) under acidic conditions. Gbandi *et al.* [3] found that photocatalysis of TiO₂ was independent of the pH of the solution, while under Fenton photocatalysis, the degradation rate of Orange II increases as the pH decreases. Duran *et al.* [8] found that the TiO₂ concentration and pH were the main factors for the TiO₂/Fenton/sunlight method for the degradation of the "blue 4" dye. Kim *et al.* [4] showed that the synergistic removal of benzoic acid by the UV/TiO₂/Fe³⁺/H₂O₂ system was very efficient between

Table 3. Comparing the removal efficiencies (%) for three degradation processes expressed by TOC and COD under acidic pH range between 5.5 and 7 of petroleum wastewater.

Removal (%)	pH	TiO ₂ /solar ^a	Fenton/solar ^b	TiO ₂ /Fenton/solar ^c
TOC	5.5	9	17	26
	7.0	15	16	23
COD	5.5	6	39	61
	7.0	24	27	38

experimental conditions: ^a1 g dm⁻³ TiO₂ and 180 min (RT); ^b1 g dm⁻³ H₂O₂, 0.04 g dm⁻³ Fe²⁺ and 180 min (RT); ^c1 g dm⁻³ TiO₂, 1 g dm⁻³ H₂O₂, 0.02 g dm⁻³ Fe²⁺ and 180 min (RT).

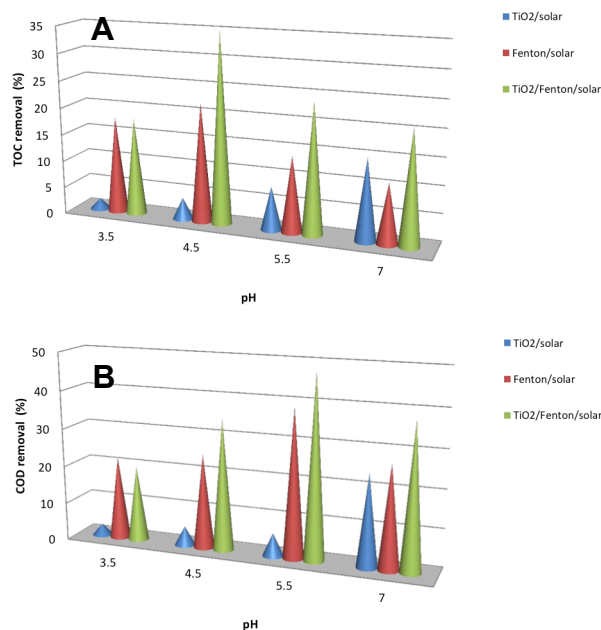


Figure 2. Comparison of the three degradation processes of TOC (A) and COD (B) under different pH values.

the pH values of 4 and 7. But, at higher pH values (pH>7), the addition of Fe³⁺ and H₂O₂ to the UV/TiO₂ system caused negative effects. However, Tony *et al.* [9] reported that the neutral pH of the oil-water solution was the optimum pH value for the degradation of COD by the Fenton/TiO₂/UV system.

3.2. Effect of Fenton Reagent and TiO₂ Concentration

The degradation of organic matter monitored by TOC and COD for solar TiO₂ photocatalysis is significantly improved by using a Fenton reagent in combination with solar photocatalysis as shown in Fig. 2 for the TiO₂/Fenton system. The excess iron has a negative effect because it reacts with hydroxyl radicals reducing the degradation rate of the pollutant [6]. Also, the excess amount of hydrogen peroxide can cause the auto decomposition of H₂O₂ to oxygen and water, and the recombination of hydroxyl radicals. Therefore, decreasing the concentration of hydroxyl radicals and

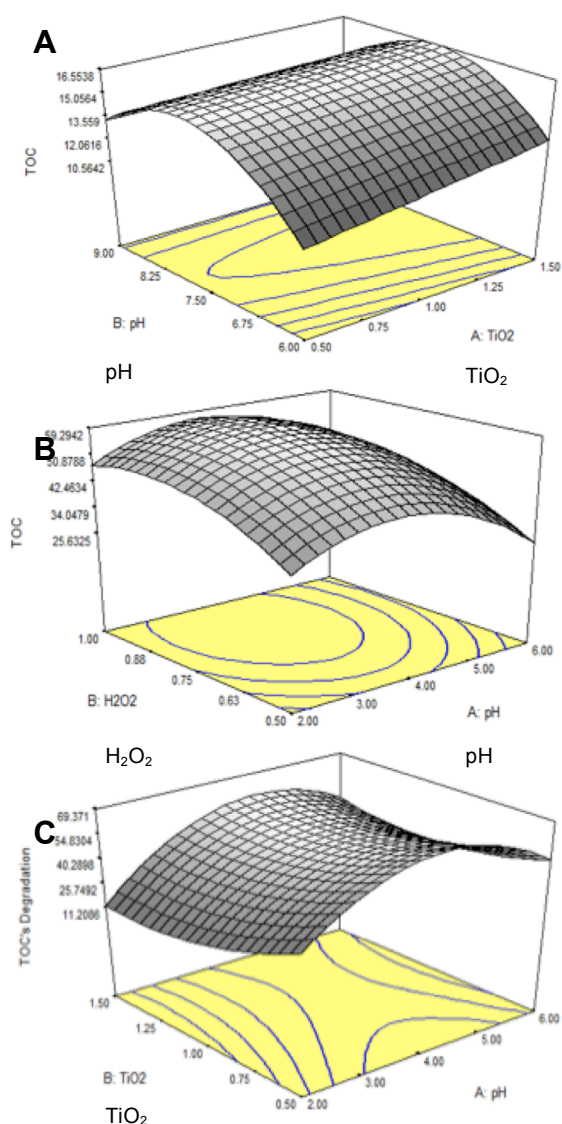


Figure 3. Response surface models for TOC pH val efficiencies for (A) solar photocatalysis by TiO_2 (B) solar photo-Fenton catalysis (C) solar photocatalysis by $\text{TiO}_2/\text{Fenton}$.

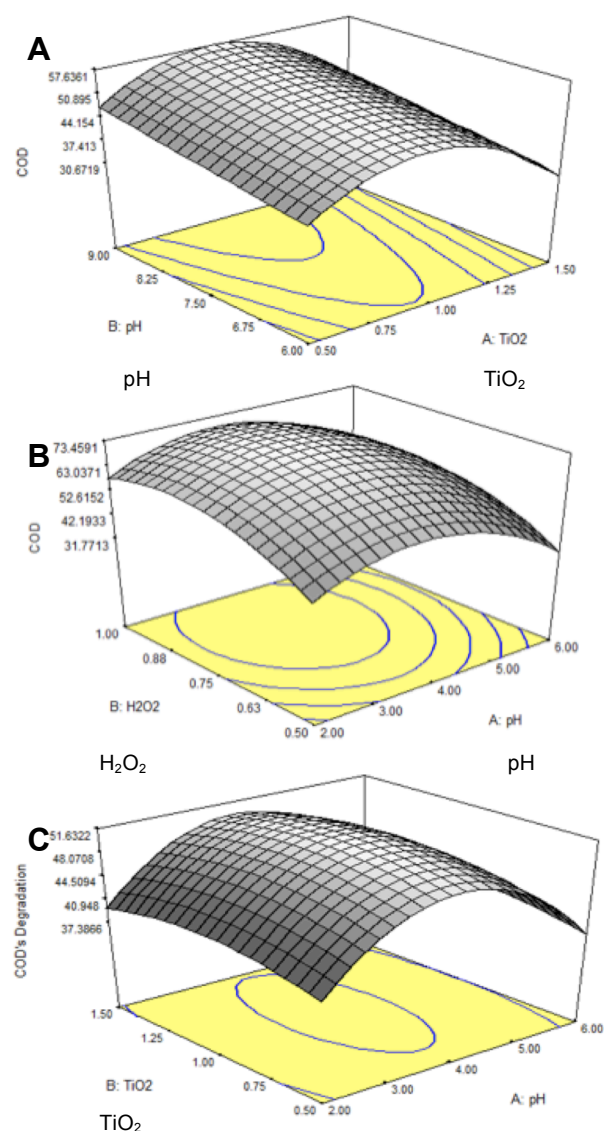


Figure 4. Response surface models for COD pH removal efficiencies for (A) solar photocatalysis by TiO_2 (B) solar photo-Fenton catalysis (C) solar photocatalysis by $\text{TiO}_2/\text{Fenton}$.

reagents reduces efficiency [9]. The degradation rate measured by COD and TOC increases as the TiO_2 concentration increases up to the optimum TiO_2 dosage in solar TiO_2 photocatalysis and solar photocatalysis using combined $\text{TiO}_2/\text{Fenton}$ processes, which were 1 g dm^{-3} and 0.66 g dm^{-3} , respectively. However, TiO_2 dosages greater than the maximum value have a negative effect on these processes since the excess TiO_2 particles increase the turbidity of the solution that decreases the penetration of light into the solution resulting in a reduction in production of hydroxyl radicals ($\bullet\text{OH}$) at the TiO_2 surface [10].

3.3. Treatment Efficiency

To assess the interactive relationships between the independent variables and the responses of certain

models, 3D surface response plots were created by Design Expert 6.0.7. As shown in *Figs.3* and *4*, the TiO_2 dosage and pH were the two main factors that improved the TOC and COD values after removal under solar photocatalysis using the combined $\text{TiO}_2/\text{Fenton}$ and solar TiO_2 photocatalysis processes, while the pH and H_2O_2 concentration were the two main factors in the solar photo-Fenton method. The greater removal rates from TOC and COD values under acidic conditions for solar photocatalysis using the combined $\text{TiO}_2/\text{Fenton}$ and solar photo-Fenton methods were achieved with pH values of 3.6 and 4.2, respectively. However, they were under alkaline conditions (pH 8) for solar TiO_2 photocatalysis. The Fenton ratio and Fe^{2+} concentration were the essential variables for solar photocatalysis using the combined $\text{TiO}_2/\text{Fenton}$ and solar photo-Fenton methods, respectively.

4. Conclusion

The given study evaluated the performance of advanced oxidation processes for the treatment of petroleum wastewater by a central composite design with response surface methodology. These processes include solar photo-Fenton catalysis, solar TiO₂ photocatalysis, and solar photocatalysis using the combined TiO₂/Fenton processes. The decomposition of organic matter was monitored by chemical oxygen demand and total organic carbon content. We obtained experimental evidence for the superior performance of solar photocatalysis using the combined TiO₂/Fenton methods over using TiO₂ only in the case of petroleum wastewater at neutral pH. Under acidic conditions, solar photo-Fenton process was found to be more efficient than solar TiO₂ photocatalysis. However, it was less efficient than the solar TiO₂ photocatalysis under alkaline conditions. The TiO₂ dosage and pH can be used to improve the TOC and COD values for solar photocatalysis using the combined TiO₂/Fenton processes and solar TiO₂ photocatalysis only. The pH and H₂O₂ concentration are the two main factors that influence the efficiency of the solar photo-Fenton process.

REFERENCES

- [1] Giri, A.S.; Golder, A.K.: Fenton, photo-Fenton, H₂O₂ photolysis, and TiO₂ photocatalysis for dipyrone oxidation: Drug removal, mineralisation, biodegradability, and degradation mechanism, *Ind. Eng. Chem. Res.*, 2014, **53**(1), 1351–1358. DOI 10.1021/ie402279q
- [2] Durán, A.; Monteagudo, J.M.: Solar photocatalytic degradation of reactive blue 4 using a Fresnel lens, *Water Res.*, 2007, **41**(3), 690–698. DOI 10.1016/j.watres.2006.06.042
- [3] Djaneye-Boundjou, G.; Amouzou, E.; Kodom, T.; Tchakala, I.; Anodi, K.; Bawa, L.M.: Photocatalytic degradation of orange II using mesoporous TiO₂ (P25) and Fenton reactivity, *Int. J. Environ. Sci., Manage. & Eng. Res.*, 2012, **1**(2), 91–96. www.ijesmer.com/web_documents/20121_2_006.pdf
- [4] Hermosilla, D.; Cortijo, M.; Huang, C.P.: Optimising the treatment of landfill leachate by conventional Fenton and photo-Fenton processes, *Sci. Total Environ.*, 2009, **407**(11), 3473–3481. DOI 10.1016/j.scitotenv.2009.02.009
- [5] Kim, H.-E.; Lee, J.; Lee, H.; Lee, C.: Synergistic effects of TiO₂ photocatalysis in combination with Fenton-like reactions on oxidation of organic compounds at circumneutral pH, *Appl. Catal. B: Environ.*, 2012, **115**, 219–224. DOI 10.1016/j.apcatb.2011.12.027
- [6] Lee, H.-S.; Hur, T.; Kim, S.; Kim, J.-H.; Lee, H.-I.: Effects of pH and surface modification of TiO₂ with SiO_x on the photocatalytic degradation of a pyrimidine derivative, *Catal. Today*, 2003, **84**(1) 173–180. DOI 10.1016/S0920-5861(03)00271-2
- [7] Malato, S.; Cáceres, J.; Agüera, A.; Mezcua, M.; Hernando, D.; Vial, J.; Fernandez-Alba, A.R.: Degradation of imidacloprid in water by photo-Fenton and TiO₂ photocatalysis at a solar pilot plant: A comparative study, *Environ. Sci. Technol.*, 2001, **35**(1), 4359–4366. DOI 10.1021/es000289k
- [8] Nogueira, R.F.; Trovó, A.G.; Paterlini, W.C.: Evaluation of the combined solar TiO₂/photo-Fenton process using multivariate analysis, *Water Sci. Technol.*, 2004, **49**(4), 195–200. hwst.iwaponline.com/content/49/4/195
- [9] Bouras, P.; Lianos, P.: Synergy effect in the combined photo degradation of an azodye by titanium dioxide photocatalysis and photo-Fenton oxidation, *Catal. Lett.*, 2008, **123**, 220–225. link.springer.com/article/10.1007%2Fs10562-008-9466-9
- [10] Tony, M.A.; Zhao, Y.Q.; Purcell, P.J.; El-Sherbiny, M.F.: Evaluating the photocatalytic application of Fenton's reagent augmented with TiO₂ and ZnO for the mineralisation of an oil-water emulsion, *J. Environ. Sci. Health A*, 2009, **44**(5), 488–493. DOI 10.1080/10934520902719894
- [11] Zarei, M.; Khataee, A.; Fathinia, M.; Seyyednadjafi, F.; Ranjbar, H.: Combination of nano photocatalysis with electro-Fenton like process in the removal of phenol from aqueous solution: GC analysis and response surface approach, *Int. J. Ind. Chem.*, 2012, **3**(1), 27–28. DOI 10.1186/2228-5547-3-27
- [12] Standard Methods for the Examination of Water and Wastewater (American Public Health Association (APHA), 21th ed., Washington, DC) 2005.
- [13] Aljuboury, D.D.A.; Palaniandy, P.; Abdul Aziz, H.B.; Feroz, S.: Treatment of petroleum wastewater using combination of solar photo-two catalyst TiO₂ and photo-Fenton process, *J. Environ. Chem. Engng.*, 2015, **3**(2), 1117–1124 DOI 10.1016/j.jece.2015.04.012

Guide for Authors

- Electronic copies of manuscripts should be uploaded to the Author's Pages at hjc.mk.uni-pannon.hu or emailed directly to hjc@almos.uni-pannon.hu.
 - Please visit the Journal's website for downloading a **Word or Latex template** and follow closely the suggested layout for the text, figures, tables, and references. Manuscripts without the recommended structure and formatting for publication will be returned without a review.
 - The use of template is highly desired in order to avoid imposing any article processing charges (APCs), page fees, or article submission charges.
- In a brief letter attached to each manuscripts, **authors must declare that their work is original** and has not previously been published elsewhere. The editorial board requests an originality evaluation score to be below 10% according to CrossCheck/Ithenticate excluding quotes, references, and three-word expressions. If originality of a given manuscript is between 10-20% the authors are kindly requested to rewrite the overlapping sections. Nothing above 20% similarity will be accepted for publication and will not be sent out for review.
- For the purposes of correspondence, the authors are asked to give their current **address, telephone, professional website (if applicable), and regularly accessed E-mail address**.
- Authors are requested to adhere to the rules** given below and follow the examples:
 - The layout of manuscripts should be A4 page size (21 cm × 29.7 cm) with double columns, single-spaced (approximately 45 characters per line, 55 lines per page), and numbered pages. **The text of the papers should be concise, and not exceed twelve pages**; even with Tables and Figures the manuscript should not exceed a total of twelve pages. These limits may be lifted for reviews and invited articles for themed issues.
 - The first page should give the title, the full name (no abbreviations please) of the author(s) in the sequence to be published, the name and address of the institution where the work was completed, and a brief summary of the article (maximum 15 lines). The title of the paper should not exceed 15 words. At least three keywords must be specified, but not more than seven.
 - The corresponding author or authors should be clearly marked.
 - The article should include the following sections: Introduction, Experimental or Theoretical Methods, Results and Analysis, Discussion, and Conclusion. A Conclusion section is mandatory with at least a paragraph presenting the main outcome(s) of the given study, not just repeating the abstract or summarizing the study.
 - Tables and Figures must be inserted into the text** at their closest position to the first mention, flushed with the top margin as much as possible. Drawings must be of high contrast and have continuous curves. Please attach the source of the figure/scheme graphics if available in at least 300 dpi resolution. Characters and labels should be sufficiently large to allow for reproduction. All figures must contain decimal points and not commas.
 - Note that the electronic deposition of the published version of the manuscript will contain colored graphics; however, the printed version will only be reproduced in black and white unless otherwise requested for a fee.
 - The Tables and Figures should not exceed one A/4 size page, (**maximum width of Figures: portrait 8 cm; landscape 16.5 cm**). If diagrams are presented, only the explanation and dimensions of the abscissa, ordinate and marking numbers are required, further explanatory texts can be given in the caption. Please remove any excess white space around the figures.
 - Equations should always be stand-alone, i.e. occupy an extra line and marked with Arabic numerals in parentheses on the right-hand margin. Efforts avoiding equations in two columns are appreciated.
 - The summary of the symbols used must be included at the end of the manuscripts after the Conclusion section under the heading: "SYMBOLS". Symbols and abbreviations that represent variables, constants, quantities, properties etc., must be defined in the text at their first occurrence.
 - Only SI (System International d'Unites) units are to be used.** If data with non-SI units are reported, they should be in parentheses following the corresponding data in SI units.
- References should be numbered throughout the text and written in square brackets and not in superscript position. The references are also to be listed at the end of the paper. *Abbreviations of journal titles should conform to international standards, as accepted by Chemical Abstracts*. The style and punctuation of the references should conform to the ACS Style Guide. For a quick reference please consult the following examples:
 - Journal articles: Debye, P.; Hückel, E.: The theory of electrolytes I. Lowering of freezing point and related phenomena, *Physik. Z.* 1923 **24**(1), 185–206
 - Books: Verwey, E.J.W.; Overbeek, J.T.G.: Stability of Lyophobic Colloids (Elsevier, Amsterdam) 1948
 - Book Chapters: Gunn, A.M.; Winnard, D.A.; Hunt, D.T.E. : Trace metal speciation in sediment and soils, in *Metal speciation: Theory, analysis and application*, Eds.: Kramer, J.R.; Allen, H.E. (Lewis, Boca Raton, FL, USA) 1988
 - Patents: U.S. Pat. 3,425,442 (1984)
 - Published lectures, conference proceedings: Hih, S.; Hhu, C.; Leech, W.J.: A Discrete Method to Heat Conduction Problems, *Proc. 5th Int. Heat Transfer Conf., Tokyo, Japan*, pp. 2.4, 1975. Citations of conference presentations are strongly discouraged and should be avoided unless the talk was made available electronically.
 - Papers that are unpublished, but have been submitted to a journal may be cited with the journal's name, followed by "submitted for publication" or "in press". This will be accepted if the author uploads the submitted manuscript as 'editorial' material. No reference to "unpublished work" or "personal communication" will be accepted.
 - All references must be provided with a digital object identifier (DOI). Please provide the editorial office with a rationale for any citations without DOI numbers and explain why these references are necessary.
- Authors receive galley proofs, which they are to be corrected and returned as soon as possible, but no later than 1 week after receipt. No new material may be inserted into the text at the time of proofreading.
- Authors who are less practiced with written English are urged to have their manuscripts checked by scientists who are working in the Author's respective field and proficient in English.**